





Review

Agar-Based Composites in Sustainable Energy Storage: A Comprehensive Review

Zeenat Akhter * , Sultan Ullah , Arvydas Palevicius  and Giedrius Janusas 

Department of Mechanical Engineering, Faculty of Mechanical Engineering and Design, Kaunas University of Technology, Studentų 56, LT-51424 Kaunas, Lithuania; sultan.ullah@ktu.edu (S.U.); arvydas.palevicius@ktu.lt (A.P.); giedrius.janusas@ktu.lt (G.J.)

* Correspondence: zeenat.akhter@ktu.edu

Abstract

The shift towards renewable resources has positioned agar, a natural seaweed polysaccharide, as a pivotal and sustainable material for developing next-generation energy storage technologies. This review highlights the transformative role of agar-based composites as a game-changing and eco-friendly platform for supercapacitors, batteries, and fuel cells. Moving beyond the traditional synthetic polymers, agar introduces a novel paradigm by leveraging its natural gelation, superior film-forming ability, and inherent ionic conductivity to create advanced electrolytes, binders, and matrices. The novelty of this field lies in the strategic fabrication of synergistic composites with polymers, metal oxides, and carbon materials, engineered through innovative techniques like electrospinning, solvent casting, crosslinking, 3D printing, and freeze-drying. We critically examine how these innovative composites are breaking new ground in enhancing device efficacy, flexibility, and thermal stability. Ultimately, this analysis not only consolidates the current landscape but also charts future pathways, positioning agar-based materials as a pivotal and sustainable solution for powering the future.

Keywords: agar; sustainable composites; gel electrolytes; supercapacitor; fuel cell; battery; future perspective



Academic Editor: JongHoon Kim

Received: 30 September 2025

Revised: 13 October 2025

Accepted: 20 October 2025

Published: 25 October 2025

Citation: Akhter, Z.; Ullah, S.; Palevicius, A.; Janusas, G. Agar-Based Composites in Sustainable Energy Storage: A Comprehensive Review. *Energies* **2025**, *18*, 5618. <https://doi.org/10.3390/en18215618>

Copyright: © 2025 by the authors. Licensee MDPI, Basel, Switzerland. This article is an open access article distributed under the terms and conditions of the Creative Commons Attribution (CC BY) license (<https://creativecommons.org/licenses/by/4.0/>).

1. Introduction

The rising interest in sustainable and eco-friendly materials has led to significant interest in polysaccharide-based biomaterials, which have unmatched advantages such as biodegradability, renewability, and versatility. Among these, agar, a natural polysaccharide extracted from red algae, has been identified as a promising candidate owing to its unique physicochemical properties such as gel-forming ability, biocompatibility, and thermal stability [1–4]. These characteristics make agar an excellent matrix for the creation of advanced functional materials, particularly for energy storage applications, where sustainability and performance need to go hand in hand. As the global energy landscape moves towards renewable sources of energy, the need for efficient, scalable, and environmentally benign energy storage systems has never been more critical. Novel Agar-based composites, with tunable properties and compatibility with several nanomaterials [5,6], carbon-based nanoparticles [7], polymers [3,8–10], ceramics [11,12], and certain inorganic clay constituents [13,14], are set to play a transformative role in this transition.

Materials scientists have advanced agar matrices significantly due to their superior integration capabilities for various conductive components, including metallic nanoparticles, graphene, and synthetic and natural polymers. Their broad applications across various fields are underpinned by their compatibility with energy technologies [15–18]. Agar-based composites are becoming increasingly popular in high-tech energy storage and conversion technologies [19–22]. The attachment of graphene carbon nanotubes with agar makes it more multifunctional [23,24]. These composites are being investigated as gel electrolytes for batteries, as they improve safety and enhance battery component durability [25–27]. These applications demonstrate the efficacy of the agar matrix in enabling functional improvements in energy devices along with possible future roles in sustainable energy technology development [28].

The exceptional performance of agar-based hybrid materials is evident in supercapacitors, fuel cells, and various batteries, as well as in gel electrolytes, due to their unique structural attributes and electrochemical properties. The porous structure of agar in supercapacitors facilitates degradation while forming a conductive matrix with carbon-based nanomaterials or metal oxides, resulting in an efficient ion storage material that enhances energy capacity and power density [29,30]. Agar composites used in fuel cells function as proton-conductive membranes due to their hydrophilic polymer structure, which retains water and facilitates efficient proton transfer while ensuring structural stability during prolonged electrochemical processes. Solid and gel-polymer electrolytes that incorporate agar leverage its adaptable gel structure for lithium–metal batteries, effectively limiting dendrite growth and accommodating expansion during charging cycles, which enhances battery safety and longevity [3,31–33]. The synergistic integration of agar with both natural and synthetic polymers, such as chitosan, gelatin, cellulose, PVA, etc., creates hybrid composites that harmonize eco-friendly attributes with enhanced mechanical and electrochemical functionality, positioning them as versatile, sustainable candidates for next-generation energy systems, from biodegradable batteries to self-healing supercapacitors [3].

Research on agar-based composites is flourishing, evolving rapidly from traditional applications in microbial cultures and electrophoresis to advanced hydrogels/aerogels for sensitive drug delivery, tissue engineering, and environmental remediation (Figure 1). Since 2021, the literature has expanded sharply, with 2022–2024 showing the fastest growth and a pivot towards adsorption, 3D printing, and hybrid systems with chitosan, cellulose, collagen, and emerging MXene pairings. Current research trends prioritize tunable mechanical properties, stabilization, and controlled release, positioning agar composites as versatile, sustainable platforms for energy storage applications.

This review explores the cutting-edge developments in agar-based composites, highlighting their transformative potential in energy storage technologies. By bridging natural polysaccharides with advanced nanomaterials, these innovative composites represent a pivotal step toward sustainable, high-performance energy solutions for a greener future. Additionally, a bibliometric analysis provides insights into research trends, key contributors, and emerging focus areas, offering a comprehensive perspective on the impact of agar-based materials in next-generation energy applications.

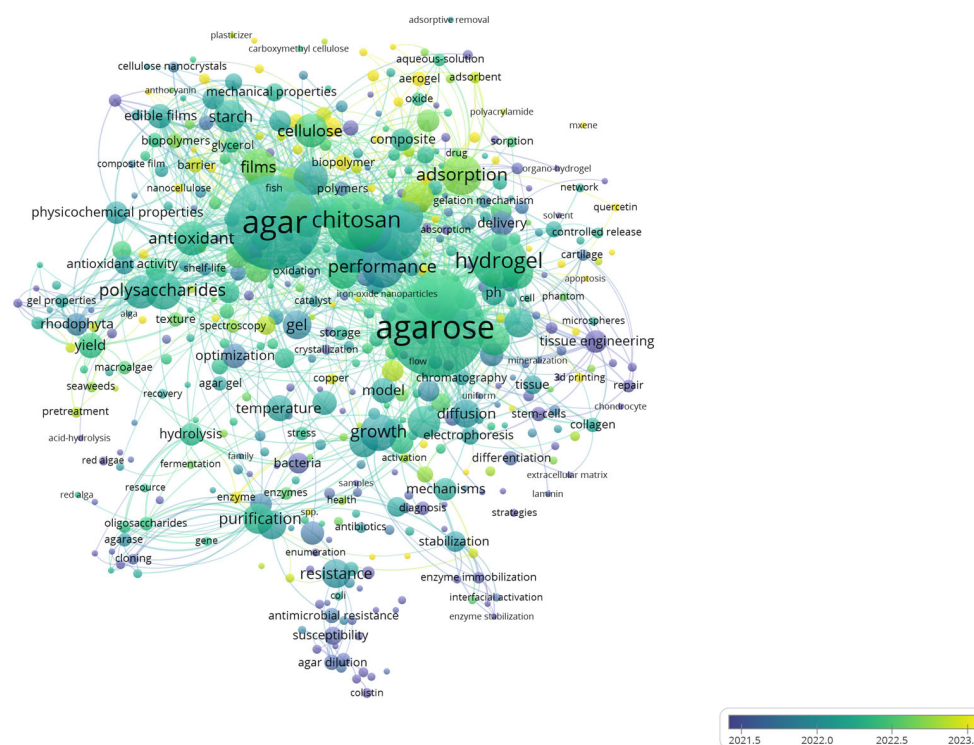


Figure 1. Overlay visualization map depicting the co-occurrence of keywords from 1631 articles retrieved from the WOS databases as of 6 February 2025. The visualization is generated using VOSviewer version 1.6.20, developed by Universiteit Leiden, Netherlands.

2. Fundamentals of Agar

Agar, a heteropolysaccharide, was first extracted from red algae (*Gracilaria* spp.) in 1658. The primary structure consists of two essential components: agarose, which makes up 70% and serves as a thermoreversible gel polymer composed of alternating β -1,4-linked D-galactose and α -1,3-linked 3,6-anhydro-L-galactopyranose units, and agaropectin, which acts as the solvent-enhancing and ion-interaction-managing heterogeneous sulfated polymer. The integration of these two primary structural units establishes the foundation for the varied physical and chemical characteristics of agar materials, facilitating their use in microbiological applications and sophisticated biomaterials. This versatility is enhanced by their customizable gel strength and compatibility with biological components, as well as their chemical diversity [34–36] (see Figure 2). The process of cooling agarose allows the formation of a thermoreversible three-dimensional network through helical coiling, which is stabilized by hydrogen bonds and hydrophobic forces, and traps water to create porous gels with mechanical stability [37,38]. Controlling cooling rates and selecting agar concentration, or adding certain substances like glycerol or salts, helps researchers achieve desired pore sizes and network densities while modifying viscoelastic properties in agarose gels [39,40]. The unique properties of agar render it a valuable substance in the study of energy storage, particularly when utilized as a gel electrolyte material in batteries and supercapacitors [41,42].

Agar demonstrates a built-in capability to form gels, which creates a dependable, biodegradable electrolyte medium that enhances ionic conductivity and structural strength. The electrochemical nature of agar allows its combination with carbon-based materials and metallic nanoparticles, which enhances electrochemical applications. Electrode performance improves through the addition of composites because they increase both surface area and electrical conductivity, which results in better energy storage efficiency and durability. Agar-based gel electrolytes integrated with composites offer an innovative solution

to boost electrochemical storage technology because they use sustainable agar as both a resource and a functional material for modern energy applications [3,43]. Agar is distinguished as a remarkable sustainable energy storage material due to its unique degradation properties and hydrolytic stability, which complement its compatibility with polymers and metals. This enables the advancement of green energy technologies by effectively harnessing viscoelastic energy dissipation in conjunction with flexible gel networks.

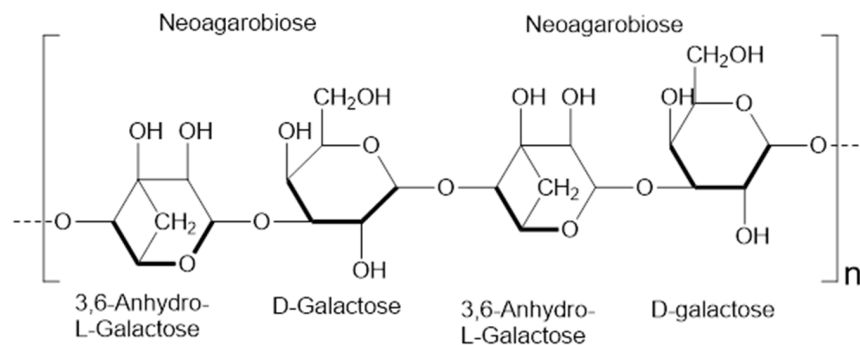


Figure 2. The repeating 3,6-anhydro-L-galactose and D-galactose units in agarose structure form agarobiose and neoagarobiose, which make up the principal component of agar.

Agar-based systems have built-in constraints that limit performance and scale-up. Their water-rich networks provide a narrow electrochemical stability window, so water splitting and gas formation can occur at modest voltages. Moisture changes cause drying, swelling, and syneresis, which shift ionic conductivity, dimensions, and self-discharge over time. The gels are relatively brittle and can creep or crack under repeated deformation, leading to contact loss at electrodes [44–47]. Thermal behavior is also restrictive: gelation occurs near room temperature, and softening or melting appears at higher temperatures, while cold conditions can embrittle the network [48]. Ionic conductivity and rate capability usually trail those of optimized liquid electrolytes unless plasticizers or high-salt formulations are used, and these fixes can weaken mechanical strength and accelerate aging. Interfaces with reactive metals (e.g., Zn) tend to require additives or protective interphases to curb dendrites and corrosion [49–51]. Robust performance depends on complex formulations, and seaweed-derived feedstocks introduce cost and batch-to-batch variability that complicate reproducibility and scaling.

3. Role of Agar in Energy Storage Applications

Agar is gaining popularity as a green source for use in energy storage devices because it is renewable, biodegradable, and not highly toxic. Agar is plentiful and environmentally friendly, unlike traditional petroleum-based polymers, and is thus in line with the objectives of green chemistry in the development of energy storage devices. Indeed, materials derived entirely or partially from algae are under consideration for batteries and supercapacitors to enhance sustainability [3,47]. The physicochemical properties of agar, e.g., its capacity to create hydrogels, to harbor ionic species, and to bind to surfaces, are reasons why agar is a good candidate for a range of electrochemical applications. Agar-based components have been added to batteries, supercapacitors, and fuel cells in recent studies, with agar being determined to be useful as a substitute for traditional binders or electrolytes that does not impair device functionality [47]. Due to its hydrophilicity and mechanical strength, agar is a flexible platform for developing functional composites in energy storage systems.

3.1. Film-Forming and Gelation Behavior

Agar has a distinct gelation property that is one of its most important characteristics. Agar is dissolved in hot water at 90 °C, then solidifies into a solid gel at temperatures below 40 °C following a thermoreversible sol–gel transition. The large hysteresis in this transition means that agar gels solidify at room temperature (approximately 35 °C) and do not melt until they are heated to approximately 85–90 °C [52,53]. During gelation, agarose chains are crosslinked physically through hydrogen-bonded double helices when chilled below the melting point. This produces a 3D network structure capable of containing large volumes of solvent. The powerful hydrogen bonding and high molecular weight of agarose give it excellent film-forming properties; agar solutions can be poured into a film or membrane, which will harden at room temperature without any extra crosslinkers (Figure 3) [54,55]. This property allows the production of thin agar-based films as solid electrolytes or separators in energy materials. In addition, agar can undergo reversibly gelation, enabling reprocessing and self-healing of materials. Kim et al. showed that an agarose composite hydrogel is moldable (into thin films, fibers, and 3D structures) and, upon being cut, the fragments could be recombined, restoring electrical activity in a short time [47]. This processing flexibility is advantageous for developing flexible and wearable energy storage devices. Structural integrity is also provided by the firm gel state of agar; e.g., an agar gel electrolyte can exist as a freestanding membrane, unlike liquid electrolytes that need a container. In general, the film-forming and gelation behavior of agar provide a basis for the development of robust, shape-conformable components within energy systems.

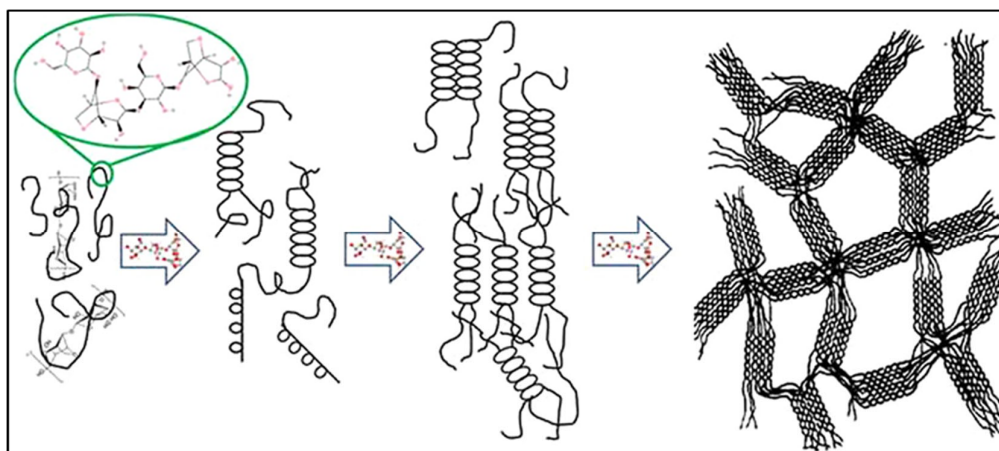


Figure 3. The gelation mechanism of agarose involves the formation of helical structures and gelation through hydrogen bonds and electrostatic interactions among agarose chains [56].

3.2. Ionic Conductivity and Electrolyte Compatibility

Even though agar is an insulator, when it is loaded with electrolytes, its hydrogel network can be used as an ion-conducting medium. The high concentration of oxygen-containing groups (hydroxyls and ethers) on the polymer can bind with cations, and therefore agar is a good polymer host for ionic conduction [57]. Gels made from agar are usually impregnated with salts or acids to make them ionically conductive. For example, initial experiments demonstrated that a basic agar–KCl gel could serve as a salt bridge and polymer electrolyte, leading to other experiments on agar-based electrolytes [58]. Swollen agar hydrogels containing aqueous electrolytes have recorded ionic conductivities on the order of 10^{-3} – 10^{-1} S/cm, close to those of liquid electrolytes. In alkaline systems, a hydrogel of PVA–agar blend with 40–50% KOH gave room-temperature conductivities of approximately 0.2–0.24 S/cm (only two to three times lower than bulk 6 M KOH solution).

This ionic conductivity is large enough to be of practical use and highlights the compatibility of agar with concentrated salt solutions. Agar gels have also been used with ammonium and lithium salts or even ionic liquids as proton- or ion-conducting membranes [59]. According to Moon et al., a NaCl–agarose gel polymer electrolyte of flexible supercapacitors allowed rapid ion movement through a 3D porous agarose scaffolding of aqueous electrolyte. Its oriented sub-micropores and bound water gave the gel agarose very efficient ionic conduction to the electrode surfaces, yielding a supercapacitor capacitance of up to about 80% of that with a liquid electrolyte. This proves that agar-based electrolytes can provide high electrochemical performance [46]. Furthermore, agar is particularly compatible with a variety of solvents: although it mainly swells in water, development of devices using organic solvents (glycerol, etc.) and ionic liquids have been investigated using agar [46].

Mohd Rafi et al. reported that, at room temperature, the ionic conductivity of CaSCN–agarose biopolymer electrolytes (0–45 wt%) increases with salt content (Figure 4a). The salt-free matrix shows $1.07 \times 10^{-8} \text{ S cm}^{-1}$, within the typical range for neat polysaccharides (about 10^{-14} to $10^{-8} \text{ S cm}^{-1}$), confirming agarose as a suitable host. Conductivity increases via a hopping mechanism in which Ca^{2+} diffuses through the agarose network and coordinates with oxygen lone pairs from hydroxyl/carboxyl groups to form polyionic interactions (Figure 4b). With added CaSCN, the density of mobile charge carriers ($\text{Ca}^{2+}/\text{SCN}^-$) grows, reaching $8.01 \times 10^{-5} \text{ S cm}^{-1}$ at 40 wt% and remaining high at $2.28 \times 10^{-4} \text{ S cm}^{-1}$ at 45 wt%. However, 45 wt% compromises mechanical/thermal integrity, failing above 353 K, so 40 wt% represents a practical optimum. Temperature-dependent data follow Arrhenius behavior, with linear log σ versus $1000/T$ plots ($R^2 \approx 1$) indicating thermally activated ion transport (Figure 4c) [60]. In conclusion, agar is a good hydrophilic network material with functional groups that can be utilized in ionic conduction when paired with suitable ion species and can be used as solid or gel polymer electrolytes in batteries, supercapacitors, and even fuel cells.

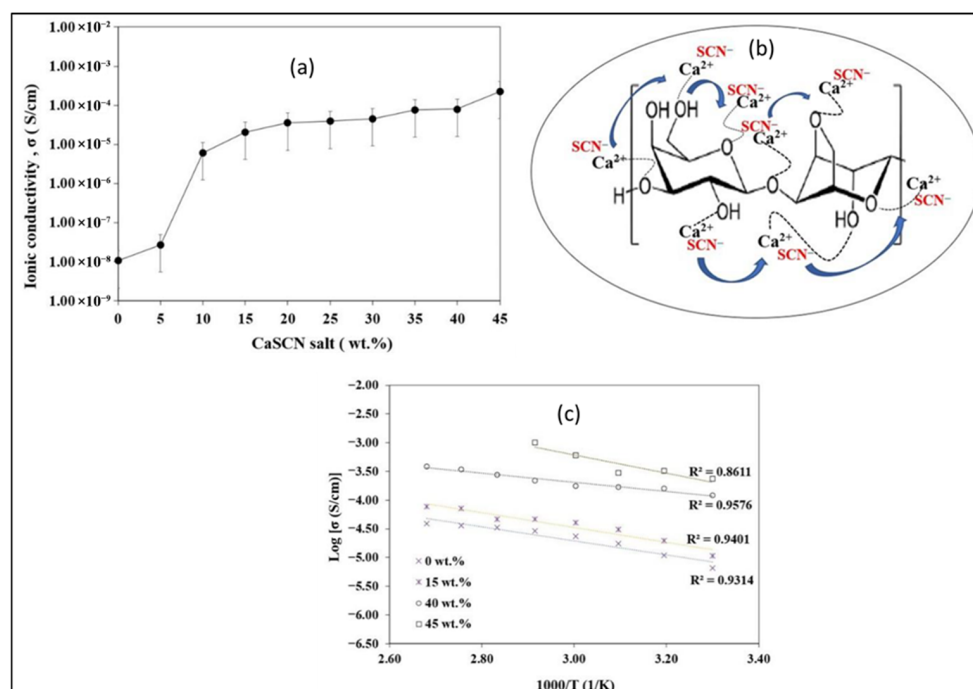


Figure 4. (a) Ionic conductivity of various concentrations of CaSCN salt at ambient temperature; (b) hopping mechanism of Ca^{2+} in CaSCN–agarose biopolymer electrolytes; (c) temperature dependency curves of different concentrations of CaSCN–agarose biopolymer electrolytes (reproduced with permission) [60].

3.3. Mechanical and Thermal Stability

Agar materials have good mechanical strength and thermal stability for energy storage applications. Agar gels are mechanically strong relative to most other biopolymer gels—agarose gels (at a few % concentration) are strong gels (maximum gel strength $> 800 \text{ g/cm}^2$) and can resist stress-induced structural damage [61,62]. This mechanical stability is essential when agar is used as a binder or membrane, since it needs to resist swelling and changes in electrode volume as well as handling. It possesses a thick network of double-helical junction regions in the agar gel, which endows it with rigidity under deformation. The mechanical toughness of agarose has also led to its implementation in the scaffold of flexible electronics [47]. Agar gels are thermostable between their melting and gelation points across a broad temperature range. As observed, agar gel remains solid up to approximately 85°C , which spans the operating temperatures of batteries and fuel cells (typically 60°C). This thermal gel stability prevents premature liquefaction or flow of agar-based electrolytes or binders under moderate heating [63,64].

Although it is a polymer, the backbone of agar is also resistant to relatively high temperatures, even in dry form. Thermogravimetric analysis reveals that dry agar (in composite gels) decomposes significantly only at about 250°C , once all the water has evaporated. This thermal strength is competitive with that of synthetic polymer binders (e.g., PVDF decomposition starts at about 300°C) and suggests that agar can withstand the heat of cell assembly (e.g., drying, solvent removal) and operation [65]. Another stability feature is the capacity of agar to retain water. Because its gels already contain high levels of water, they retain moisture through extensive hydrogen bonding [66]. In a fuel cell scenario, this is advantageous—the agar hydrogel binder maintains the electrode wet, promoting ion conduction—whereas a conventional binder would dry out. Nevertheless, it is important to control water activity: excessive drying of an agar electrolyte may lead to shrinkage and loss of conductivity, whereas excessive heat may melt the gel [65,67].

Zhang et al. reported the shear rheology of agar, PVA, and PVA–agar double networks (Figure 5a–c). In amplitude sweeps (Figure 5a), agar shows a high linear viscoelastic region modulus around 49 kPa but a low yield strain near 5%, indicating brittleness. PVA cryogels have lower modulus, higher yield strain, and the highest-molecular-weight sample shows clear strain hardening. Double networks combine strength and ductility, with moduli around 5.7, 11.7, and 14.1 kPa (for 61, 145, and 195 kg mol^{-1}) and yield strains near 26% and 86% (61 and 195 kg mol^{-1}). Frequency sweeps (Figure 5b) show weak frequency dependence, consistent with permanent-like networks in the tested window. Flow tests (Figure 5c) show shear-thinning for agar and PVA; double networks exhibit a nonmonotonic viscosity trend, and the 145 kg mol^{-1} PVA–agar sample reaches the instrument torque limit [68]. In general, agar has a combination of mechanical rigidity and thermal endurance that allows it to be used in composite electrodes and solid-state electrolyte membranes, and its safety profile (non-flammable, with no toxic degradation materials) is better than that of most traditional materials.

3.4. Role as Matrix or Binder in Composite Electrodes

Agar may also be used as a matrix or binder in composite electrodes (including batteries, supercapacitors, fuel cells, etc.) to bind together active materials, conductive additives, and current collectors. The role is similar to PVDF in Li-ion batteries or Nafion in certain fuel cells, but agar has specific advantages in terms of sustainability and performance. Research has demonstrated that agar-based binders have the potential to maintain electrode cohesion and interparticle contact intact throughout cycling. As an example, Tang et al. used a chemically modified agar (oxidized to expose carboxyl groups) as a water-soluble binder for lithium–sulfur battery cathodes [69]. The agar binder maintained close contact

between sulfur and carbon black and the aluminum current collector, and its polar functional groups immobilized lithium polysulfides, inhibiting the shuttle effect. This led to a Li-S electrode with an initial discharge capacity of approximately 700 mAh g^{-1} , and high capacity retention of 90.7% after 100 cycles, which is much higher than that of the traditional PVDF-bound electrode [69]. This demonstrates the stability of the agar binder for electrode structure and chemistry during repeat charging/discharging. Similarly, agar binders have been promising in Zn-based batteries. An alkaline Zn-air battery anode with an agar binder outperformed a binder-free electrode in mechanical integrity and cycle life, as agar inhibited active-material shedding in the very alkaline KOH environment [65]. A crosslinked agar hydrogel binder was used to replace the Nafion ionomer in the catalyst layer in fuel cells. The electrode bound with ACH had a higher peak power density compared to the one bound with Nafion, due to agar's hydrophilic, water-retaining character, which facilitates mass and charge transport [65]. It is worth noting that the water-processability of agar enables electrode fabrication with benign solvents (replacing NMP with water), which makes the process easier to manufacture and less harmful to the environment. When incorporated and dried on the electrode, agar is not involved in side reactions (electrochemically inert) and is therefore stable during cell operation [69]. Its excellent adhesive and film-forming qualities make it possible to tolerate even high-volume-change materials (such as Si anodes or conversion-type cathodes) better, since the binder can gel and reharden to accommodate strain. Overall, agar represents a useful binder matrix that not only holds the composite electrode together but also has added advantages of entrapping deleterious species (e.g., polysulfides) and enhancing ionic percolation within the electrode.

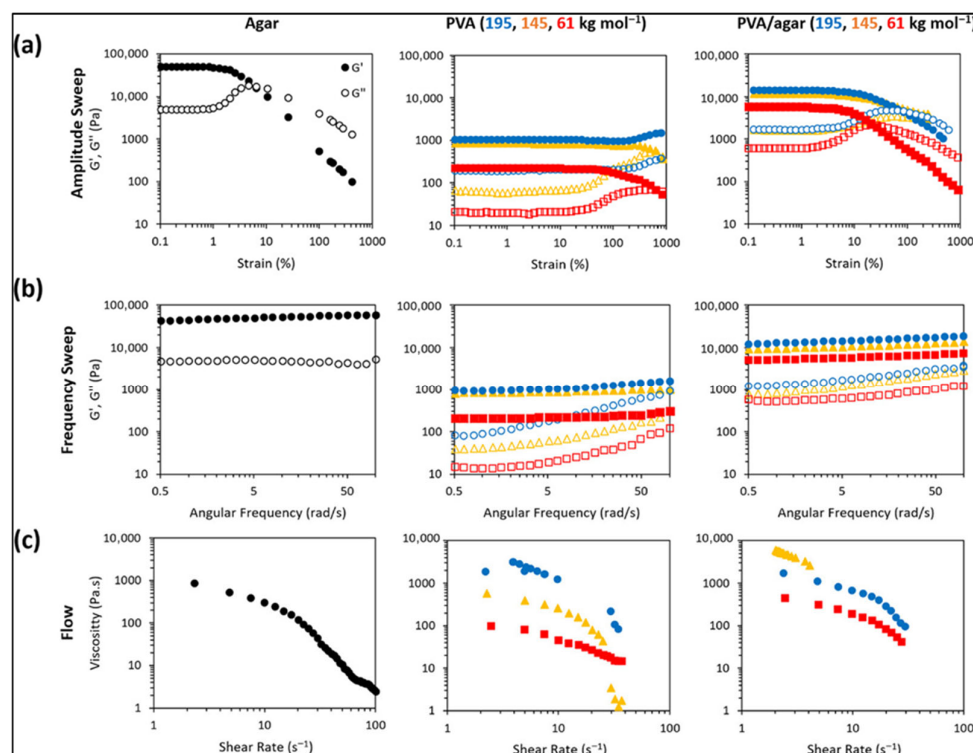


Figure 5. Rheological evaluation of agar, PVA, and PVA/agar double-network (DN) hydrogels, including (a) amplitude sweeps, (b) frequency sweeps, and (c) flow rheology (reproduced with permission) [68].

3.5. Synergistic Effects with Conducting Constituents

The applications of agar in energy storage are mostly in composite form, wherein the agar acts synergistically with conductive carbons and metal oxides to form functional

hybrids. Agarose is a gel-forming polymer and thus is able to evenly disperse filler materials to enhance the structural homogeneity of the composite. In the case of carbon materials, agar establishes a complementary relationship: the agar network offers mechanical strength and ionic transport, and carbon (e.g., activated carbon, carbon nanotubes, graphene) offers conductivity [3,65]. Agarose-based soft electrodes have recently been developed in which high-surface-area carbon is incorporated into an agarose hydrogel matrix. Kim et al. prepared an agarose–spherical activated carbon (agar/SAC) gel, which could be cast in different shapes (films, fibers, and 3D structures) and had similar electrical properties [47]. Agar forms a reversible gel, allowing the molding and even recycling of these electrodes, and the carbon content gave them conductivities in the 10^{-4} –100 S/cm range. These composites benefit from hydrogel–carbon interactions: agarose chains can cover and separate carbon nanoparticles to avoid agglomeration and expose the large surface area of nano-carbons to store charge. Additionally, the wetting of carbon surfaces by electrolytes can be enhanced by the moisture in agar. It has also been demonstrated that carbon–agarose gels can be made conductive by the addition of conducting polymers (e.g., polyaniline, PEDOT), and that conductivity and pseudocapacitance can be increased further, suggesting the versatility of agarose as a host matrix [47,70].

Agar in combination with metal oxides has the potential to enhance the performance and stability of electrodes in a variety of ways. One particular example is the use of an ultrathin film of agar (sometimes called an agar microskin) on MnO_2 cathode particles to make Zn-ion batteries. This wetted agar layer was observed to have a positive effect on electrode wettability (to help diffusion of Zn^{2+} ions) and also serve as a physical barrier that reduced dissolution of manganese in the electrolyte [71]. The agar-covered MnO_2 cathode had a significantly higher discharge capacity ($\sim 240 \text{ mAh g}^{-1}$ at 0.5 A g^{-1}) than the bare cathode (160 mAh g^{-1}) and it maintained 85.6% of its capacity after 500 cycles, whereas the non-protected one maintained only 51%. This dramatic change can be attributed to the properties of agar in preserving the structural integrity of the α - MnO_2 framework during the cycling process by avoiding excessive contact with the electrolyte and compensating for the change in volume [71]. As a rule, in the case of agar as a binder or a matrix to hold metal-oxide-based electrodes (e.g., Fe_3O_4 , TiO_2 , MnO_2 , etc.), the agar allows strain accommodation and prevents the pulverization of particles because of its cushioning effect as a gel. It also provides functional groups to interact with the surface, and this may help in increasing electron transfer at the particle–binder interface. In dye solar cells and supercapacitors, for example, agar-based gels doped with metal oxides (TiO_2 , Co_3O_4) had higher ionic conductivity and superior dispersion of the oxide than the oxide in a dry polymer [57,72,73]. As a result, agar is effective as a small additive (coating) or a bulk material (bulk matrix) with inorganic materials to benefit from the film-forming, ion-conducting, and flexible characteristics of agar combined with electrical or faradaic characteristics of conducting additives. This synergy enables the design of next-generation composite electrodes that are high performance and derived from sustainable materials.

Despite these advantages, research on agar used as an electrochemical material remains, compared to other polymers, at a very immature level. Therefore, there are several aspects of future work to pursue in order to achieve the maximum value of agar. For example, chemical modification of agar/agarose has been demonstrated to be a viable means of controlling the solubility and behavior of the compound—oxidized agar has been shown to improve polysulfide binding in Li-S batteries, and crosslinked agar has been shown to improve stability in fuel cells. These modifications may improve the ease of use of agar in non-aqueous media and/or its ionic conductivity. In addition, a more fundamental characterization of ion transport in agar networks and predictive modeling would be desirable for the design of agar electrolytes with predetermined pore structures

or ionic liquids that have broad electrochemical stability ranges. In addition to this, more practical aspects of the matter should also be considered—for example, how an agar-based component breaks down after cell disassembly, and whether this can simply be repurposed to rerecycle batteries in an environmentally friendly way.

4. Agar vs. Other Biopolymers in Energy Storage Applications

Compared with other bio-based polymers used in energy storage, agarose offers a uniquely advantageous balance of ionic transport, mechanical integrity, processing simplicity, and interfacial compatibility that makes it particularly promising for supercapacitors and batteries. First, agar forms robust, water-gelled networks at low polymer loadings, so its quasi-solid electrolytes can approach liquid-like ionic conductivities while tightly retaining solvent, reducing leakage and self-discharge [74,75]. Cellulose matrices, by contrast, typically need derivatization (e.g., CMC) or plasticizers to reach comparable conductivities, trading off mechanical strength or adding processing steps; nanocellulose separators are mechanically excellent but require a separate gel/electrolyte infusion to conduct ions efficiently [76,77]. Chitosan can form proton-conductive films, yet it relies on acidic dissolution and often becomes brittle without plasticizers, limiting durability under repeated bending [78]. Alginate gels readily via Ca^{2+} crosslinking, but those ionic bridges are environmentally sensitive (ion exchange, pH, humidity), and carboxylate coordination can immobilize multivalent charge carriers, depressing net ion mobility [79–81]. Second, agar's hydrogen-bonded double-helix network produces self-standing, flexible films with tunable porosity and thickness by simple aqueous casting, enabling leak-free, bend-tolerant gel electrolytes and separators [82,83]; chitosan and cellulose often require harsher solvents or complex regeneration routes, while alginate's performance can drift as crosslinkers redistribute. Third, agar's abundant hydroxyl and ether groups provide a neutral yet sticky surface chemistry that binds well to both organic (conducting polymers such as PANI/PPy) and inorganic additives (carbon blacks, graphene, CNTs, metal oxides), promoting uniform dispersion and strong electrode–binder adhesion; chitosan's cationic amines can interact too strongly with anionic species, complicating electrochemistry, and alginate's carboxylates can sequester active cations, whereas cellulose's relatively inert backbone may require extra functionalization to achieve comparable interfaces [84–86]. Next, agar gels exhibit broad thermal and electrochemical stability: they resist drying-induced cracking, reduce solvent evaporation, and help extend the usable voltage of aqueous devices by maintaining a sealed microenvironment; cellulose and chitosan films are heat-stable as solids but can undergo phase or chemical changes in alkaline or highly oxidative regimes, and alginate networks soften as crosslink ions are displaced. In practical architectures, agar has proven effective as a gel electrolyte for flexible supercapacitors (stable capacitance under bending/twisting), as a green binder for high-expansion anodes (improved adhesion and cycling vs. conventional binders), and as a dendrite-suppressing host for aqueous metal-ion batteries (smooth plating/stripping and wide operating temperatures) [17,31,86,87]. Taken together, high ionic flux at low polymer fraction, simple and benign processing, resilient mechanics, and additive-agnostic interfacial chemistry are traits that consistently position agar ahead of cellulose, chitosan, and alginate for next-generation, flexible, and sustainable energy storage devices.

5. Agar-Based Composites

Agar-based composites represent a paradigm shift from native agar, transcending its inherent limitations by integrating diverse functional particles to achieve multidimensional enhancements. Unlike native agar, which exhibits modest thermal stability, mechanical fragility, and limited electrical conductivity, composites reinforced with metallic nanoparticles (e.g., Fe, Ag, Cu) or carbon derivatives (graphene, carbon nanotubes) demonstrate

remarkable thermal resilience, withstanding high-temperature environments in battery systems or catalytic processes [3,14]. The incorporation of fillers like graphene oxide (GO) or reduced graphene oxide (rGO) introduces exceptional mechanical strength, transforming brittle agar into flexible, fracture-resistant films ideal for bendable supercapacitors [88–90]. Electrically insulating native agar gains conductive pathways through additives such as silver nanowires or polyaniline, enabling efficient charge transport in electrodes. Additionally, hybridizing agar with polymers (e.g., chitosan, PVA, etc.) or silica nanoparticles enhances hydrophobicity and structural integrity without compromising its biodegradability. These composites also retain agar's eco-friendly essence while addressing critical challenges like swelling in aqueous electrolytes or cycle instability in energy devices [91–93]. By synergizing agar's natural versatility with advanced nanomaterials, these composites redefine performance benchmarks, offering tailored solutions for thermal management, mechanical durability, electrochemical activity, and environmental sustainability in energy storage technologies.

The addition of various additives to agar-based polymeric matrices yields positive outcomes, as demonstrated through systematic physicochemical and thermal characterization techniques. Kumar et al. [94] demonstrated that native agar behaves very differently from its composites, as shown through FTIR spectroscopy and thermogravimetry studies (see Figure 6a,b). The native agar film exhibited peaks corresponding to $-NH_2$, $-OH$, $-CH_3$, and $C=O$ groups. However, these peak intensities were reduced in the agar–ZnOPs composite films, suggesting a transformation of native agar into a different form within the composite, without major structural changes. Thermogravimetric analysis further highlighted the distinct behavior between native agar and its composites (see Figure 6b). The composite films showed higher thermal stability, with a shift in maximum weight loss from 225 °C in the composites, indicating enhanced stability due to the incorporation of ZnONPs. This enhanced thermal stability is consistent with moisture removal, degradation of glycerol, and removal of organic groups.

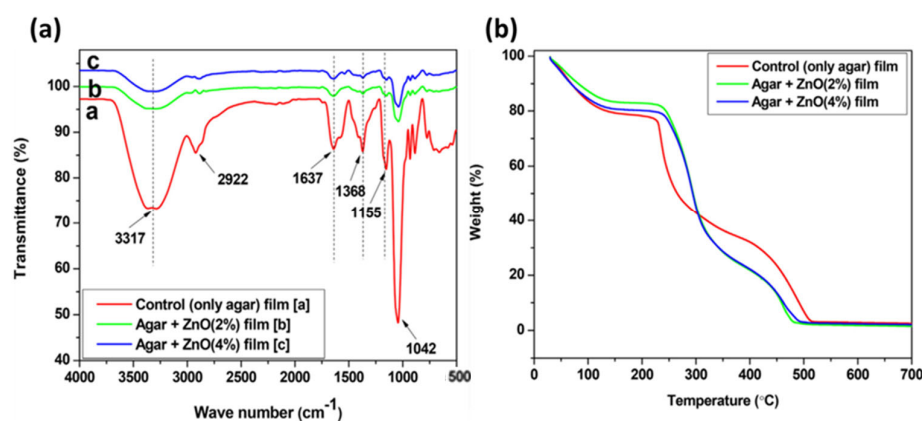


Figure 6. (a) FTIR spectra of agar, and agar/ZnO composite films; (b) TGA profile of agar, and agar/ZnO composite films (reproduced with permission) [94].

5.1. Types of Agar-Based Composites

Agar-based composites are formed through the dynamic binding forces between the polysaccharide matrix of agar and various reinforcing materials, including metallic nanoparticles, carbon derivatives, and polymers (see Figure 7) [3]. The agar network, characterized by numerous hydroxyl groups, facilitates the formation of hydrogen bonds and contributes to the uniform stabilization of reinforcing components within the structure. The combination of these composites yields enhanced properties, wherein metallic nanomaterials augment electrical conductivity and antimicrobial functionality, while carbon-based additives enhance mechanical properties and thermal stability [95,96]. Addi-

tionally, polymers like chitosan [97,98] or synthetic elastomers [99,100] contribute flexibility and stimuli-responsive characteristics. The structural combination of agar preserves its biodegradability while incorporating the additional features of secondary materials into unified hybrid units. Such hybrid materials are utilized in antibacterial wound dressings for medical applications, stretchable conductive sensors, and sustainable, degradable packaging. The molecular structure of these materials enables them to combine with other elements for improved macroscopic properties in environmental and biomedical research.

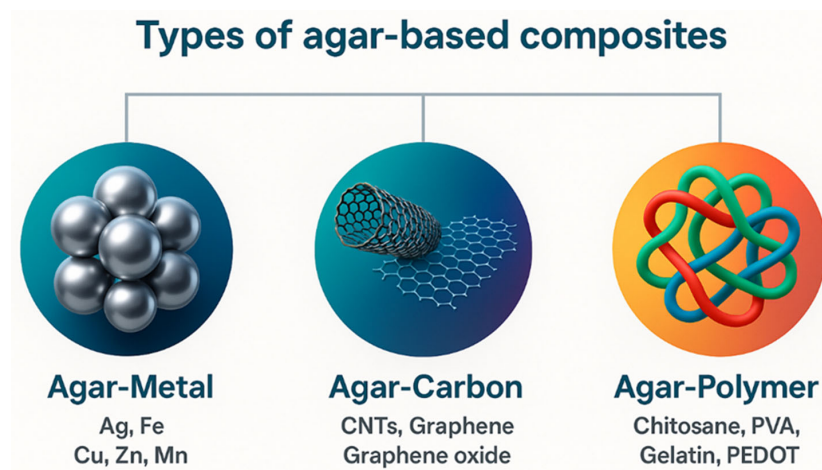


Figure 7. Various types of agar-based composites.

5.1.1.1. Agar–Polymer Composites

Innovative applications are made possible by agar’s wide compatibility with polymers, including PVA [101], butylene adipate [102], chitosan [97], gelatin [103], starch [104], and polyethylene glycol [105–108]. Agar’s idiosyncratic nature enables researchers to craft cutting-edge composites that revolutionize sustainable synthetic methods, biodegradable films, electroactive scaffolds, and environmentally friendly applications. Various agar–polymer hybrids are shown in Figure 8.

Agar serves as a strong structural matrix for numerous conducting polymers, e.g., PANI, PEDOT, PPy, etc., for improved electromechanical behavior. The intrinsic biodegradability of agar and the adjustable conductivity of conductive polymers are the main advantages that distinguish these hybrids [27,109–113]. When combined, they offer a highly flexible and environmentally benign framework for creating cutting-edge energy storage materials that are suited to particular performance requirements. These composites, which combine the sustainability of agar with the capabilities of conductive polymers, open the door to creative, high-performing energy storage solutions that are both technologically and environmentally sophisticated [70,114].

Kang et al. examined the application of κ -carrageenan–agar (κ C-Agar) composite materials as biodegradable elements in triboelectric nanogenerators (TENGs). The research demonstrates that a composite material with an optimal concentration exhibits a 57.5% enhancement in electron-donating properties, attributed to improved charge trapping enabled by Ca^{2+} cations and sulfate ester groups. The material exhibited enhanced biocompatibility, as indicated by positive MTT assay results and diminished inflammation in subdermal assessments, due to its hydrophilic properties. A thin, flexible TENG was developed, demonstrating significant output and highlighting the potential of κ C-Agar composites for self-powered transient electronics [115]. Lin et al. synthesized quaternary polysaccharide gels utilizing konjac glucomannan (KGM), xanthan gum, κ -carrageenan, and agar, achieving optimal springiness and thermal stability at their ideal composition. The gels demonstrated pseudoplastic properties and enhanced solid-like behavior at higher

temperatures, rendering them suitable for practical applications [116]. Qiao et al. investigated ternary systems comprising agar, KGM, and κ -carrageenan, revealing that κ -carrageenan concentrations below 25% increased both the sol–gel transition temperature and gel hardness. Ternary composites demonstrated superior performance compared to binary agar/KGM composites in terms of stable mechanical properties and hydrophilicity across varying relative humidity levels, indicating their potential for diverse applications with improved material characteristics [117]. Shakya et al. demonstrated that the addition of TEMPO-oxidized bacterial cellulose to agar matrices enhanced the hemostatic and mechanical properties of the resulting agar and oxidized bacterial cellulose composite cryogels. The cryogels exhibited a rapid blood-clotting capability of 90 s *in vitro*, comparable to the performance of commercial products Axiostat and Surgispon [118]. In another study, the development of environmentally friendly nanocomposite fibers through dry-jet wet spinning involved all-biomass agar and cellulose nanocrystals. The developed fibers improved mechanical stability while demonstrating rapid methylene blue (MB) adsorption, which implies their potential to reduce water pollution from plastic wastes. The study illustrates how sustainable materials present a solution to environmental issues that appear when fiber-based commodities become waste products [119]. Manna et al. synthesized Fe(III)-crosslinked cellulose–agar beads via sol–gel methods for phosphate removal in water. The optimal conditions facilitated the beads' adsorption of 94% of phosphate, achieving a maximum adsorption capacity of 73.13 mg/g at pH 5. The adsorbents demonstrated stable performance, retaining 42% of their initial removal capacity over six adsorption–desorption cycles utilizing sodium chloride as the desorption agent. This study shows that hydrogel beads are effective in water purification systems [120].

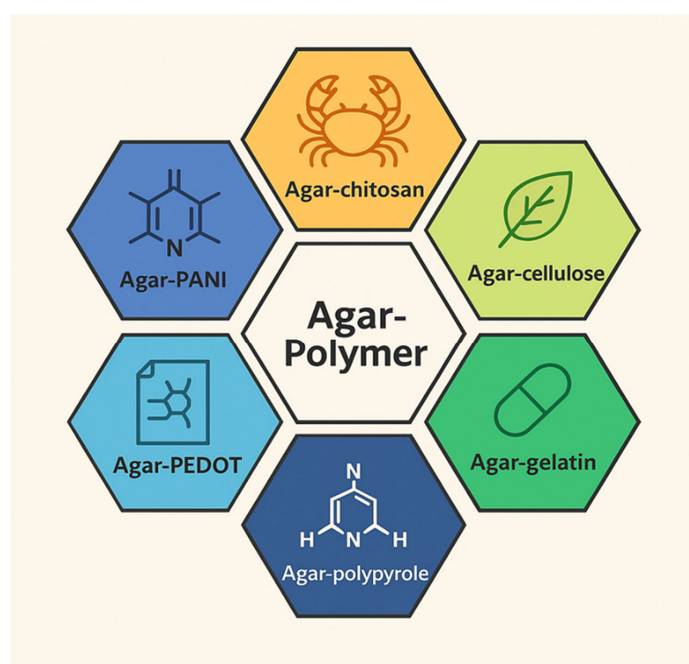


Figure 8. Various types of agar–polymer hybrids.

Namasivayam et al. synthesized biocomposites using starch, gum acacia, agar, chitosan, and PVA via environmentally friendly methods. The chitosan–starch–gum acacia biocomposite demonstrated significant herbicidal effects, resulting in necrotic lesions that expanded from 6 h to a maximum size of 30.0 mm. These biocomposites released herbicidal metabolites in controlled patterns under *in vitro* and in soil conditions, preserving soil health and promoting plant growth without toxic effects, thereby demonstrating their

agricultural potential [91]. Safarimehr et al. developed a triple-layer intelligent film composed of chitosan, gelatin, and agar, incorporating 4% *w/v* roselle anthocyanin extract for monitoring the freshness of red snapper fish. The film demonstrated pH-sensitive color changes from dark red to pale red with greenish hues, indicating spoilage when volatile basic nitrogen levels in fish surpassed safety thresholds over a 7-day storage period at 4 °C [121]. Safarimehr et al. synthesized Fe₃O₄ microspheres coated with chitosan and agarose, subsequently immobilizing palladium nanoparticles to generate Fe₃O₄ MPs@CS-agar/Pd NPs, which exhibited efficacy in Suzuki–Miyaura reactions. The nanocatalyst demonstrated durability due to its nanostructured characteristics, allowing up to eight consecutive applications without a decline in activity [122]. Table 1 shows various types of agar–polymer hybrids and their applications in energy storage devices.

Table 1. Different types of agar–polymer composites, their methods of synthesis, properties, and applications in energy storage devices.

Composite	Polymer Type	Synthesis	Properties	Application in Energy Storage	Ref.
PVA/agar/PANI/PPy composite	PVA, PANI, PPy	Chemical crosslinking and in situ polymerization	Flexible; high areal capacitance (750.13 mF/cm ²); high energy density (103.02 μWh/cm ²); excellent cyclic stability (149% retention after 15,000 cycles)	All-in-one, lamination-free, flexible supercapacitors	[27]
PVA–agar hydrogel (PAGH) crosslinked with copper-doped carbon dots	PVA	Crosslinking with copper-doped carbon dots	Ca ²⁺ recognition; fluorescence and electrical response; non-cytotoxic; bactericidal; flexible; biocompatible; ionic conductivity	Wearable biosensors for calcium ion monitoring in sweat	[123]
PVA/HPMC/agar hydrogel	PVA, HPMC, methyl cellulose,	Utilizes citric acid as a crosslinking agent in lieu of conventional PVA crosslinkers to promote polymerization of hydrogel	Mechanical property: 1.77 MPa; elongation at break: 766%; good recovery, fatigue resistance, and adhesion	Flexible hydrogel sensors capable of detecting mechanical strain and environmental changes (temperature and humidity)	[124]
PVA–CMC–SiO ₂ –Cr ₂ O ₃ NCs	PVA, CMC	Solution-casting technique with varying concentrations of SiO ₂ and Cr ₂ O ₃ nanoparticles	Uniform morphology; amorphous structure; improved optical characteristics; enhanced antimicrobial efficacy	Optoelectronic nanodevices	[125]
PVA/agar/GO–EMIMBF ₄ –Li ₂ SO ₄	PVA, graphene nanosheets	Freeze–thaw cycles	High specific capacitance (130 F g ^{−1}); excellent ion conductivity (39.2 mS cm ^{−1}); outstanding self-healing; wide temperature range (−30–80 °C); long cycle life	Wearable supercapacitors for energy storage devices	[126]
PVA/agar–EMIMBF ₄ –Li ₂ SO ₄	PVA, ionic liquids	One-pot physical crosslinking; freeze–thaw cycles	Better tensile properties; excellent flexibility; temperature tolerance (−30 °C to 80 °C); high self-healing efficiency	Flexible supercapacitors for energy storage devices	[127]
PVA/agar hydrogel electrolytes	PVA	Chemically crosslinked	Biodegradable; cost-effective; environmentally friendly	Electrolytes in supercapacitors	[27]
PANI/PPy electrodes	PANI, PPy	Binder-free growth on hydrogel	High areal capacitance; energy and power density; excellent cyclic stability	Electrolytes in supercapacitors	[27]
Combined PVA/agar with PANI/PPy	PVA, PANI, PPy	Fabrication on hydrogel base	Areal capacitance: 750.13 mF/cm ² ; energy density: 103.02 μWh/cm ² ; power density: 497.22 μW/cm ² ; 149% capacity retention after 15,000 cycles	High-performance flexible energy storage devices	[27]
Solid-state Ag/AgCl reference electrode	PVA, polydimethylsiloxane (PDMS)	Modified with KCl–agar–PVA gel and PDMS liquid-junction layer	Low sensitivity to chloride; excellent potential stability; minimal drift; reliable electrochemical performance	pH sensing in culture-substrate online detection	[128]

5.1.2. Agar–Metal Composites

Due to nano-metals' unique functional properties and agar's biocompatibility, composites of metals and agar have many innovative applications. Silver's significant antimicrobial effects are used in wound dressings and antibacterial coatings [129–132], and zeolite–agar hybrids break down contaminants and absorb heavy metals in environmental cleanup due to iron's magnetic characteristics [131,133,134]. Agar–magnetic composites have versatile applications in biomedical, environmental, and electrical fields [13,14]. The customizable porosity and environmentally friendly degradability of these composites make them suitable for healthcare and packaging applications. Eco-friendly agar and multi-purpose metals create sustainable materials with significant technological potential for biomedical, environmental, and industrial uses. Figure 9 shows various agar–metal functional hybrid composites.

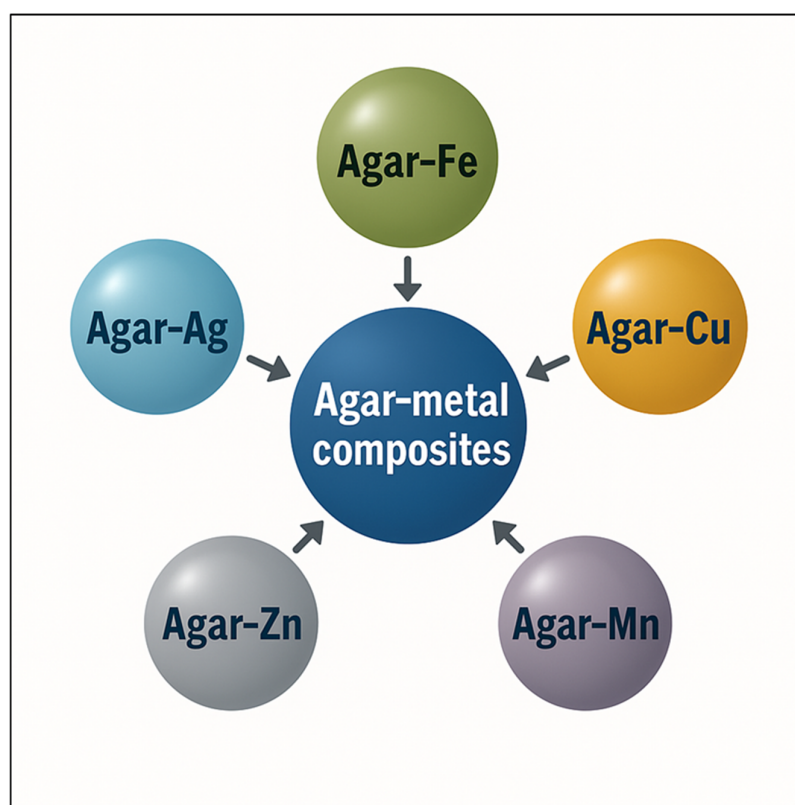


Figure 9. Different types of agar–metal composites.

Magesh et al. developed ZnO nanoparticles using agar biopolymer, which influenced their morphology and optical properties. The study demonstrated that agar/ZnO nanocomposites exhibit antibacterial activity against Gram-positive and Gram-negative bacteria and show dose-dependent cytotoxicity in normal and cancer cell lines [135]. Roy et al. developed a pectin/agar-based composite film enhanced with zinc sulfide nanoparticles, which improved the film's mechanical strength and UV protection. The film maintained its transparency and original properties, showing strong antibacterial activity against *E. coli* and *L. monocytogenes*, suggesting potential for active packaging applications [136]. Hu et al. developed a biosafe composite hydrogel (MSG-Zn²⁺) by crosslinking sodium alginate and agar with Ti3C2Tx MXene and zinc ions for wound-dressing applications. This hydrogel combines the photothermal properties of MXene and the antimicrobial activity of zinc, offering effective photothermal and chemical antibacterial therapies. It demonstrated broad-spectrum antibacterial effects against both

Gram-positive *Staphylococcus aureus* and Gram-negative *Escherichia coli*, with excellent biocompatibility and enhanced cell migration, indicating its potential as an economical and efficient wound dressing [137].

Agar–silver composites not only revolutionize biomedical and environmental research but also hold promising potential in enhancing energy storage technologies. Rhim et al. prepared composite films using silver nanoparticles (AgNPs) and agar, where the AgNPs were synthesized through an environmentally friendly reduction method involving trisodium citrate and heating. These films showed enhanced water-vapor barrier properties and increased surface hydrophobicity with higher AgNP concentrations while maintaining mechanical strength. Films with more than 1 wt% AgNPs demonstrated strong antimicrobial activity against both Gram-positive (*Listeria monocytogenes*) and Gram-negative (*Escherichia coli* O157:H7) bacteria [138]. Ghosh et al. developed highly stable Ag/agar films that demonstrated strong and sustainable antimicrobial effects against *E. coli*, *S. aureus*, and particularly *C. albicans*, with retained mechanical strength even after multiple use cycles [139]. Mostafa et al. developed an agar–carboxymethylcellulose–AgNP nanocomposite, which demonstrated a high adsorption capacity for MB dye. The adsorption process conformed to the Langmuir isotherm and pseudo-second-order kinetics, indicating its potential as a reusable biosorbent, although its efficacy decreased after multiple cycles [140].

Agar–iron-based composites, particularly those incorporating magnetic particles, are transforming diverse research fields with their versatile applications. For instance, Shah et al. synthesized highly intercalated magnetic composites using montmorillonite clay, agar, and magnetic iron oxide nanoparticles through a thermo-physicomechanical method. These composites demonstrated increased hydrophobicity and improved thermal stability, showing significant antibacterial activity against *Escherichia coli* and notable antioxidant properties, along with conductor-like electrical behavior [14]. Gautam et al. prepared agar-based aqueous suspensions with lignin magnetic nanocomposites using a pH-driven co-precipitation method. The study demonstrated that adding low concentrations of lignin-coated Fe_3O_4 nanoparticles to the suspension enhances thermal conductivity by up to 10% at 45 °C. Additionally, varying magnetic fields at room temperature initially increased the thermal conductivity, with a peak at 0.02 T, before decreasing at higher fields due to nanoparticle aggregation [141].

Gupta et al. demonstrated that using agar in a sol–gel synthesis technique enhances the structural and electrochemical properties of $\text{LiNi}_{0.8}\text{Co}_{0.1}\text{Mn}_{0.1}\text{O}_2/\text{C}$ cathodes for lithium-ion batteries. The agar-assisted method produced bi-pyramidal particles with a high specific discharge capacity of 182 mAh/g and improved capacity retention of 78% after 50 cycles. This approach resulted in lower charge-transfer resistance and better ion diffusion, significantly boosting cell efficiency compared to traditional methods [142]. Lu et al. developed olivine-structured $\text{LiMn}_{0.5}\text{Fe}_{0.5}\text{PO}_4$ cathode materials for energy storage applications. The optimal synthesis at 700 °C yielded cathodes with superior electrochemical performance, characterized by lower charge-transfer resistance and high capacity retention of 95% after 40 cycles at a C/3 rate. This method demonstrated that agar effectively facilitates the synthesis of phase-pure $\text{LiMn}_{0.5}\text{Fe}_{0.5}\text{PO}_4$, enhancing the structural and functional properties of the cathode material [143]. Table 2 indicates various agar-metal composites, synthesis and energy storage devices applications.

Table 2. Various agar–metal composites, their methods of synthesis, properties, and applications in energy storage devices.

Composite	Metal Type	Synthesis	Properties	Application in Energy Storage	Ref.
Agar–agar CoWO ₄	Co, W	Proteic sol–gel	Particle size: 284 nm; crystallite size: 84 nm; paramagnetic behavior; magnetic moment: 4.926 μ B	Used as electrodes in batteries for high-capacity energy storage in alkaline media	[144]
Agar–agar and LiCl electrolyte	Li	Solution-casting technique	Highly amorphous nature; low glass transition temperature (37 °C); high ionic conductivity (3.12×10^{-2} S/cm); good thermal and cyclic stability	Solid-state primary and secondary Li-ion batteries	[145]
Agar-based gel polysulfide electrolyte	Cd, Ti	Electrophoretic deposition	Conductivity comparable to liquid electrolytes; high wettability and permeation into TiO ₂ films	Enhanced performance and stability in solar cells	[146]
Agar-loaded felts	V	Agar-solution treatment on felts	Increased hydrophilicity; good catalytic activity for V ⁴⁺ /V ⁵⁺ and V ²⁺ /V ³⁺ redox couples; enhanced oxygen-functional groups on fibers	Electrode material in all-vanadium redox flow batteries for improved energy efficiency and discharge capacity retention	[147]
Agarose-based GPE	Zn	One-pot encapsulation of KOH in agarose	High ionic conductivity (0.45 S cm ^{−1}); excellent water retention; reduced zinc corrosion; high zinc utilization; good cyclability	Gel-polymer electrolytes in Zn-air batteries for stationary applications	[45]
LiMn _{0.5} Fe _{0.5} PO ₄	Li, Mn, Fe	Agar-assisted sol–gel	Orthorhombic structure; reduced calcination temperature; enhanced particle size control; lower charge-transfer resistance	Cathode material for lithium-ion batteries	[143]
Sulfidated mZVI	Fe	Milling mZVI with elemental sulfur at 0.05 S/Fe molar ratio for 10 h	Improved stability in 2.0 g/L agar solution; decreased capacity and reaction kinetics for chromate reduction when coated with agar	Groundwater remediation for chromate reduction	[148]
Agar-coated MnO ₂ electrode	Mn	Agar as a microskin coating	Improved wettability; enhanced diffusion rate of Zn ²⁺ ; reduced interface impedance; increased reversibility of MnO ₂ /Mn ²⁺	Enhanced cycle life and stability in Zn/MnO ₂ batteries	[71]
High-strength agarose gel electrolyte	Al	Quasi-solid electrolyte interface	Extended discharge duration (20.1 h); high specific capacity (2148.5 mAh g ^{−1} , 2766.9 Wh kg ^{−1})	Driving LED arrays and smartphones in wearable applications	[149]
Agarose/PVA gel-polymer electrolyte	Li	-	Specific capacitance: 697.22 mF cm ^{−2} at 5 mA cm ^{−2} ; enhanced diffusion coefficient for Li ⁺	High-performance solid-state supercapacitors	[150]
Fe–Ni–NC electrocatalyst	Fe, Ni		Enhanced ORR activity; methanol tolerance of 67.3%; Tafel slope: 93.24 mV dec ^{−1} ; low H ₂ O ₂ yield (3.31%); high electron transfer number	Electro-catalyst for DMFCs, particularly in oxygen-reduction reaction	[151]

5.1.3. Agar–Carbon Composites

Agar–carbon composites (see Figure 10) represent a significant advancement in the development of functional materials applicable to energy storage devices. These composites leverage the unique properties of agar and carbon-based materials, such as graphene, graphene oxide, and carbon nanotubes, by incorporating them into the agar matrix [152–157]. Agar provides two critical functions: it serves as a biocompatible scaffold that facilitates the distribution of carbon materials and enhances both electrical conductivity and structural strength. The electrochemical performance of composites is significantly enhanced due to graphene’s superior electrical conductivity and high surface area, rendering them suitable for applications in supercapacitors and batteries. The incorporation of carbon nanotubes in electrode design enhances structural integrity and electrical connectivity [158–162]. The synergy between agar and carbon materials enhances energy storage capability and cyclic reliability in devices, while also promoting flexible and environmentally sustainable designs for advanced energy systems as summarized in Table 3.

Next-generation energy storage technologies necessitate innovations that ensure high efficiency and environmental sustainability.

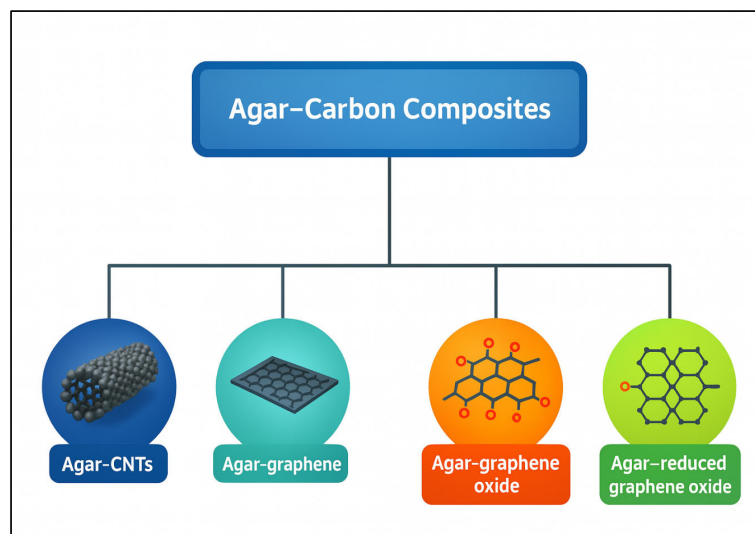


Figure 10. Various types of agar-carbon composites.

Yang et al. presented a double-network hydrogel electrolyte that functions as a component of a flexible zinc-air battery (FZAB), demonstrating significant ionic conductivity alongside robust mechanical stability. The hydrogel electrolyte comprises two networks: a rigid agar network and a secondary polyvinyl alcohol (PVA) network, achieving a power density of 123.7 mW/cm^2 , a stretchability of 246%, and a maximum tensile strength of 388 kPa. The electrolyte system enables FZABs to function effectively under various bending conditions, demonstrating significant potential for flexible energy storage applications [163]. Ji et al. developed biomass agar-derived N-doped porous carbon (NPC) at varying carbonization temperatures, optimizing the NPC-900 variant for sodium-ion batteries (SIBs). NPC-900 demonstrated a superior reversible capacity and excellent rate capability, achieving a high practical energy density of 267 Wh/kg when paired with a $\text{Na}_3\text{V}_2(\text{PO}_4)_3$ cathode, highlighting its potential for efficient sodium storage [164]. Chen et al. developed a three-dimensional agar/GO composite aerogel with a high MB adsorption capacity of 578 mg/g , showcasing endothermic and spontaneous adsorption kinetics. The aerogel maintained over 91% of its adsorption capacity after three recycling rounds, using a dilute NaOH solution for regeneration [10].

In another study, a novel triple-network hydrogel combining PVA, agar, and graphene nanoplatelets was developed through a one-pot, green solution-mixing method. This hydrogel exhibited high strength, toughness, and rapid self-healing within 10 min, making it suitable for various biomedical applications [165]. Belay et al. enhanced the mechanical properties and water resistance of agar by incorporating GO and reduced RGO, which increased the tensile strength by 118.4% and 69.4%, respectively, at 2% loading. The composite films showed improved hydrophobicity and resistance to swelling, although the tensile strength decreased at higher reinforcement concentrations due to pore formation [7]. De Araujo et al. developed nano-biocomposite hydrogel samples using GO and agar, which were effective in adsorbing cationic dyes Nile Blue A (NB) and MB from water, achieving maximum adsorption capacities of 284.69 mg/g for NB and 141.48 mg/g for MB. The hydrogels maintained consistent adsorption capacity through five cycles, demonstrating significant regenerative potential [166]. De Araujo et al. synthesized a hydrogel biocomposite using GO and agar biopolymer (agar-GO) for fixed-bed adsorption in textile wastewater treatment, showing high adsorption capacities for dyes like Nile Blue A, MB, Malachite

Green, and Basic Fuchsin. The biocomposite demonstrated eco-friendly attributes, effectively treating over 6 L of wastewater and displaying significant regenerative capacity, suitable for industrial applications [167]. In a recent study, a one-step gelation process produced an agar–GO hydrogel that demonstrated effective water treatment capabilities for the removal of chloroquine diphosphate and safranin O. Batch adsorption experiments showed significant binding properties for both contaminants. The Sips model ($R^2 > 0.98$) effectively represented the safranin O data, while the Freundlich model was appropriate for the chloroquine data. The presence of multiple contaminants in solution reduced the adsorption capacity of both pollutants by approximately 10 mg g^{-1} per molecule, yielding capacities of 41 mg g^{-1} for safranin O and 31 mg g^{-1} for chloroquine. The fixed-bed column assessment demonstrated effective removal of chloroquine at 63 mg g^{-1} , while safranin O achieved 100 mg g^{-1} , exhibiting excellent regeneration capabilities. The agar–GO biocomposite demonstrated its efficacy as an environmentally sustainable, reusable system for the effective dual elimination of pollutants in water purification applications [168]. Felipe Melo Lima Gomes et al. developed an agar–GO hydrogel to adsorb Cd(II) and Methyl Violet from water, demonstrating high adsorption capacities and effective fitting with the Sips model for isotherm data. The hydrogel showed excellent regeneration potential, maintaining strong adsorption performance through multiple adsorption–desorption cycles [169].

Tang et al. developed an environmentally friendly method to synthesize agar–rGO (ArGO), achieving controlled topological features and physical properties by varying water content. The resulting ArGO materials, ranging from water-stable dehydrated films to highly swellable hydrogels, exhibited enhanced mechanical strength and chemical stability, promising for applications in water purification and tissue engineering [170]. Belay et al. developed agar/rGO composites with enhanced tensile strength and thermal properties, showing a 55% increase in strength with just 2% rGO loading. These composites not only serve as biodegradable packaging materials but also have potential uses in supercapacitors and electric-field-induced wound healing [22]. Bagheri et al. optimized the electro-Fenton process using an agar-functionalized GO-immobilized copper ferrite aerogel to degrade MB in wastewater. They achieved 99.9% degradation under optimal conditions of 20 mg catalyst, 2 mL H_2O_2 , 40 °C, and pH 6, demonstrating the process's effectiveness through pseudo-second-order kinetics [171].

Table 3. Different types of agar-carbon composite their methods of synthesis and properties and applications in energy storage devices.

Composite	Carbon Type	Synthesis	Properties	Application in Energy Storage	Ref.
Agar-N-doped porous carbon	N-doped porous carbon	Sol–gel process followed by freeze-drying and activation with KHCO_3	Ultra-high SSA of $3184 \text{ m}^2/\text{g}$; hierarchical porous structure; specific capacitance of 443.0 F/g at 0.5 A/g in 6 M KOH ; excellent rate capability (255 F/g at 50 A/g)	Used in supercapacitors; achieved energy density of 35.5 Wh/kg with a capacitance retention of 99.7% after 20,000 cycles	[172]
Nitrogen-doped porous carbon (NPC-750), coupled with LiFePO_4 cathode	N-doped porous carbon	One-pot pyrolysis of agar at 750°C	High surface area ($2914 \text{ m}^2/\text{g}$); N content (2.84%); excellent capacity and cycle life; fast charging	Anode material for lithium-ion batteries	[173]
Water-soluble graphene (WSG)-incorporated agar gel-electrolyte	Graphene	-	Ionic conductivity: $8.62 \times 10^{-2} \text{ S cm}^{-1}$; OCV: 1.7–1.6 V; high discharge capacity ($1010.60 \text{ mAh g}^{-1}$); high energy density ($1406.09 \text{ mWh g}^{-1}$)	Electrolyte for magnesium–air batteries	[174]
Agar/graphene conductive organoge	Graphene	-	Excellent adhesion to various substrates; rapid self-healing via hydrogen bonding; wearable	Wearable electronic devices for motion and physiological activity detection	[175]
Agarose/GO	GO	-	Ionic conductivity 73.8 mS cm^{-1} ; specific capacitance ($791.67 \text{ mF cm}^{-2}$)	Solid-state supercapacitor	[176]

6. Fabrication Routes

Diverse methodologies enhance the inherent qualities of agar, rendering it more advantageous for environmental technology and medicinal science. The properties of agar-based composites in energy storage depend strongly on the chosen fabrication route. Electrospinning can produce agar/PVA nanofiber mats with extremely high porosity and surface area, enhancing ion diffusion and double-layer capacitance. However, pure agar gels are not directly spinnable (hence PVA blends are required), which complicates uniform fiber formation and scale-up [101]. Solvent casting is simpler: cast agar gels or films (used as electrolytes or binders) are mechanically robust and can exhibit broad voltage-stability windows. For example, a solvent-cast agar/ Na_2SO_4 gel showed an expanded electrochemical window (1.8 V) and excellent flexibility [177]. Likewise, a cast agar-PAM electrolyte had high Zn^{2+} conductivity and enabled stable Zn plating/stripping from $-25\text{ }^\circ\text{C}$ to $50\text{ }^\circ\text{C}$. Casting is readily scalable (e.g., roll-to-roll film formation) but tends to yield dense gels, which may limit ionic mobility. Three-dimensional (3D) printing (e.g., direct ink writing) allows customized architectures [178], but agar's low viscosity and wide gelling range make precise printing difficult [179] (additives like alginate are usually needed). In summary, electrospun agar mats maximize surface area (raising capacitance) but require complex processing [101], whereas cast agar gels offer flexibility and wide voltage windows [50]. Three-dimensional-printed agar structures provide design flexibility but currently face rheological and throughput limitations [178,179]. These fabrication choices directly affect device conductivity, capacitance, and structural integrity. Figure 11 represents various techniques for the fabrication of agar-based composites.

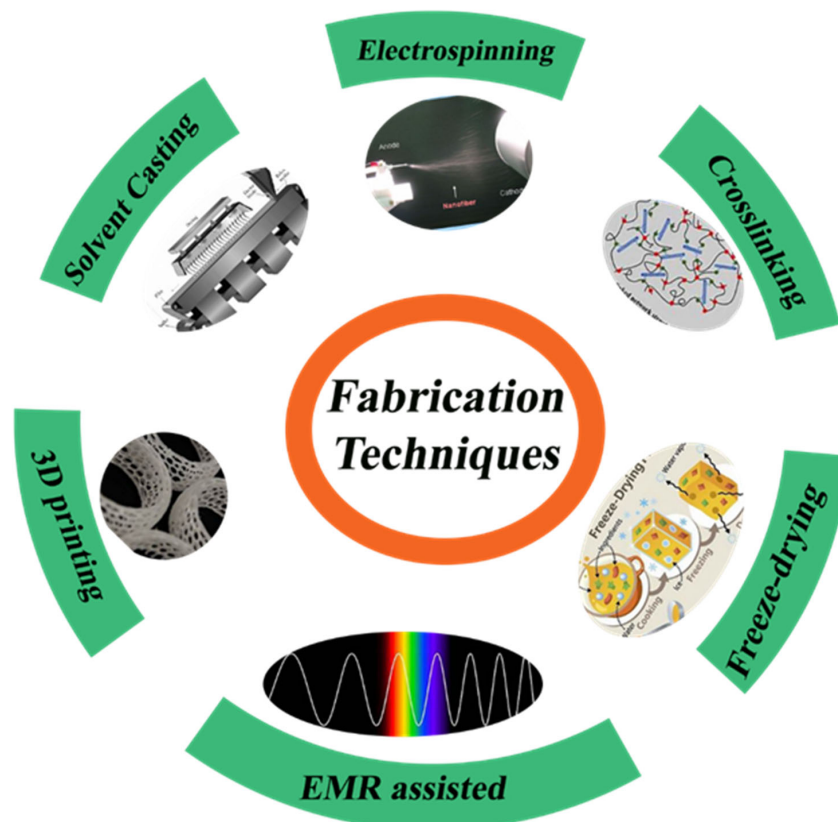


Figure 11. Various techniques for the synthesis of agar-based composites.

6.1. Solvent Casting

The solvent casting strategy is a cost-effective approach for producing thin films and membranes. This process involves dissolving polymers in suitable solutions, followed by

pouring or spreading the mixture into molds or onto flat surfaces, leading to the formation of dried solid polymer products. The fundamental manufacturing technique allows for the utilization of diverse polymers and additives, facilitating the production of smooth and uniform film surfaces. However, this method presents several drawbacks, as it necessitates careful management of volatile organic compounds that pose environmental and health risks. Additionally, it introduces challenges in maintaining solvent-free films, producing defect-free thicker materials, and requires precise drying processes for industrial-scale implementation [180–182].

Rhim et al. synthesized their films using solvent-casting methods, incorporating agar with silver nanoparticles (AgNPs), with agar serving as both the structural component and a protective nano-scale coating for the nanoparticles. The nanoparticles were produced using an environmentally friendly method employing trisodium citrate and heat to reduce AgNO_3 . Research efforts involved incorporating varying amounts of AgNPs into the agar solution during the preparation process. The presence of AgNPs within the films resulted in the generation of plasmonic colors. The films exhibited enhanced water-vapor-barrier properties and surface water resistance, while preserving structural integrity as AgNPs concentration increased [138]. Han et al. synthesized Agar/CMC films incorporating HAP nanoparticles by dissolving the components and subsequently employing a solvent-casting method. HAP nanoparticles were mixed into a uniform agar–CMC solution, resulting in the formation of films in molds through the solvent-casting process. The films retained their healing properties under suitable drying conditions, facilitating applications in bone repair [183]. Jayaram et al. extracted nanosized *Acalypha indica* (Ai) components from ethanol to develop wound treatments via solvent-casting methods. The solvent-casting technique facilitated the effective combination of herbal extract with guar gum and chitosan, while also incorporating PVA into the formulation. The study produced a medically effective and physically stable wound-dressing film, PBTFAi, utilizing a solution-casting technique [184]. The advancements in wound healing are attributed to the two-layered dressing developed by Rathore et al., which integrates agar with Janus nanofiber materials. The hypodermic support layer was developed through solvent casting utilizing silver nitrate and agar to provide extended bacterial protection. The electrospun polycaprolactone and agar incorporating gallic acid functioned as the secondary layer, imparting antioxidant properties to the system. The dressing effectively facilitated fluid absorption while allowing water vapor to escape through its porous structure, as indicated by test results. The wound-care dressing demonstrated significant inhibition of bacterial growth, safe removal of oxidizing agents, and environmentally friendly degradation. Application of this dressing resulted in accelerated wound healing and skin-tissue restoration in animal trials. Evidence of its wide applicability suggests its effectiveness in treating diverse wound types [185]. Using a layer-by-layer solvent-casting approach, Diop et al. prepared double-layered films as shown in Figure 12a. First, an agar and chitosan blend solution was formed by dissolving agar powder with glycerol as a plasticizer in distilled water under stirring while heating. The blend was then spread on a Teflon plate and allowed to gel at room temperature. An additional layer composed of agar, PVA, and citric acid was also produced and cast over the first layer. After standing at room temperature, both layers were allowed to dry in an air-circulating oven. The physical properties of the films were affected by the temperature of the drying process and were stored in a desiccator until testing. Apparently, this method successfully produced bilayer composite films with tunable properties [186]. Guo et al. used solvent-casting technique to prepare an agar composite containing activated carbon, suitable for energy storage applications (Figure 12b). The process involved creating foamy carbon (activated at 700–900 °C) while agar–sodium-sulfate solution cast on glass produced a solid gel electrolyte, together yielding efficient energy-storage-ready materials [177].

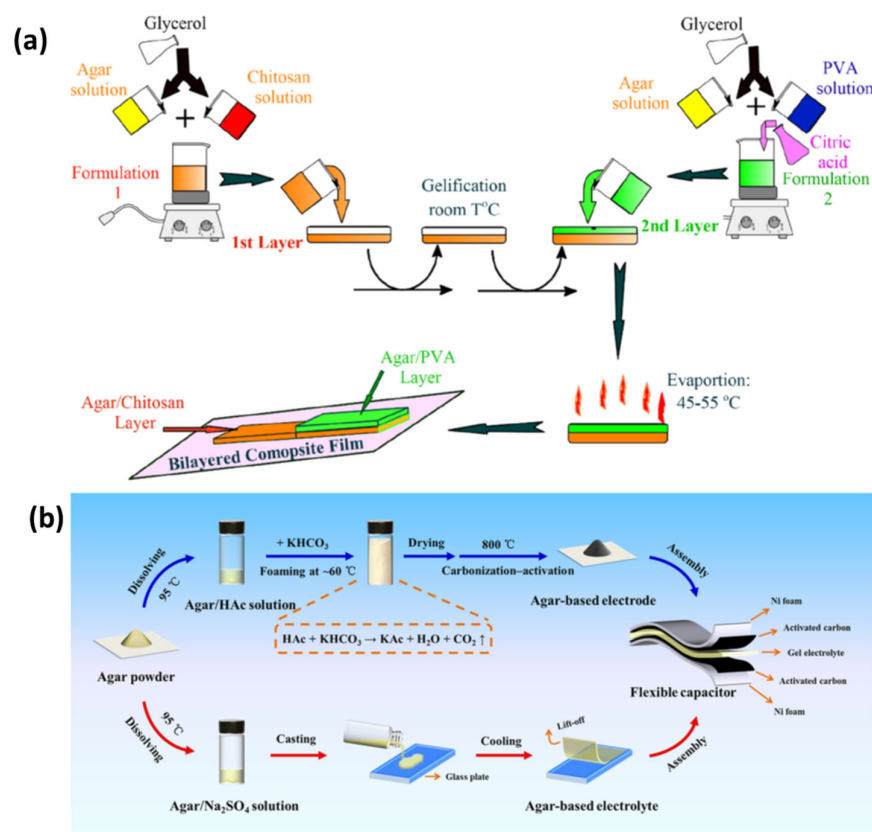


Figure 12. (a) Preparation process of agar/chitosan and agar/PVA double-layered composite films: enhanced physical properties in the layer-by-layer solvent-casting approach with optimized drying conditions (reproduced with permission) [186]; (b) exploring agar-based porous electrodes and electrolytes for ultra-high energy density in flexible symmetric supercapacitors (reproduced with permission) [177].

6.2. Electrospinning Technique

Electrospinning creates fine polymer fibers through a powerful yet straightforward production method. The process employs a high-voltage electric field to form fibers from a liquid polymer or melted material. Upon entering the spinneret, the electrical charge disrupts the surface tension of the polymer liquid, producing a fluid jet that elongates toward the collector. As the solvent evaporates, solid polymer strands deposit on the collector surface as a fabric-like material [187–189]. The method provides precise control over fiber dimensions and structural properties to achieve optimal surface performance.

Sousa et al. created agar-based nanofibers through water-based electrospinning (Figure 13). They operated a tubeless spinneret inside an electrospinning chamber maintained at 50 °C to prevent agar from gelling. An initial 1% agar solution showed poor spinning results, which improved after adding PVA. Agar/PVA blends ranging from 100/0 to 0/100 were tested under various electrospinning conditions. Mixing 30% agar with 70% PVA and 20% agar with 80% PVA produced the best agar/PVA nanofiber outcomes, indicating prospective applications for agar nanofibers in medical fields [101]. Duman et al. used a series of processing steps to clean oil-contaminated water and created advanced PVA-based membranes with superhydrophobic properties. Electrospinning was used to spin fibers into membranes, which were then treated with methyltrichlorosilane in petroleum ether to increase water resistance and hardened using glutaraldehyde. The PVA and agar water-treatment membranes exhibited exceptional efficacy in eliminating organic solvents and oily contaminants from water in a cost-effective and sustainable manner [190]. Rathore et al. developed a two-layer medicated skin patch utilizing agar-based nanofiber

technology for transdermal medicinal applications. To produce optimal nanofibers, precise parameters were utilized: the material was delivered at a rate of 10 $\mu\text{L}/\text{min}$ over a distance of 7 cm from the nozzle to the collector, while a voltage of 15 kV was applied and the collector rotated at 700 rpm. The second layer, composed of a PVA matrix with cephalixin hydrate and agar–PCL fibers, was designed to retain and gradually release the medication. Both membrane layers had exceptional physical properties, featuring a tensile strength of 7 MPa, an eightfold increase in swelling, and a moisture-permeability rate of 2174 $\text{g}/\text{m}^2/\text{day}$. These mats demonstrated antibacterial efficacy and compatibility with blood and cellular systems, indicating their significant potential as drug-delivery methods in medical technology [191].

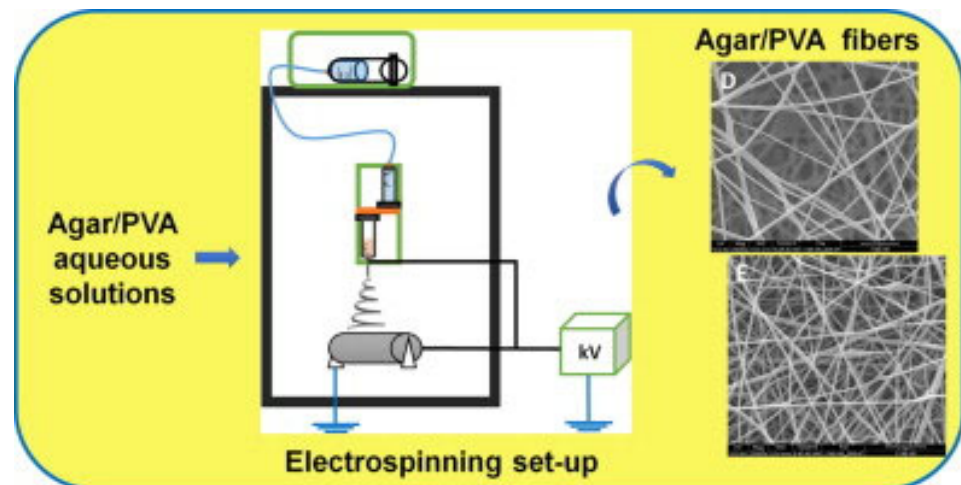


Figure 13. The combination of agar-based nanofibers with a PVA co-blending polymer enhances their spinnability during electrospinning, forming continuous fiber mats when using 30/70 or 20/80 ratio blends of agar/PVA (reproduced with permission) [101].

6.3. Chemical and Physical Crosslinking

Chemical crosslinking agents form new covalent bonds between agar polymer chains, thereby enhancing mechanical strength, heat tolerance, and the structural properties of composites. The hydroxyl groups in the polysaccharide backbone of agar interact with crosslinking agents, including glutaraldehyde, epichlorohydrin, or genipin, to form robust three-dimensional networks. This procedure offers the advantage of enhancing mechanical strength and thermal stability of the composite, allowing for more durable and reliable hybrid materials for a wide range of sustainable applications [192,193].

Belay et al. tested how agar performance could improve with succinic acid crosslinking combined with bacterial cellulose. Agar treated with succinic acid crosslinking and bacterial cellulose reinforcement together increased its tensile strength by 101%, compared with separate improvements of 70% and 56%, respectively. Once the agar was crosslinked, the material's water absorption was greatly decreased. This technique makes agar appropriate for use in the production of food containers and medical devices by strengthening it while preserving its cell compatibility [194]. Wang et al. engineered a three-layer hydrogel combined with different linking approaches to make it more durable and stable. Agar molecular chains connected as a physical network through hydrogen bonding during freezing. They mixed acrylic acid (AAc) with a chemical crosslinker to produce a free-radical-polymerization-based chemically linked network. PVA addition created semi-crystalline zones that improved molecular chain organization. The strength of the polymer network increased when Fe^{3+} bonded to PAAc carboxyl groups, and the introduction of carbon nanotubes enhanced material performance. The experimental Agar/PAAc-

Fe^{3+} /PVA/CNTs hydrogel demonstrated superior mechanical characteristics, instantly returning to its original shape after repeated compression, highlighting its promise for demanding applications requiring strong and tough materials [195]. Gürkan Polat et al. produced new hydrogels by combining agar/ κ -carrageenan with montmorillonite and crosslinking them through a free-radical process using triethylene glycol divinyl ether as the crosslinker (Figure 14a). Through careful adjustment of chemical composition and temperature while balancing agar and carrageenan, they created hydrogels that could expand to 2523% of their own volume. These special hydrogels absorb liquids through nonstandard methods, making them promising for medical use [196]. Yang et al. prepared a double-network hydrogel electrolyte for flexible Zn–air batteries by thermally gelling stiff agar (primary network) and subsequently adding poly(vinyl alcohol) crosslinked through repeated freezing–thawing to form microcrystalline contacts (secondary network) (Figure 14b). The resulting gel operates in both alkaline and neutral media, provides high ionic conductivity in alkaline KOH, retains water well in neutral salt, and allows shape-adaptive Zn–air cells that maintain output when bent, exemplifying its potential for safe, low-cost, high-performance wearable power sources [163].

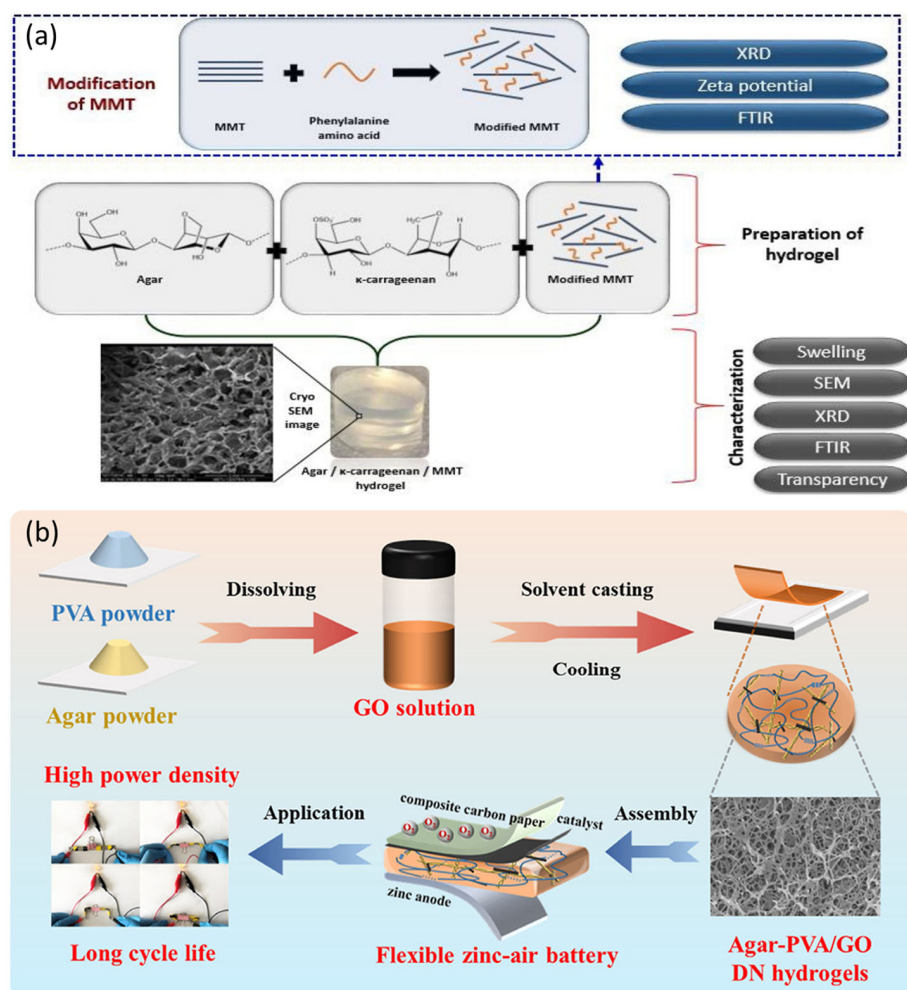


Figure 14. (a) Crosslinking new agar/ κ -carrageenan/MMT hydrogels with TEGDE produced substances that absorbed water up to 2523% while exhibiting non-Fickian absorption patterns that varied with MMT content (reproduced with permission) [196]; (b) agar–PVA–GO crosslinked double-network gel composite electrolyte for extraordinary performance FZABs (reproduced with permission) [163].

Physical crosslinking processes in agar-based composites leverage the biopolymer's intrinsic capacity to form reversible, non-covalent networks through hydrogen bonding, ionic interactions, or chain entanglements with natural or synthetic polymers. These processes enable tailored mechanical strength, stimuli-responsive behavior, and self-healing properties essential for cutting-edge energy storage and flexible electronic applications [197,198]. For instance, Mahamoud et al. developed biocompatible hydrogels made from PVA and agar incorporating tannic acid as a physical crosslinker to enhance mechanical strength for medical and water-treatment purposes. They subjected the hydrogels to repeated freezing–thawing cycles, observing that each cycle increased their mechanical strength. According to the results, the samples' tensile strength rose from 1.56 MPa after one cycle to 3.77 MPa after five cycles while using less crosslinking agent. These hydrogels showed both lower swelling volume and improved water-retention capacity. By using tannic acid as a crosslinking agent and improving hydrogel performance through F/T cycles, the study demonstrated that PVA hydrogels become more suitable for wound-care and artificial-cartilage applications [199]. Through a single-step physical crosslinking technique, Li et al. produced a PASA hydrogel from PVA and agar with in situ-formed silk–AgNPs. AgNPs formed directly within the silk hydrogel because tyrosine in silk fibroin naturally reduces silver ions during synthesis. PVA crystallites and hydrogen-bonded agar networks strengthened the hydrogel structure. This method creates a strong bandage material that fights off bacteria that can help treat infected wounds [200]. Huang et al. developed a new type of physically crosslinked composite for advanced water-filtration systems. Agar physically bonded with sodium alginate bound by calcium ions forms the basis of this new aerogel system. When sodium alginate enters the agar system, it forms a stronger network that resists deformation and retains more material [201].

6.4. Freeze-Drying

Freeze-drying, or lyophilization, is as a vital method for preparing agar-based composite materials, especially when preservation of probiotic substances is required. Through freeze-drying, samples are solidified before the pressure is reduced, which turns ice directly into vapor and preserves the original biological structure and functionality of encapsulated substances. The process generates a spongy structure that supports many uses in the biotechnology and food industries for creating customized solutions [202–204].

Ajisafe and Raichur et al. developed a 3D scaffold for cartilage repair when they freeze-dried agarose and snail mucus into AGSMu. Their scaffold combines agarose's biodegradable nature with snail mucus's healing properties. The process added mechanical stability to the scaffold and supported the growth of C28/I2 human chondrocyte cells. The AGSMu scaffolds demonstrate strong potential for repairing and regenerating joint cartilage tissue [205]. Liu et al. synthesized a porous carbon material exhibiting a surface area of 3184 m²/g via concurrent sol–gel and freeze-drying techniques, prior to activation (Figure 15a). Agar functioned as the carbon source, while L-arginine served as the nitrogen source, resulting in N-doped porous carbon that stored 443.0 F of electricity when evaluated at 0.5 A/g in 6 M KOH. They constructed a symmetrical supercapacitor utilizing their material and an agar–sodium-sulfate gel as electrodes, achieving an energy storage capacity of 35.5 Watt-hours per kilogram and 99.7% capacity retention over 20,000 cycles [172]. Xie et al. synthesized oxygen/nitrogen/boron codoped carbon aerogels through one-pot sol–gel polymerization of resorcinol/formaldehyde precursors with heteroatom sources, followed by freeze-drying and high-temperature carbonization (Figure 15b). The multi-element codoping strategically introduced lattice distortion, generating abundant neighboring active sites that provided high potassium-ion adsorption (1.62 eV) and very low diffusion barriers (0.12 eV) along N- or O-decorated rings. These structural benefits

gave the prepared sample exceptional capacity, rate capability, and long-term retention, maintaining 83% of its capacitance after 10,000 cycles. A symmetric K-ion supercapacitor constructed from the material achieved 51.8 Wh kg^{-1} energy density at 443 W kg^{-1} power density, demonstrating the potential of heteroatom-codoped aerogels as building blocks of next-generation potassium-ion energy devices [206].

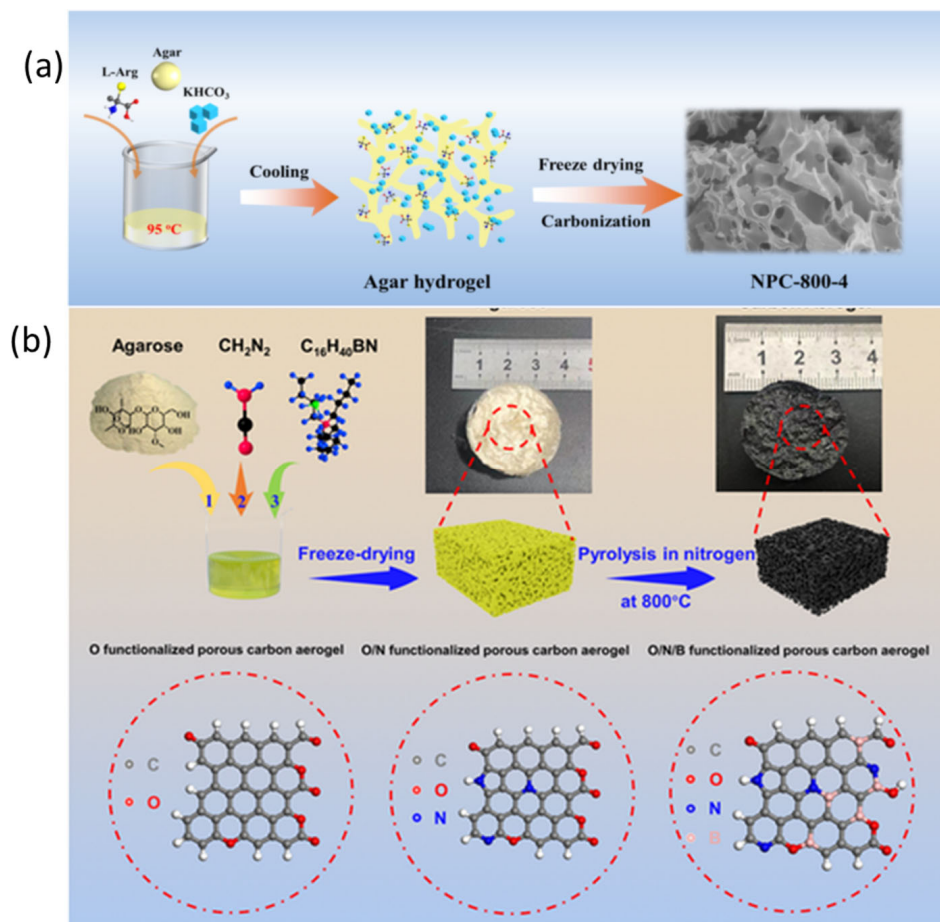


Figure 15. (a) N-doped porous carbon synthesis: activation of agar-based gel for enhanced supercapacitor performance (reproduced with permission) [172]; (b) schematic representation of heteroatom-doped carbon aerogel synthesis: the agarose-derived hydrogels are freeze-dried and pyrolyzed at 800°C in N_2 , and nitrogen and boron are doped using cyanamide and tetrabutylammonium borohydride to obtain the O-CA, ON-CA, and ONB-CA porous carbon structures (reproduced with permission) [206].

In another work, the freeze-drying process produced agar/PVA aerogels that effectively extract oil from water while being environmentally sustainable. These aerogels absorbed substantial volumes while attaining 99.3% separation purity for chloroform and water mixtures via their oil–water and solvent–water separation mechanism. Research indicates that these materials may aid in the removal of oil spills from aquatic systems [207]. Sang et al. fabricated agarose–chitosan scaffolds via freeze-drying, subsequently coating them with collagen at a concentration of 3 mg/mL , which exhibited superior mechanical properties for dermatological research applications [208]. Kumar et al. dissolved 3% agarose in water, added varying amounts of chitosan from acetic acid, and stirred continuously to create agarose scaffolds with embedded AgNPs coated in chitosan. The mixture changed from its initial state to a brownish-yellow color when the nanoparticles formed, and they used 1% glutaraldehyde to fix them in place. The AG-CHNp1 to AG-CHNp4 scaffolds were freeze-dried at -80°C to produce natural pores by direct ice-crystal sublimation [209].

6.5. 3D Printing

The research capabilities in composite material creation were transformed by the precise delivery capabilities and robust design scaling mechanisms of 3D printing technology. The sequential building method facilitates the accurate placement of materials, thereby optimizing the mechanical, thermal, and electrical properties of the composite structure. FDM, along with other sophisticated manufacturing methods such as SLA and DIW, allows users to fabricate intricate, lightweight components that exceed the constraints of traditional manufacturing by integrating diverse matrices, including polymers and hydrogels, with reinforcements like nanoparticles and fibers [210,211]. The process has three main advantages: reduced waste production, expedited model creation, and tailored design possibilities for aerospace components, biomimetic implants, tissue scaffolds, battery electrodes, and electronic materials. Functional additives, including conducting polymers or ceramics, can be integrated to produce a wide range of smart devices, sensors, and sustainable infrastructure [212–214].

Ghaedamini et al. used 3D printing to create PCL scaffolds and applied a 2% Ag hydrogel coating layer. They assessed the physical characteristics and water-absorption capacity of PCL and PCL/Ag scaffolds. Using MTT testing, which was carried out every day for three days and then once a week, the experiment evaluated the behavior of L929 cells with regard to attachment and proliferation on PCL and PCL/Ag surfaces [215]. Yang et al. improved the GelMA used in 3D printing by incorporating embedded printing with agarose microgel support to enhance printing properties. Initially, the standard LAP solution was prepared, and GelMA was combined with red dye in a heated water bath. Agarose was first melted in hot water and subsequently fragmented into small beads upon cooling. A liquid appropriate for printer spraying was created by integrating these components. The research evaluated the printing performance of the GelMA and agarose blend, confirming its suitability for optimal print formation and cell viability. The method seeks to improve the flexibility and water absorption of printed scaffolds while preserving their structural integrity, thus avoiding rapid changes in shape. This enables the creation of specialized medical tissue repair products [216]. Wang et al. employed thermal methods to fabricate calcium alginate/agar composites, resulting in customizable, high-resolution filaments. The combination of alginate and agar mitigated the Barus effect, resulting in a thicker and sharper ink suitable for enhanced printing. Calcium ions interconnected the alginate chains during printing to enhance layer adhesion, regulate liquid absorption, and modify stiffness. They enhanced the bond between printed stripes by including a soft polyacrylamide network at the junctions of the stripes. These enhancements facilitate the application of 3D-printed CA/Ag hydrogels in healthcare, particularly in the construction of biological tissues [217]. Vijayaraghavan et al. produced 3D-printable sheets from GelMA/agarose hydrogels by pneumatic extrusion to construct scaffolds that replicate the architecture of an adult cornea. These gel materials facilitate enhanced cellular growth and maintain transparency equivalent to natural corneal tissue, presenting significant potential for the development of novel corneal tissues [218]. Mukundan et al. functionalized agarose with methacrylate groups to achieve thermogelling, photo-curable bio-ink (Figure 16a). The warm fluid is extruded, rapidly gels on cooling, and is subsequently UV-crosslinked to fix a rigid, cell-compatible lattice for osteogenic applications [219]. Satrip et al. combined agarose and PEGDA and added nano-hydroxyapatite to increase the viscosity and shear-thinning properties (Figure 16b). The composite is extruded as stable lattice scaffolds that correspond to the geometry of the cartilage and facilitate cell growth [220].

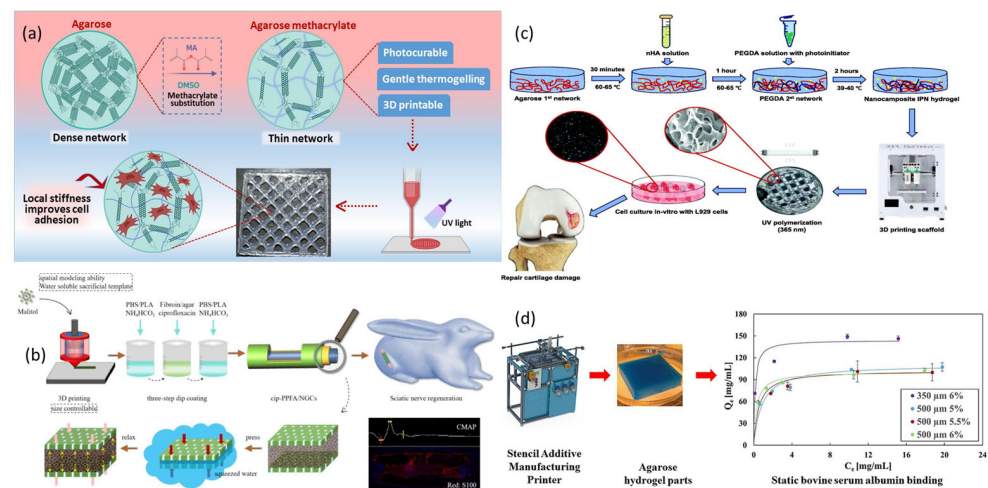


Figure 16. Various 3D-printed agar-based composites: (a) Agarose hydrogel tailoring to control its 3D printability and mechanical properties in stem-cell-mediated bone tissue engineering (reproduced with permission) [219]. (b) The three-layer membrane neural guidance conduit successfully fabricated with the combination of 3D printing–sacrificial template and dip-coating technology. The sandwich tube wall structure gives the conduit very good compressive and shape-recovering characteristics. Conduits overcome implant-induced infections by using drug sustained-release technology; cip-PPFA/NGCs can guide regeneration of a 10 mm neural bridge in rabbits, and restore sciatic nerve function (reproduced with permission) [221]. (c) Designing and testing of 3D printed agarose/poly(ethylene glycol) diacrylate/hydroxyapatite nanocomposite hydrogel for cartilage tissue engineering (reproduced with permission) [220]. (d) Three-dimensional manufacturing protocol to produce agarose hydrogel structures for protein sorption (reproduced with permission) [222].

Zhang et al. co-printed a three-layer sandwich conduit: porous PBS/PLA sleeves on the outside, and a fibroin/agarose hydrogel core that also encapsulates ciprofloxacin on the inside (Figure 16c). The architecture provides a nerve guide that is antibacterial and resistant to compression [221]. Cao et al. patterned agarose hydrogels with stencil additive manufacturing in fine-resolution grids (Figure 16d). The use of reusable stencils and layer-by-layer deposition results in neat walls, adjustable porosity, and low die-swell—enabling fine-scale hydrogel printing of agarose [222].

6.6. EMR-Assisted Routes

The fabrication process of agar-based composites greatly benefits from techniques involving electromagnetic radiation, such as microwave irradiation, ultraviolet curing, and plasma treatment [223–225]. The use of microwave irradiation accelerates the polymerization process and enhances the uniform distribution of nanoparticles within agar matrices, while reducing processing times [226,227]. UV curing facilitates the rapid crosslinking of agar blends with biopolymers, thereby improving their mechanical strength and water resistance. Plasma treatment enhances the surface properties of agar, improving its compatibility with cellulose and graphene materials, thereby increasing the functionality of the resulting composites [228–231]. The benefits of EMR-assisted techniques include rapid manufacturing processes and enhanced mechanical properties, alongside environmental advantages due to reduced chemical usage and improved surface bonding. These methods are crucial for the advancement of agar-based composites suitable for biomedical applications, packaging solutions, and environmental purposes.

Qi et al. prepared carboxymethyl agar (CAG) using both conventional and microwave-assisted techniques. The agar powder (5 g) was mixed with 50 mL of 80% ethanol and stirred until complete swelling was achieved over 0.5 h. The CAG alkalization necessitated the addition of NaOH at 40 °C for 2 h using conventional heating, whereas it was achieved

at 45 °C for 20 min with microwave-based technology. The MAS II synthesizer functioned during this phase via microwave application. In the synthesis, MCA and NaOH were utilized at molar ratios of 2.0 nNaOH/nAgar and 1.00 nMCA/nAgar prior to heating the solution to 55 °C. A procedure for MAg production involved cooling to 20 °C, neutralizing with glacial acetic acid, followed by filtration and washing with 60% ethanol until chloride was removed, and drying at 60 °C to yield 80-mesh particles. The evaluated products from conventional and microwave-assisted synthesis were designated as CAg and MAg, respectively [225]. Chang et al. developed agarose microspheres with large pores for antibody purification through the integration of microfluidics and microwave-assisted synthesis techniques. In the process of microwave heating, a solution of 1.2 g of agar dissolved in 30 mL of deionized water was subjected to specific time intervals until complete liquefaction was achieved. The continuous phase was prepared using 1.5 mL of EM90 and 50 mL of liquid paraffin. The stability of gas flow was ensured through the utilization of an air compressor in conjunction with a preheated water bath maintained at 85 °C. By altering the flow rates of fluids in both the continuous and dispersed phases, the FluidicLabSuite control system measured the size of the microspheres. After the gathered microspheres were cleaned with petroleum ether, they were put in a 20% ethanol solution and kept at 4 °C. Liquid paraffin with different EM90 concentrations (1–4%) combined with the surfactants TWEEN80 and SP80 was used for morphological study [232]. Wang et al. reported using ultraviolet-assisted reaction techniques to combine zinc oxide–polyethylene glycol methyl ether methacrylate with 4-azidobenzoic agarose to create nanocomposite hydrogels with interpenetrating polymer networks. The hydrogels demonstrated an open porous network, exceptional mechanical strength, and light transparency greater than 85%. In order to combat *Escherichia coli* and *Staphylococcus aureus*, the hydrogels' anti-adhesive and bactericidal qualities increased as their zinc oxide–polyethylene glycol methyl ether methacrylate content rose. The synthetic membrane material is a promising option for wound-dressing applications because it maintained its biocompatibility [233].

7. Applications in Energy Storage Devices

The exploration of sustainable energy storage technology leverages agar-based composites due to their effective ion-conducting capabilities and biodegradable properties. Agar-based composites facilitate greater operational stability in supercapacitors while also enhancing storage capacities. They contribute to advancements in battery technology by delivering superior performance alongside environmental sustainability. The implementation of agar-based composites enhances the performance level of fuel-cell electrochemical operations while also providing environmental benefits. Research statistics indicate that agar-based composites exhibit significant potential, facilitating advancements in power storage methodologies.

Their adaptable networks enable three complementary roles: carbon precursors that yield high-surface-area, heteroatom-rich electrodes; gel-polymer electrolytes that combine ionic transport with safety and flexibility; and structural scaffolds that stabilize interfaces during repeated cycling [45,176,234,235]. Agar-derived carbons facilitate rapid ion access and robust charge storage through interconnected porosity and abundant surface functionalities, while agarose-based hydrogels suppress leakage, buffer mechanical strain, and harmonize electrode–electrolyte contact in flexible and integrated devices [173,236,237]. Together, these attributes anchor agar-based materials as eco-friendly, low-cost candidates that reconcile transport, mechanics, and durability across supercapacitors, zinc-ion and metal–air batteries, and fuel-cell platforms, as summarized in Table 4.

Table 4. Different types of agar-based composites and their electrochemical characteristics in various energy storage devices.

Composite	Device Type	Specific Capacitance (F g ⁻¹)	Energy Density (Wh kg ⁻¹)	Power Density (W kg ⁻¹)	Cycle Life (Retention %/Cycles)	Ref.
3D porous carbon from agar (N,O,S-doped APC)	Symmetric supercapacitor	272	20.4	449	103.2%/10,000	[234]
Agarose gel electrolyte with 8 M KOH	Zinc–air battery	-	20.77		57.8%/302	[45]
N,O-codoped agar porous carbon (APC)	Symmetric supercapacitor	272 (at 0.5 A g ⁻¹)	20.4	449	100%/10,000	[234]
Agar–agar-derived carbon	Supercapacitor (integrated with solar cell)	170	17.7		85%/15,000 (at 1 A g ⁻¹)	[41]
Agar-based porous electrode + agar electrolyte	Flexible supercapacitor	-	22.1	450		[172]
Agarose-derived hierarchical porous carbon	Symmetric supercapacitor	64 (1 A g ⁻¹)	14.4	2000	~100%/10,000	[160]
Agarose-gel-templated 3D wrinkled graphene electrode	Symmetric supercapacitor	-	1.2–10	45–562	-	[21]
Agarose/PVA gel polymer electrolyte	Solid-state supercapacitor	(697 mF cm ⁻² at 5 mA cm ⁻²)	-	-	-	[150]
High-modulus agarose gel electrolyte (AGE)	Aqueous Zn-ion battery	-	-	-	90%/10,000	[25]
N-doped agar-derived porous carbon	Symmetric supercapacitor	-	70.2	1810	83.3%/50,000	[235]
PVA/agar hydrogel electrolyte	Symmetric supercapacitor	200 (CV at 5 mV s ⁻¹)	-	-	-	[27]
PEDOT-OH/PEO electrodes in agarose gel electrolyte	Symmetric supercapacitor	195.2 (10 mV s ⁻¹)	-	-	-	[238]
Agar-based hydrogel polymer electrolyte (agar + PAM)	Aqueous Zn-ion battery	-	-	-	85%/50,000	[50]

7.1. Agar-Based Composites in Supercapacitors

Agar-based composites have garnered interest due to their emphasis on green, renewable components, serving a dual purpose as both electrodes and electrolytes in supercapacitors. The inherent sponge-like structure and hydrophilic properties of agar render it an ideal medium for incorporating conductive materials like carbon nanotubes, graphene, or metallic nanoparticles that facilitate electrical conduction. The additives significantly enhance the materials' capacity to conduct electricity and retain electrical charges. The utilization of porous agar-based composite electrodes in supercapacitors facilitates enhanced ion flow, thereby elevating the performance of the device during both charging and power delivery [239–244]. The establishment of hydrogel electrolytes using composite materials results in a system that demonstrates elevated electrical conductivity along with flexible properties, making it ideal for use in flexible electronic devices [245–249]. Agar-based materials demonstrate efficacy in supercapacitors due to their environmental safety, compatibility with living organisms, enhanced energy storage capabilities, and reliable performance across diverse applications. The incorporation of agar into sophisticated energy storage systems is essential because of its significance.

Guo et al. designed a flexible supercapacitor that utilizes agar material as both the active electrode component and the electrolyte agent. The treatment of foaming-cured carbon material with KHCO₃ and HAc enhanced its surface area and pore structure, resulting in an electrode capacitance of 313.7 F g⁻¹. The Na₂SO₄ hydrogel electrolyte, produced via a solvent-casting method, exhibited an electrochemical potential window of 1.8 V and flexibility. The novel supercapacitor achieved an energy storage capacity of 22.1 Wh kg⁻¹, thereby validating agar as a viable candidate for developing high-performance flexible

energy storage devices [177]. Hwang et al. developed a method to create porous carbons since agarose is renewable. Potassium oxalate was added to heated agarose to create pores when the salt disintegrated during carbonization. The process produced porous carbon units with electrochemical activity and tunable internal properties that are suitable for supercapacitors. Agar-based electrodes showed significant energy storage potential by delivering 166.0 F g^{-1} of specific capacitance at slow rates and maintaining 64.1 F g^{-1} after 10,000 charging cycles at rapid rates [160]. Lv et al. investigated the combination of agarose derived from the ocean with GO to create a gel-polymer electrolyte matrix in solid-state supercapacitors. DFT research demonstrates that agarose exhibits a distinct layered structure, promoting improved lithium mobility and enhancing ion transport. Ag/GO-GPE exhibits exceptional performance, achieving a specific capacitance of $791.67 \text{ mF cm}^{-2}$ while maintaining consistent electrochemical properties under flexion. The Ag/GO-GPE material exhibits significant resistance to physical pressure and fire, rendering it suitable for flexible wearable energy applications [176].

Guo et al. investigated agar-based porous electrodes for flexible symmetric supercapacitors, concentrating on ultra-high energy density assessment. The CV analysis of AAC-700, AAC-800, AAC-900, and AC-800 electrodes conducted in a 6 M KOH electrolyte demonstrates their CV results at a scan rate of 50 mV s^{-1} , as illustrated in Figure 17a. The CV curves of AAC electrodes exhibit a nearly rectangular shape, indicating superior double-layer capacitive performance for efficient electrical charge storage. The GCD curves of AAC electrodes depicted in Figure 17b indicate specific capacitance values of 227.2 F g^{-1} , 313.7 F g^{-1} , 289.1 F g^{-1} , and 69.4 F g^{-1} at a current density of 0.5 A g^{-1} for AAC-700, AAC-800, AAC-900, and AC-800, respectively. The CV curves of AAC-800 in Figure 17c exhibit rectangular-like morphologies when assessed at 100 mV s^{-1} , as well as at other scan rates ranging from 10 to 100 mV s^{-1} , indicating exceptional charge-transfer capacity and outstanding rate capability. The material exhibits exceptional electrochemical stability and high-power performance, as evidenced by its GCD curves spanning a broad current density range from 0.5 A g^{-1} to 100 A g^{-1} , as depicted in Figure 17d. Next-generation flexible supercapacitors with high energy density can benefit from materials produced from agar due to these promising results (see Figure 17) [177].

Guo et al. investigated the practical application of agar-based activated carbon electrodes by creating a flexible supercapacitor entirely composed of agar, utilizing an Agar/ Na_2SO_4 gel electrolyte for operation. The electrochemical stability assessments included CV, GCD, and cycling-stability evaluation. The operational voltage ranges of 1.0–1.8 V enabled the CV curves (Figure 18a) to exhibit near-rectangular forms, confirming double-layer capacitor behavior. The device exhibited significant electrode polarization due to water breakdown at 2.0 V, resulting in an ESPW determination of 0–1.8 V, a range that surpasses that of existing hydrogel-based supercapacitors. The capacitance response remained consistent across scan rate experiments ranging from 10 to 100 mV s^{-1} (Figure 18b), indicating steady performance. The devices fabricated at $0.5\text{--}10 \text{ A g}^{-1}$ (Figure 18c) preserved optimal isosceles triangular configurations with a minimal internal-resistance reduction of 0.06 V at 0.5 A g^{-1} . Consequently, favorable ionic conductivity was maintained. The agar/ Na_2SO_4 system exhibited superior energy density at 22.1 Wh kg^{-1} for 450 W kg^{-1} , in contrast to 8.6 Wh kg^{-1} for 250 W kg^{-1} PVA/KOH electrodes and 10.8 Wh kg^{-1} for 400 W kg^{-1} PVA/ Na_2SO_4 electrodes (Figure 18d). A broadly anticipated stable working potential window of 1.8 V exceeded previous performance outcomes of carbon-based solid-state supercapacitors utilizing diverse polymer hydrogel electrolytes. The entirely agar-based supercapacitor exhibited steady CV curves when bent to 90° and 180° angles (Figure 18e). A practical test demonstrated the feasibility of employing a wearable electronic device utilizing a series connection of four supercapacitors to power an LED under

applied strain (Figure 18f). Cycling-stability assessments performed at 2 A g^{-1} (Figure 18g) demonstrated long-term durability, as the specific capacitance retained its initial value over 50,000 cycles, and the system attained a Columbic-efficiency stability of about 100%. This work demonstrates that supercapacitors made from agar exhibit improved energy density, greater stability, and flexibility, making them suitable for wearable energy storage applications [177]. Hasan et al. developed binder-free conducting polymer hydrogel electrodes by combining PVA/agar hydrogels with polyaniline and Ppy to enhance the energy density and electrochemical performance of supercapacitors. A complete supercapacitor structure was developed using flexible hydrogel systems, eliminating the need for lamination. The PAP2 device demonstrated outstanding performance in electrochemical evaluations, achieving an area capacitance of 750.13 mF/cm^2 , alongside energy- and power-density values of $103.02 \text{ } \mu\text{Wh/cm}^2$ and $497.22 \text{ } \mu\text{W/cm}^2$, respectively, with a notable capacity retention of 149% over 15,000 cycles [27]. Zhang et al. synthesized deoxygenated agar-based activated carbon, resulting in enhanced specific-energy metrics for hybrid lithium-ion supercapacitors. Hybrid supercapacitors were developed by integrating advanced carbon materials with a multilayer-protected lithium anode and a 21 m LITFSI water-in-salt electrolyte, leading to a notable improvement in specific energy performance of 308.3 Wh/kgAC at a specific power of 0.7 kW/kgAC . The electrolyte's broad operational potential window, along with the cell's high working voltage, allowed the system to maintain 89% of its specific energy after 8000 charge/discharge cycles [250].

Kim et al. demonstrated agarose gel composite fiber electrodes including bundled CNTs that exhibit electrical conductivity of 8.3 S cm^{-1} within a filament of approximately $120 \text{ } \mu\text{m}$ in diameter. The mechanically stable electrodes yield flexible two-ply microsupercapacitors exhibiting a capacitance of around 1.2 F cm^{-3} , with exceptional rate retention (almost 90%) amid variations in discharge current density and sustained performance following 10,000 deformation cycles. The utilization of poly(dimethylsiloxane) coating enhances the operational lifespan of batteries in aqueous environments, thereby illustrating the endurance of devices designed for wearable energy storage systems [251]. Agar-PANI, utilized as a synthesis template for polyaniline electrochemistry, demonstrates an electrical conductivity of 1.5 S cm^{-1} and a bulk density of 1.53 g cm^{-3} , surpassing the electrical properties of C-PANI. The capacitance ranges of agar-PANI electrodes span from 200 to 500 F cm^{-3} at 5 mHz due to their comparable crystallinity, which facilitates high energy-density performance. The ion storage capacity of agar-PANI attains $1.5 \times 10^{-3} \text{ mol cm}^{-3}$, surpassing PPy electrodes by two orders of magnitude [110]. Liu et al. reported that the synthesis of crosslinked hierarchical porous carbon materials, featuring a specific surface area of $3184 \text{ m}^2 \text{ g}^{-1}$, is accomplished through sol-gel processes, followed by activation via freeze-drying with KHCO_3 . The nitrogen-doped porous carbon serves as an electrode in a 6M KOH electrolyte, demonstrating remarkable electrochemical properties with a capacitance of 443.0 F g^{-1} at 0.5 A g^{-1} and maintaining 255 F g^{-1} at 50 A g^{-1} . Laboratory testing showed that constructing supercapacitors by this method achieves an energy density of 35.5 Wh kg^{-1} , while exhibiting 99.7% capacitance retention throughout 20,000 cycles, indicating its potential to power high-performance energy storage systems [172]. Vijayakumar et al. combined agar-agar-based, high-performance activated-carbon supercapacitors with commercial photovoltaic modules to build a self-sustaining power pack (Figure 19a,b). Symmetric SCs provide 170 F g^{-1} , 17.7 Wh kg^{-1} , with 85% of initial capacitance remaining after 15,000 cycles at 1 A g^{-1} , and thus three cells in parallel can easily supply 120 mA DC to drive a fan (Figure 16c). The same three cells are wired in series (5.4 V) to get the higher output voltage to light up 40 LEDs in the shape of the ARCI logo and to drive a solar lantern (Figure 19d,e). The stack charges on the photovoltaic panel of the lantern in seconds under sunlight and then powers the LEDs in the dark—a smooth process of

solar-energy conversion, electrochemical storage, and on-demand delivery—an ultrafast and low-cost pathway to next-generation renewable energy modules [41].

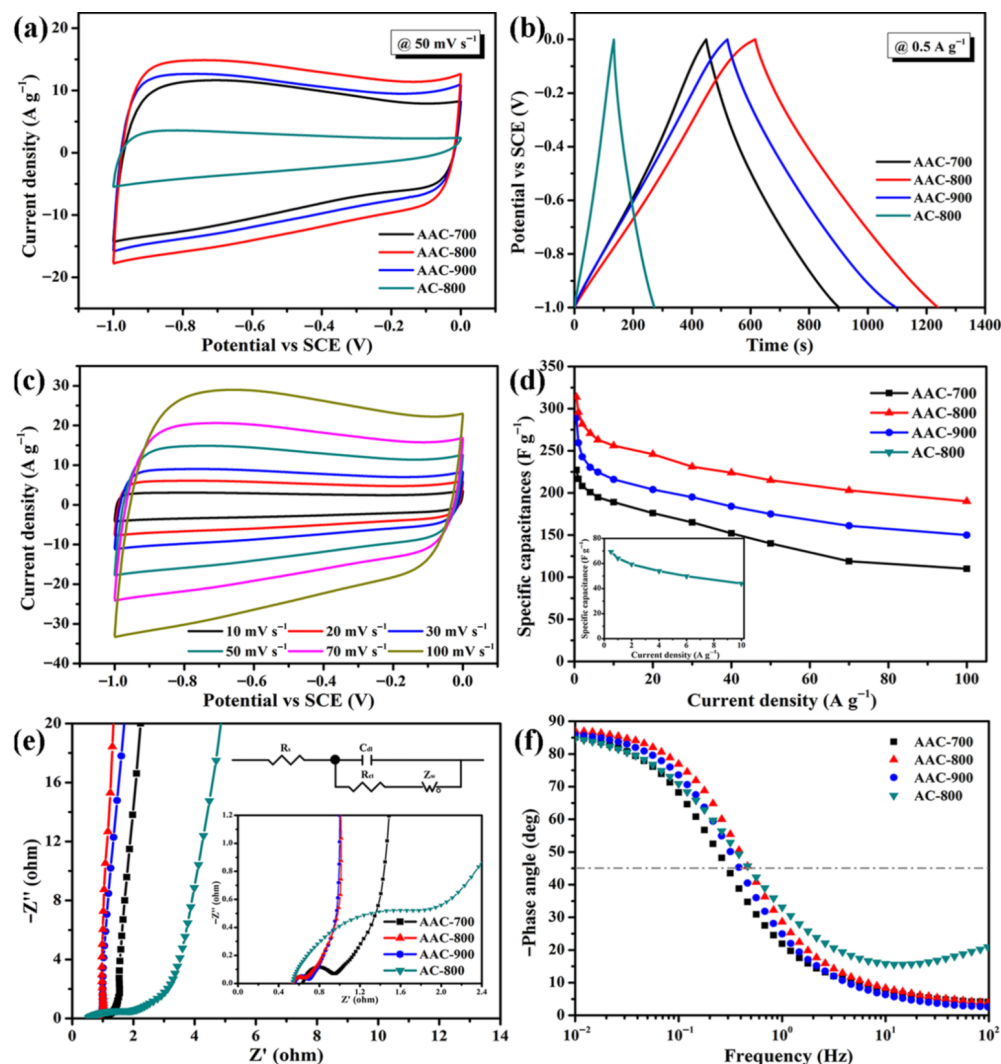


Figure 17. Electrochemical characterization of agar-AAC electrodes in 6 M KOH electrolyte. (a) CV curves obtained at a scan rate of 50 mV s⁻¹, demonstrating the capacitive performance of the electrodes. (b) GCD profiles at a current density of 0.5 A g⁻¹, showing the charge-storage capacity. (c) CV curves for AAC-800 at various scan rates, highlighting its stability and charge-transfer capabilities. (d) Specific capacitances of AACs at different current densities, illustrating the electrodes' performance under varying loads. (e) Nyquist plots ranging from 0.01 to 100 Hz, reflecting the electrochemical impedance. (f) Phase-angle and frequency diagrams, providing insights into the frequency response of the electrodes (reproduced with permission) [177].

Hwang et al. reported that their activated porous carbon, PC-6-700, exhibits near-ideal electric-double-layer characteristics, as rectangular CV profiles are preserved at increasing scan rates (Figure 20a) and linear charge-discharge profiles at various current densities (Figure 20b). The specific capacitance decreased linearly from 135.9 F g⁻¹ at 0.125 A g⁻¹ to 48.8 F g⁻¹ at 10 A g⁻¹ (Figure 20c), and more general comparisons supported that high surface area is advantageous under slow rates, high mesoporosity is desirable under high rates, and chemical activation is critical (Figure 20c). The impedance showed low series resistance and charge-transfer resistance of 0.49 Ω and 9.120 Ω, respectively, which improved after cycling, indicating effective ion transport (Figure 20d). As Figure 20e reveals, the estimated power density amounted to 20 kW kg⁻¹ and the estimated energy density

was 18.9 Wh kg^{-1} . It is the best-performing and longest-lasting carbon supercapacitor electrode that has ever been reported, where the electrode still holds only a small fraction of its original capacitance after 10,000 cycles (after an initial capacitance-enhancing activation, Figure 20f) [160].

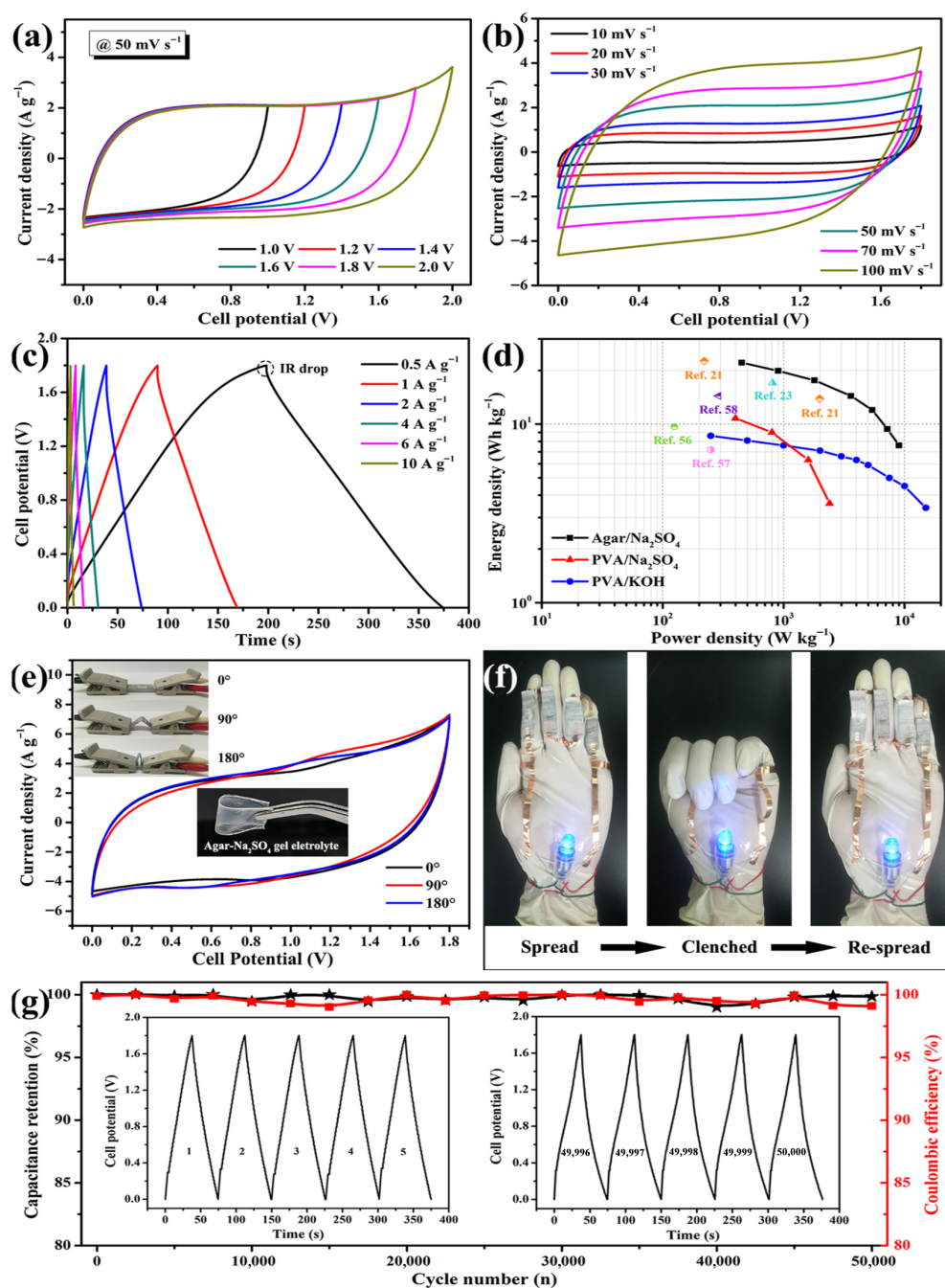


Figure 18. Electrochemical assessments of the all-agar-based supercapacitor in a two-electrode configuration. (a) CV curves across various potential operational windows, indicating capacitive behavior; (b) CV curves recorded at sweep rates ranging from 10 to 100 mV s^{-1} , showcasing response consistency; (c) GCD curves at different current densities, demonstrating energy storage capacities; (d) Ragone plots comparing performance across various electrolytes, highlighting energy and power densities; (e) CV curves measured at diverse bending angles, illustrating mechanical flexibility; (f) an image of a blue LED illuminated by a wearable device equipped with four supercapacitors connected in series, exemplifying practical application; (g) cycling stability of the coin-type all-agar-based supercapacitor at a current density of 2 A g^{-1} , confirming durability over repeated use (reproduced with permission) [177].

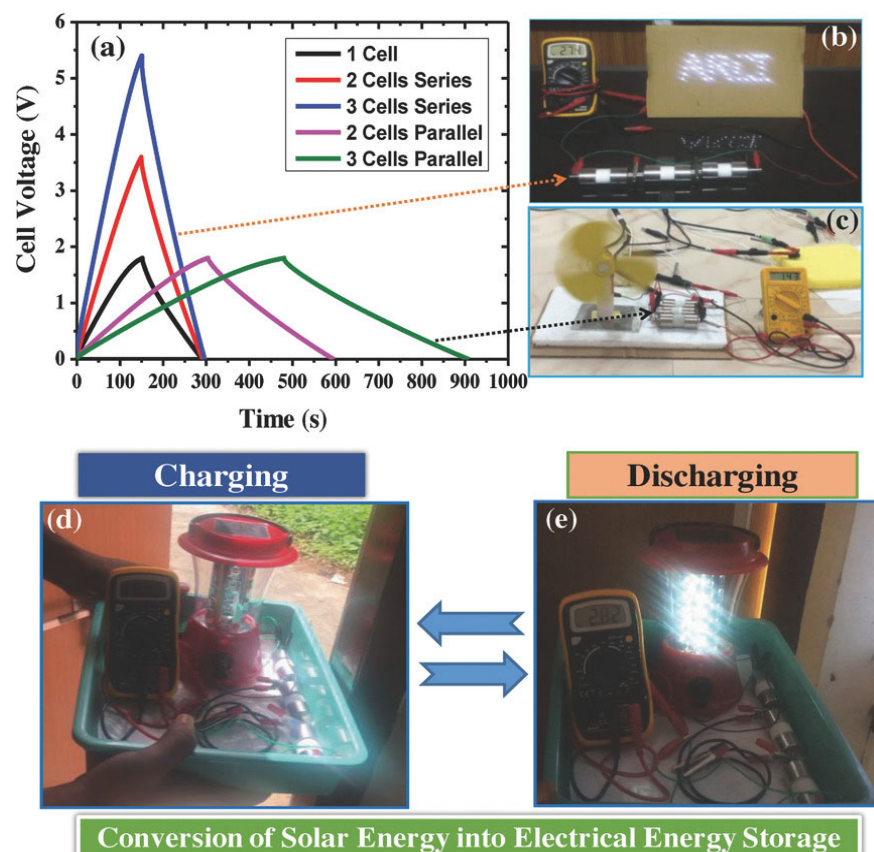


Figure 19. Biomass-derived carbon symmetric supercapacitors: practical validation. A comparison of parallel and series assemblies of three single cells: (a) galvanostatic charge/discharge curves; (b) picture of the three-cell series stack, providing approximately 5.4 V at higher voltages. The boost in overall capacitance is demonstrated by (c) three-cell parallel stack powering a micro-fan at approximately 120 mA; (d) rapid charging of series stack by an integrated photovoltaic panel; (e) off-sunlight lighting: solar-charged supercapacitors driving a commercial lantern equipped with forty light-emitting diodes (reproduced with permission) [41].

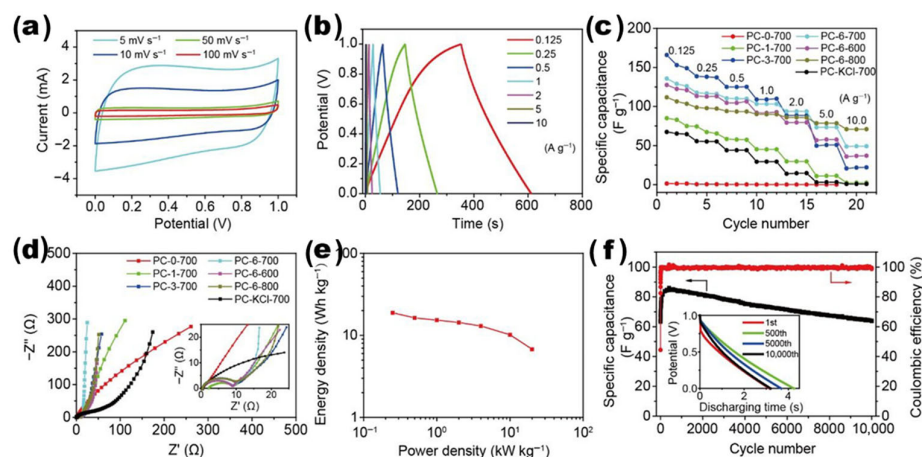


Figure 20. Electrochemical properties of supercapacitors produced with different PC materials. (a) CV data recorded at varying scan rates using an electrode with PC-6-700; (b) charge/discharge curves at various current densities (denoted) on an electrode that holds PC-6-700; (c) electrode rate performance of the various electrodes at different current densities (indicated); (d) the profiles of various electrodes (marked) before cycling; (e) Ragone current plot of electrode with PC-6-700; (f) stability of PC-6-700 supercapacitor at a current density of 5 A g⁻¹ and discharge curves of the 1st, 500th, 5000th, and 10,000th cycles (reprinted with permission) [160].

Moon et al. designed a NaCl–agarose gel electrolyte with its three-dimensional agarose backbone and water-filled sub-micropores providing mechanical integrity and continuous ion pathways to achieve a MnO₂ (parallel) NaCl–agarose planar interdigitated supercapacitor with a capacitance of 286.9 F g^{−1} and approximately 80% of the capacitance seen with a liquid electrolyte at 100 mV s^{−1}. The electrochemical signatures are essentially the same when the device is flat, compressed in-plane, or tensile out-of-plane to a 1.16 cm radius (Figure 21a–c), and Nyquist plots under each deformation show almost identical semicircles, confirming stable charge-transfer resistance (Figure 21d). The sealed cell using moisture-retaining encapsulation with PTFE and polypropylene tape has ~80% of the initial capacitance at 1200 cycles, compared to only 34% for an unenveloped analog, and can power a red LED, demonstrating practical robustness (Figure 21e,f). This nontoxic, scalable, and simple NaCl–agar electrolyte hence offers an attractive basis for mechanically compliant energy storage devices that perform well [46].

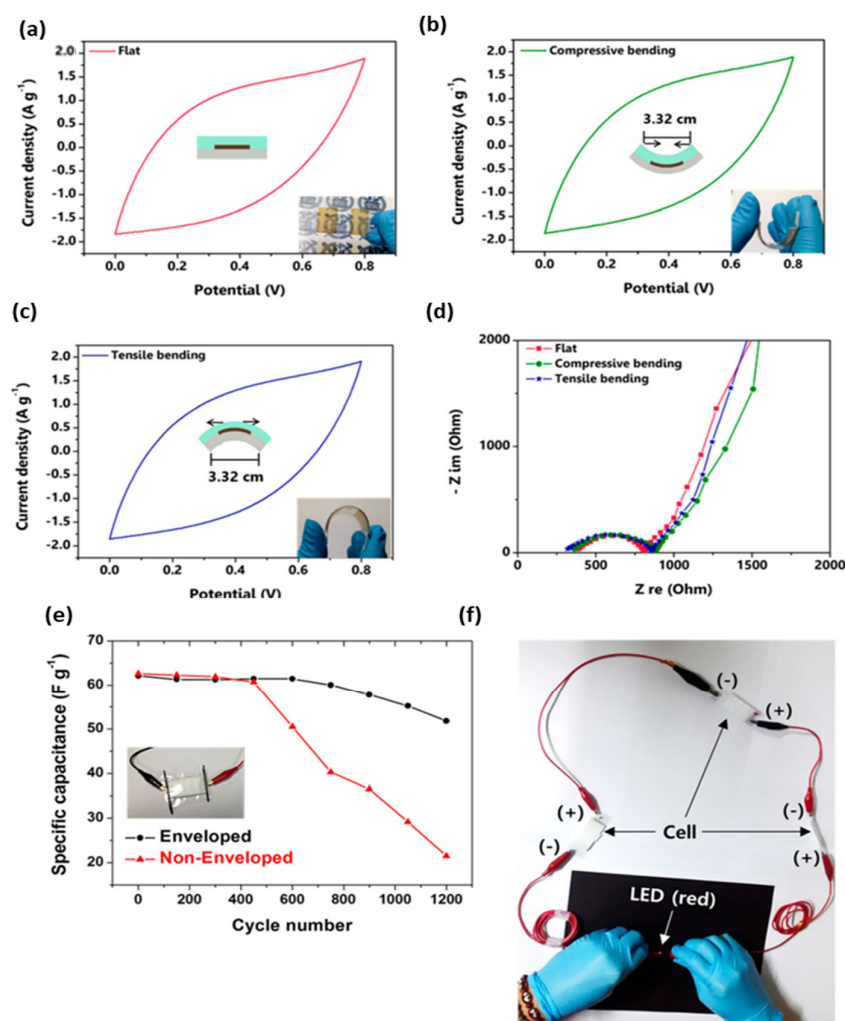


Figure 21. Comparison of CV at a scan rate of 20 mV s^{−1}; EIS profile of the as-synthesized sample; and digital photo of three various bending states: (a) flat; (b) compressive bending; (c) tensile bending; (d) EIS profiles under the three bending states; (e) long-term cycling-stability test profile of enveloped and unenveloped NaCl–agar supercapacitors at a scan rate of 100 mV s^{−1}; (f) digital image of an LED energized by the NaCl–agar supercapacitors (reproduced with permission) [46].

7.2. Agar-Based Composites in Battery Technology

Agar-based hybrid materials are gaining increasing attention as multifunctional constituents in advanced battery systems, including lithium-, sodium-, potassium-, and zinc-

ion batteries, and have demonstrated great potential in next-generation electrochemical energy-storage systems. The gel-stabilization properties of agar materials allow for efficient creation of demonstrative systems that host battery components along with enabling effective ion movement. The application of agar in lithium-ion batteries produces solid yet adaptable gel electrolytes that improve ionic movement alongside increased safety through decreased leakage and reduced fire hazard relative to conventional liquid electrolytes [252–254]. The environmentally friendly nature, alongside the plentiful availability, of agar makes it a desirable option for developing sustainable battery materials. Agar displays adaptability across various battery technologies while aiding electrode–interface stabilization and cycle-life enhancement in sodium-ion and zinc–air cells. Agar composites represent a significant advancement in battery technology by delivering advanced device performance and meeting environmental requirements for safe and sustainable energy storage systems [31,164,255].

Hazaana et al. fabricated biopolymer electrolytes from agar and lithium chloride (LiCl) by using the solution-casting technique to enhance solid-state Li-ion batteries. The 20 mol% agar and 80 mol% LiCl composition showed a high amorphous structure together with optimal ionic conductivity of $3.12 \pm 0.11 \times 10^{-2}$ S/cm and a glass-transition temperature of 37 °C, demonstrating superior battery performance. Both structural integrity and thermal stability with good cyclic stability were confirmed through extensive characterization using X-ray diffraction, Fourier transform infrared spectroscopy, differential scanning calorimetry, scanning electron microscopy, thermogravimetric analysis, and CV, which show the electrolyte is ready for primary and secondary Li-ion battery use [145]. Zuo et al. improved FZAB by designing an agar gel solid-state electrolyte that combines environmental sustainability with increased performance through a melamine-foam skeleton, resulting in a melamine–agar SSE structure. Through this innovative formulation, the electrolyte showed enhanced properties: improved mechanical strength and water retention alongside better ionic conductivity. They reported the FZAB outfitted with M-agar SSE reached an areal charge storage of 24 mAh cm^{−2} and delivered a maximum energy output of 126 mW cm^{−2}. Thanks to its powerful construction, this battery functions at exceptional levels under severe conditions, demonstrating compatibility with flexible electronics [26]. Lu et al. utilized an innovative agar-assisted sol–gel method to synthesize TiNb₂O₇ powders, successfully obtaining phase-pure samples at a calcination temperature of 800 °C, in contrast to the conventional solid-state technique, which required 1100 °C. This method resulted in enhanced particle morphology characterized by submicron sizes and porous structures, leading to improved electrochemical kinetics. Additionally, it increased the electrochemically active surface area, allowing the double-layer capacitance to reach 145 mF cm^{−2}, in contrast to 22 mF cm^{−2} achieved through the solid-state approach. TiNb₂O₇ synthesized using agar demonstrates exceptional discharge capacities and capacity retention in performance tests, highlighting its potential as a high-performance anode material for lithium-ion batteries [256].

Ji et al. enhanced SIB performance by creating nitrogen-distilled porous carbon materials from biomass agar, which underwent carbonization at various thermal settings (Figure 22). The NPC-900 variant demonstrated superior performance compared to other materials due to its optimal layer spacing and extensive surface area, resulting in enhanced anode functionality. Benchmarks indicated that NPC-900 exhibited exceptional performance due to its strong reversible capacity and impressive cycling characteristics. The implementation of Na₃V₂(PO₄)₃ in sodium battery storage applications offers significant advantages, achieving an impressive energy density of 267 Wh/kg [164]. Sowmiya and Shanthi synthesized agar–agar solid biopolymer membranes incorporating sodium nitrite, achieving an ionic conductivity of 5.07×10^{-3} S cm^{−1}. Primary sodium batteries utilizing agar–agar membranes demonstrated viability for power applications, achieving

open circuit voltages of 3.02 V with V_2O_5 and 2.69 V with MnO_2 cathodes [257]. Zhang et al. created agar/magnesium-carbonate-coated silicon nanocomposites to boost the performance of silicon anodes by improving electrical conductivity and minimizing volume expansion during lithium-ion battery operations. The amalgamation of self-solidifying agar with the electron-conducting surface generated by a lithium–magnesium alloy yields nanocomposites that reduce the propagation distance for lithium ions and electrons, thereby enhancing battery performance. Following 200 cycles at elevated current density, the improved composite exhibited an initial discharge capacity of $2060.2 \text{ mAh g}^{-1}$, accompanied by an 86.28% Coulombic efficiency, culminating in a reversible capacity of 801.5 mAh g^{-1} , thereby enhancing the longevity and efficiency of lithium-ion batteries [258].

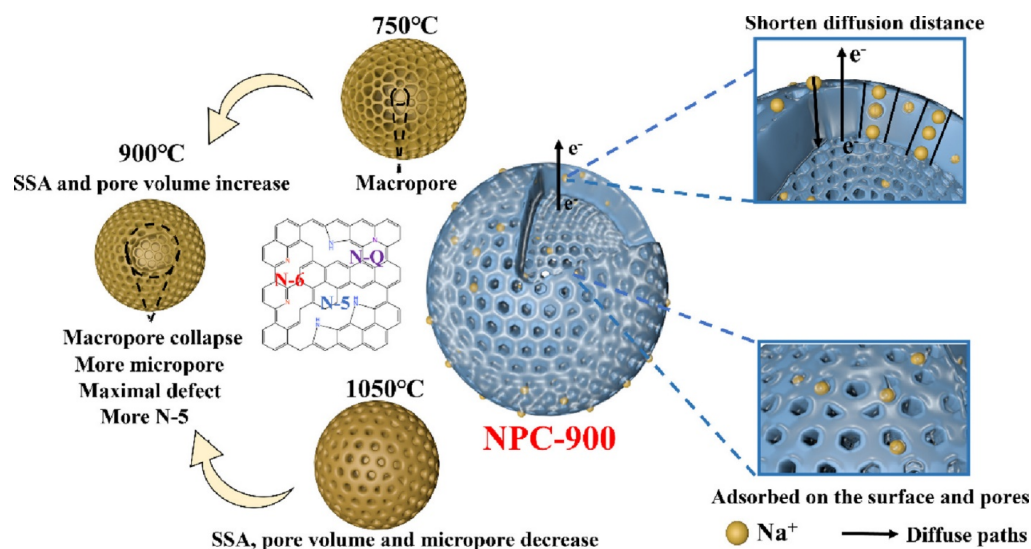


Figure 22. Enhanced performance of NPC-900 as SIB anode: achieving ultra-high reversible capacity and superior capacity retention due to optimal activation and nitrogen configuration (reproduced with permission) [164].

Lu et al. examined the electrochemical charge–discharge characteristics of $LiFePO_4$ ceramic particles in relation to their production parameters, while assessing the influence of agar concentration and calcination temperature on energy conversion mechanisms. Enhanced specific discharge capacities were seen as the agar concentration increased from 6 wt% to 12 wt% at a calcination temperature of 700°C , according to research findings. The ideal calcination temperature was 600°C , yielding the maximum specific discharge capacity of 147 mAh/g , in contrast to 133 mAh g^{-1} at 500°C and 142 mAh g^{-1} at 700°C . The synthesis of the $LiFePO_4$ phase commenced at temperatures as low as 500°C ; however, optimal electrochemical performance was achieved only at elevated temperatures, underscoring the significance of synthesis conditions in optimizing material functionality [259]. Another study utilized the image casting approach to fabricate an agarose– $Mg(ClO_4)_2$ polymer electrolyte containing $Mg(ClO_4)_2$ concentrations ranging from 0 to 35 wt%. A 30 wt% concentration of $Mg(ClO_4)_2$ yielded the maximum recorded ionic conductivity of $6.247 \times 10^{-4} \text{ S}\cdot\text{cm}^{-1}$. The polymer electrolyte exhibited elevated ionic conductivity at ambient temperature, indicating its potential for use in electrochemical energy storage systems [260]. Hu et al. presented a flexible $Zn || \text{PASMD-gel} || \beta\text{-MnO}_2$ battery where its architecture (Figure 23a) combines both electrolyte and separator in one freestanding PASMD film. Following cyclic-voltammetry scans between 0.1 and 1 mV s^{-1} (Figure 23b), sharp, symmetrical redox peaks enveloped by quasi-rectangular curves confirm a pseudo-capacitive response; $\log i$ vs. $\log \nu$ plots (Figure 23c) give b-values of 0.73 to 0.80, reflecting a mixed surface-controlled and diffusion-controlled charge-storage mechanism. The high

specific capacity of 205 mAh g^{-1} at 0.2 A g^{-1} and the good retention at higher currents can be observed in galvanostatic curves measured at different current densities (Figure 23d,e), whereas long-term testing (Figure 23f) retains 67 mAh g^{-1} after 1000 cycles at 1 A g^{-1} with $\sim 100\%$ Coulombic efficiency. Practicality is demonstrated by one cell illuminating a 0.3 W red LED at 1.8 V (Figure 23g) and two cells in series driving a 0.75 W white LED at 3 V (Figure 23h), both of which continue to work even when bent or when buried in the snow (Figure 23i,j). Taken together, these data demonstrate PASMD gel as a strong platform of high capacity, long life, and mechanical robustness for aqueous Zn batteries [261].

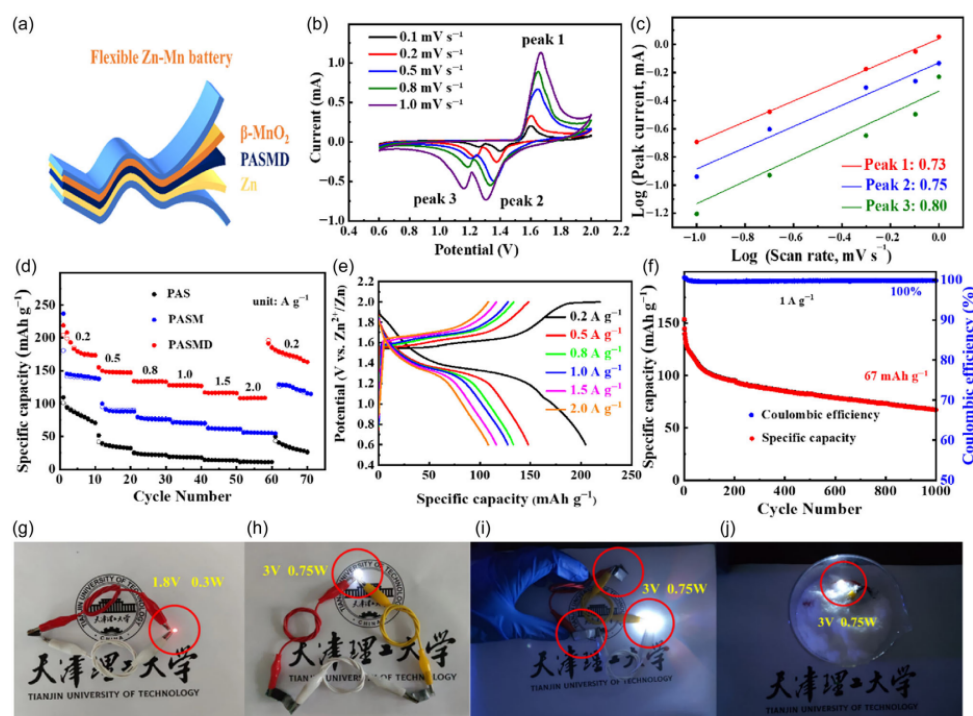


Figure 23. Electrochemical performance of the flexible battery Zn//PASMD//beta-MnO₂: (a) flexible battery configuration diagram; (b) CV curves at various scan rates; (c) log plots of peak current versus scan rate at different redox peaks; (d) analysis of rate capability; (e) GCD profiles at multiple current densities; (f) long-term cycling stability at 1 A g^{-1} ; (g) picture of a battery driving a 0.3 W red LED at 1.8 V ; (h) 3 V to light a 0.75 W white LED with two batteries in series; (i) flexibility of battery: a curved device drives a 0.75 W white LED at 3 V ; (j) operational stability exhibited by a battery buried in the snow, driving a 0.75 W white LED at 3 V (reproduced with permission) [261].

Mittal et al. presented a completely transient zinc-ion battery with an agarose-carboxymethyl cellulose (AG:CMC 50:50) hydrogel electrolyte, in which the agarose-based composite serves as an ion-conductive and biodegradable matrix (Figure 24a). The flexible battery assembled with a zinc metal anode and a polydopamine-modified activated carbon cloth (CC-AC/PDA) cathode, offered an initial capacity of 264 mAh g^{-1} at 0.5 A g^{-1} , and retained $\sim 197 \text{ mAh g}^{-1}$ after 1000 cycles, as shown in the Figure 24a(I,II). EIS (Figure 24a(III)) showed that the hydrogel electrolyte exhibited a greater resistance of ~ 6.80 compared to 2.450 for the liquid electrolytes due to moderate wettability of the cathode by the hydrogel. The agarose-based electrolyte remarkably allowed long-term cycling stability, maintaining more than 10,000 cycles at 1 A g^{-1} (Figure 24a(IV)). Additionally, the pouch-cell structure, which was packaged in agarose (Figure 24a(VI)), had an open-circuit voltage of $\sim 1.1 \text{ V}$ (Figure 24a(VII)) and exhibited a capacity of $\sim 157 \text{ mAh g}^{-1}$ after 200 cycles at 50 mA g^{-1} (Figure 24a(V)). This research indicates the importance of agarose composites in offering ionic conductivity, mechanical flexibility, and environmental degradability for sustainable and high-performance transient ZIBs [262]. Li et al. designed a

flexible ZAB that can operate at low temperatures; the gel electrolyte is composed of polyacrylamide/agar/dimethyl sulfoxide (PAAm/agar-DMSO). The ionic conductivity of this gel electrolyte was 24 mS cm^{-1} at -30°C , which makes it suitable for cold-temperature batteries. The flexible ZAB provided reproducible power densities of 57.14, 34.30, and 30.34 mW cm^{-2} at 25°C , 0°C , and -30°C , respectively (Figure 24b(I)), and only a slight loss of discharge plateau (147 mV) and specific capacity of 212.8 mAh g^{-1} between 25°C and -30°C (Figure 24b(II)). The thermal adaptability of the device in response to changes in temperature was excellent through charge–discharge cycling, which kept the voltage profiles stable (Figure 24b(III)). Also, the device showed strong cycling characteristics at 25°C to 50 h and at -30°C to 45 h at 1 mA cm^{-2} (Figure 24b(IV)). Practical feasibility was demonstrated with the battery able to power an LED at -30°C and maintain a stable energy supply in extreme cold (Figure 24b(V)). This work proposes a successful approach to developing flexible ZABs with the ability to work reliably in subzero conditions [263]. In a study already reported in this section, Mittal et al. systematically correlated the electrochemical behavior of their agar-based composite (AG:CMC 50:50) hydrogel electrolyte with four diagnostic measurements (Figure 24c(I–IV)). With the hydrogel protective at $1 \text{ mA cm}^{-2}/1 \text{ mAh cm}^{-2}$, the flat 40 mV polarization of the hydrogel-protected Zn | Zn cell is observed for over 4000 h = 2000 cycles, but the liquid 2 m ZnSO_4 cell shorts after 605 h. The endurance at a moderate setpoint of $0.25 \text{ mA cm}^{-2}/0.25 \text{ mAh cm}^{-2}$ is confirmed in Figure 24c(II), which reveals that the lifetime can exceed 8500 h without voltage drift. To investigate plating kinetics, Figure 24c(III) shows chrono-amperometry throttled to -150 mV : the hydrogel cell shows a finer, smoothly softening current, due to its controlled two-dimensional nucleation and flat Zn^{2+} distribution, whereas the liquid cell shows a larger diffusion-limited current attributed to dendritic growth. In Figure 24c(IV), post-mortem analysis reveals the presence of $\text{Zn}_4(\text{OH})_6\text{SO}_4 \cdot 5\text{H}_2\text{O}$ (in situ electrodeposited) only on the respective electrodes, meaning that the beneficial effect of the hydrogel platform lies in conformity (mechanically) and Zn^{2+} -coordinating behavior and not in changed corrosion chemistry. Collectively, panels a–d clearly show that the inert AG:CMC matrix provides non-coring, long-lasting Zn cycling that outperforms mainstream as well as many so-called, non-transient strategies [262].

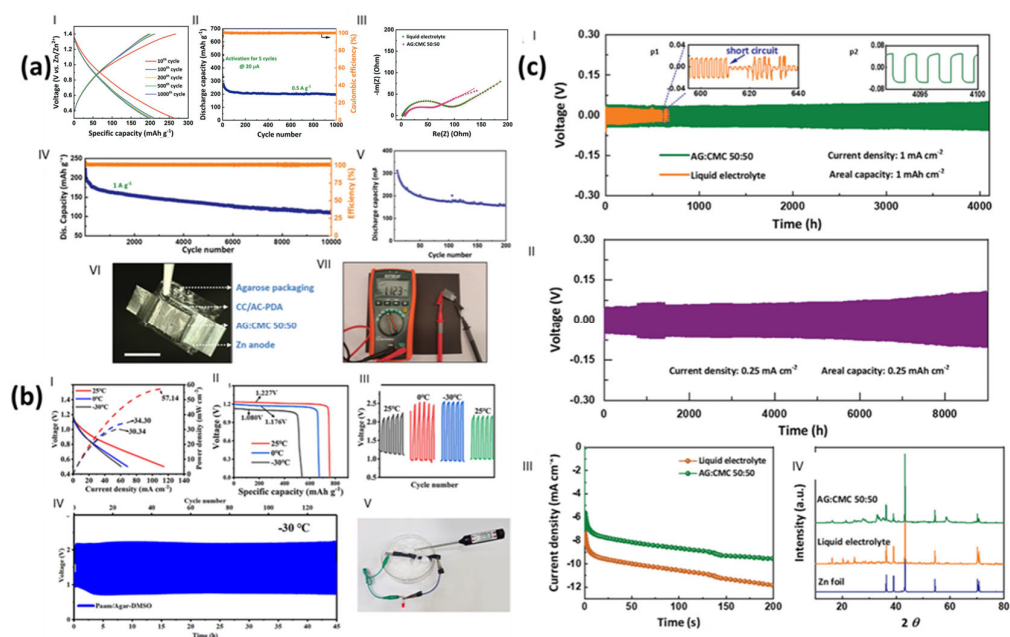


Figure 24. (a) The electrochemical properties of the Zn-ion battery with a Zn anode, CC-AC/PDA cathode, and AG:CMC 50:50 hydrogel electrolyte: (I) galvanostatic charge/discharge curves of 0.5 A g^{-1} ;

(II) matching cycling performance over 1000 cycles; (III) EIS spectra of ZIBs with glass-fiber-liquid electrolyte and hydrogel electrolyte; (IV) duration of cycling at 1 A g^{-1} over 10,000 cycles. Description of the fabricated pouch cell with Zn anode, CC-AC/PDA cathode, AG:CMC 50:50 hydrogel electrolyte, and agarose packaging; (V) cycling activity at 50 mA g^{-1} ; (VI) digital picture of the pouch cell (scale bar = 1 cm); (VII) pouch-cell open-circuit voltage (reproduced with permission) [262]. (b) PAAm/agar-DMSO-based flexible Zn-air batteries' electrochemical behavior at different temperatures: (I) discharge and power-density curves; (II) specific discharge capacity at various working temperatures; (III) cycling performance at different temperatures; (IV) cycling stability of PAAm/agar-DMSO-based ZABs over the long term at -30°C ; (V) pictures with LED illumination at -30°C (reproduced with permission) [263]; (c) Zn/Zn symmetric cells at room temperature with an AG:CMC (50:50) hydrogel (blue) versus 2m ZnSO_4 liquid electrolyte (orange): (I) $1 \text{ mA cm}^{-2} | 1 \text{ mAh cm}^{-2}$ voltage trace; insets show the liquid-cell short at 605 h (p1) and the polarization of the hydrogel at 4000–4100 h (p2). (II) $0.25 \text{ mA cm}^{-2} | 0.25 \text{ mH cm}^{-2}$. (III) Chronoamperometry at -150 V along with post-cycling XRD of the Zn anodes (reproduced with permission) [262].

Wang et al. showed that P-doped hard carbon (P-HC-2) based on agar has a unique puparium-like nano-morphology that supports slope-dominated Na^+ storage essential to high-performance SIB anodes. CV (Figure 25a) at 0.2 mV s^{-1} showed irreversible SEI formation in the initial cycle, but subsequent cycles were remarkably reversible. The materials all had slope-dominated profiles (Figure 25b), with P-HC-2 recording a record slope capacity of 363 mAh g^{-1} (vs. 238 mAh g^{-1} undoped HC; Figure 25c) owing to increasing interlayer distance (3.91 \AA), reducing lateral size (9.4 nm), and P=O/P-C functional groups that improve surface adsorption. At 0.1 A g^{-1} , P-HC-2 showed a capacity of 394 mAh g^{-1} and maintained 310 mAh g^{-1} after 500 cycles (Figure 25d), and a high rate capability (140 mAh g^{-1} at 5 A g^{-1} ; Figure 25e). It was also astounding that it retained 178 mAh g^{-1} after 10,000 cycles at 5 A g^{-1} (Figure 25f), among the best in biomass-derived carbons. The kinetic analysis (Figure 25g,h) as well as GITT (Figure 25i,j) confirmed that 90% of the contribution is pseudocapacitive at 8 mV s^{-1} and that Na^+ diffusion was faster in P-HC-2 than in HC due to defect-rich surfaces. Lower charge-transfer resistance and improved wettability caused by P-doping were also confirmed by EIS (Figure 25k,l) [236]. The same work also demonstrated the practical feasibility of the P-HC-2 anode developed by Wang et al. by assembling and testing a working sodium-ion battery using a commercial cathode $\text{Na}_3\text{V}_2(\text{PO}_4)_3$ (NVP), as shown in Figure 26a. The full cell (NVP//P-HC-2) was cycled between 1.5 V and 3.9 V based on half-cell performance (Figure 26b) (NVP: $\sim 90 \text{ mAh g}^{-1}$ at $\sim 3.5 \text{ V}$ vs. Na/Na^+ P-HC-2: $\sim 400 \text{ mAh g}^{-1}$). This structure provided a large reversible capacity of 132 mAh g^{-1} and a remarkable energy density of 261 Wh kg^{-1} at 0.05 A g^{-1} (capacity based on total electrode mass; Figure 26c). The cell showed a respectable rate capability (Figure 26d): capacities of 123, 92, 68, 54, and 47 mAh g^{-1} at 0.1, 0.2, 0.5, 1.0, and 1.5 A g^{-1} , respectively, with good recovery (120 mAh g^{-1} on recharging at 0.1 A g^{-1}). Moreover, the complete cell showed remarkable cycling stability (Figure 26e) retaining 111 mAh g^{-1} after 100 cycles at 100 mA g^{-1} from an initial 128 mAh g^{-1} (86% retention). Importantly, a button-packaged NVP//P-HC-2 cell was able to power an electronic watch (Figure 26f), highlighting its functionality, meaning the watch can withstand pressure up to 5 atmospheres (non-english part). The overall results show that the low-cost P-HC-2 is a very promising anode candidate for commercial sodium ion batteries. This paper highlights agar as a sustainable precursor of morphology-engineered carbons, in which P-doping and pore-structure control can be achieved simultaneously to deliver ultrafast kinetics and record longevity. The slope-dominated design removes plating risks and graphite-layer collapse, making P-HC-2 well suited to fast-charging SIBs. This method opens the path to cost-effective, bio-derived anodes in commercial sodium-ion batteries owing to scalable low-temperature synthesis (750°C) and demonstrable full-cell viability [236].

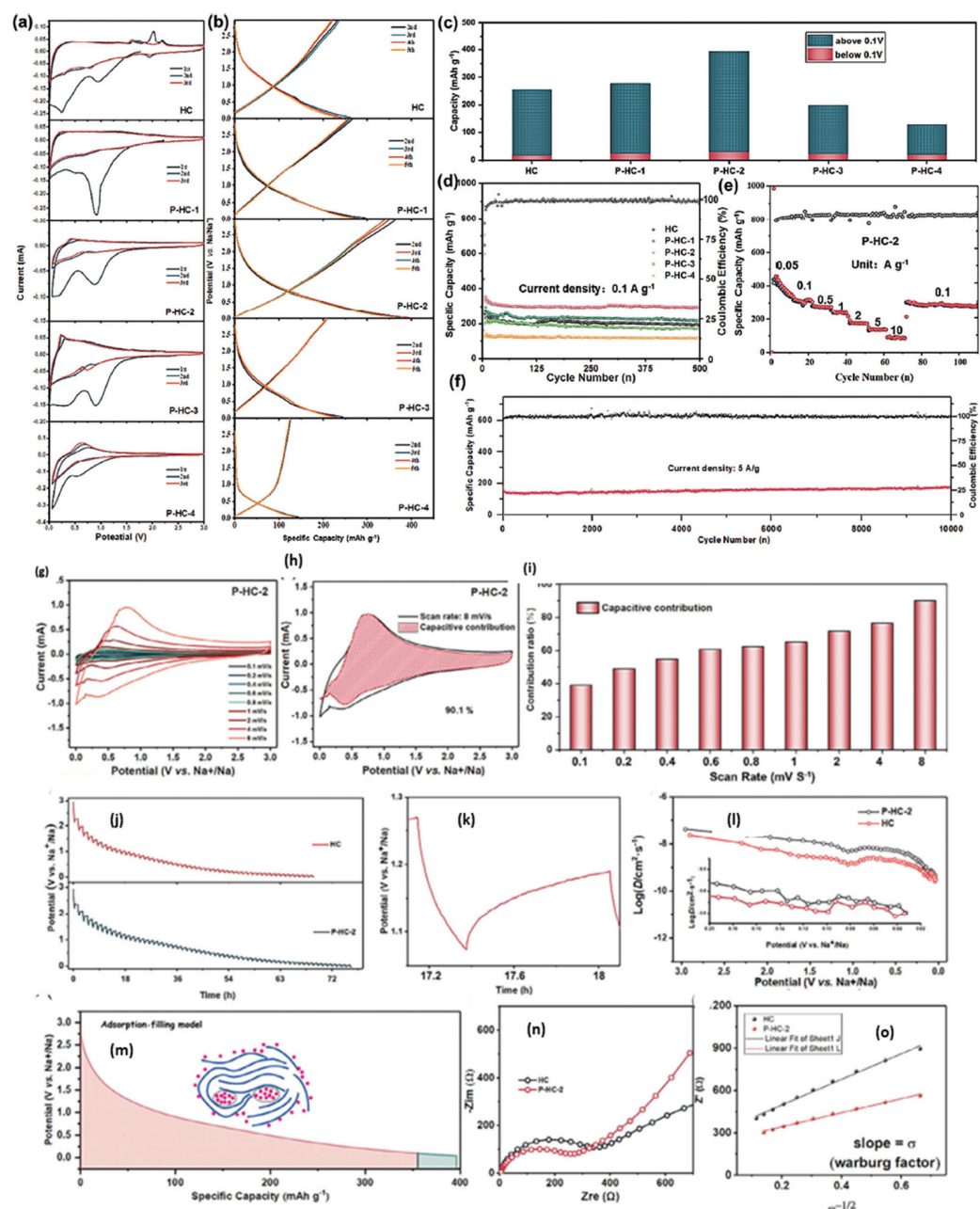


Figure 25. Half-cell electrochemical performance: (a) CV curves of HC and P-HC-*x* electrodes; (b) HC and P-HC-*x* electrode discharge/charge voltages at 0.1 A g^{-1} ; (c) comparison of the contributions of the capacitors above and below 0.1 V for HC and P-HC-*x* electrodes; (d) HC and P-HC-*x* electrodes cycling stability at 0.1 A g^{-1} ; (e) the rate capability of the P-HC-2 electrode tested at different current densities (0.1 to 5 A g^{-1}); (f) long cycle life of P-HC-2 at a high current density of 5 A g^{-1} . Kinetic analysis (g–o): (g) CV curves of P-HC-2 at various scanning rates; (h) capacitive contribution of P-HC-2 at the scanning rate of 8 mV s^{-1} calculated from the CV; (i) capacitive contribution of P-HC-2 calculated from the CV curves at various scan rates; (j) galvanostatic intermittent titration technique (GITT) curves of HC and P-HC-2; (k) high-magnification GITT curve of P-HC-2 during discharge; (l) Na-ion diffusion coefficients computed as a function of voltage for the HC and P-HC-2 anodes during discharge; (m) P-HC-2 mechanism of Na^+ storage; (n) Nyquist plots of EIS and the fitted data of HC and P-HC-2; (o) the fitted EIS results (reproduced with permission) [236].

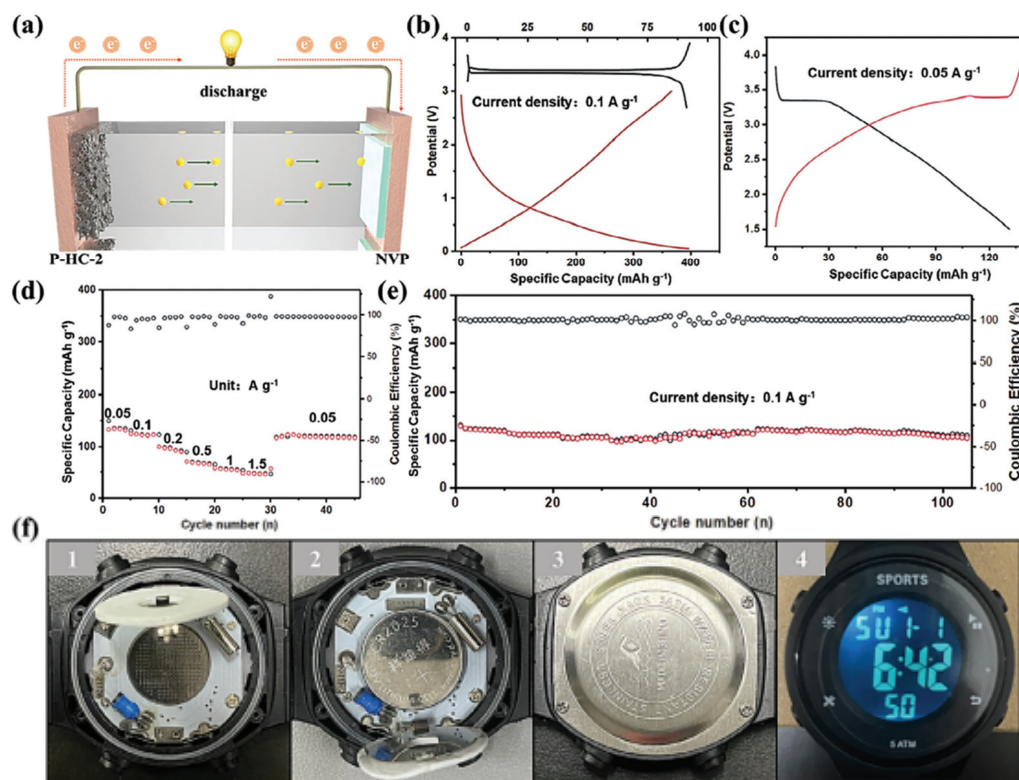


Figure 26. Full-cell electrochemical performance: (a) NVP//P-HC-2 full-battery system outline; (b) charge–discharge voltages of the single electrodes: P-HC-2 anode (down curve) 0.1 A g^{-1} and the NVP cathode (up curve) 0.1 A g^{-1} ; (c) charge–discharge voltage curves of NVP//PHC-2 full cell at 0.05 A g^{-1} ; (d) rate performance; and (e) cycling performance of the full cell between 1.5 and 3.9 V. (f) Photographs showing a button-type full cell powering an electronic watch (5 ATM) (reproduced with permission) [236].

Yang et al., as shown in Figure 27a, initially depict the complete constructed flexible Zn–air pouch cell where agar–PVA/GO gel electrolyte is placed between a Zn-foil anode and a breathable air cathode, indicating the thin, flexible structure needed in wearable electronics. The open-circuit voltage (OCV) of the two versions, alkaline and neutral, is monitored over time (Figure 27b): the alkaline cell has a higher initial potential, but the neutral cell exhibits a nearly constant OCV over 300 h, indicating better resistance to Zn corrosion and dendrite formation. Electrochemical polarization data in Figure 27c show that the charge–discharge gap in the alkaline electrolyte is much narrower—this translates, through the Ragone-type analysis in Figure 27d, to a peak power density of 123.7 mW cm^{-2} versus just 11.3 mW cm^{-2} in the neutral cell. Figure 27e also demonstrates reversible kinetics by rate-capability tests showing that discharge voltages of both chemistries scale with current density and recover when the load is stepped back. Another key feature brought out by Figure 27f is the durability trade-off: at 0.5 mA cm^{-2} the neutral cell lasts 30.4 h and delivers $595.8 \text{ mAh g}^{-1} \text{ Zn}$, whereas the alkaline higher-voltage version only lasts 5.8 h at $230.6 \text{ mAh g}^{-1} \text{ Zn}$. With the power of each complementing the other, one neutral and one alkaline cell were connected in series, giving a total OCV of 2.28 V, sufficient to drive an LED array (Figure 27h). Lastly, the series stack continues to illuminate LEDs upon bending angles evaluated in Figure 27i at 0° , 45° , 90° , and 180° , confirming that the agar–PVA–GO gel also offers electrochemical stability and mechanical strength required for the creation of practical and bendable energy storage devices [163].

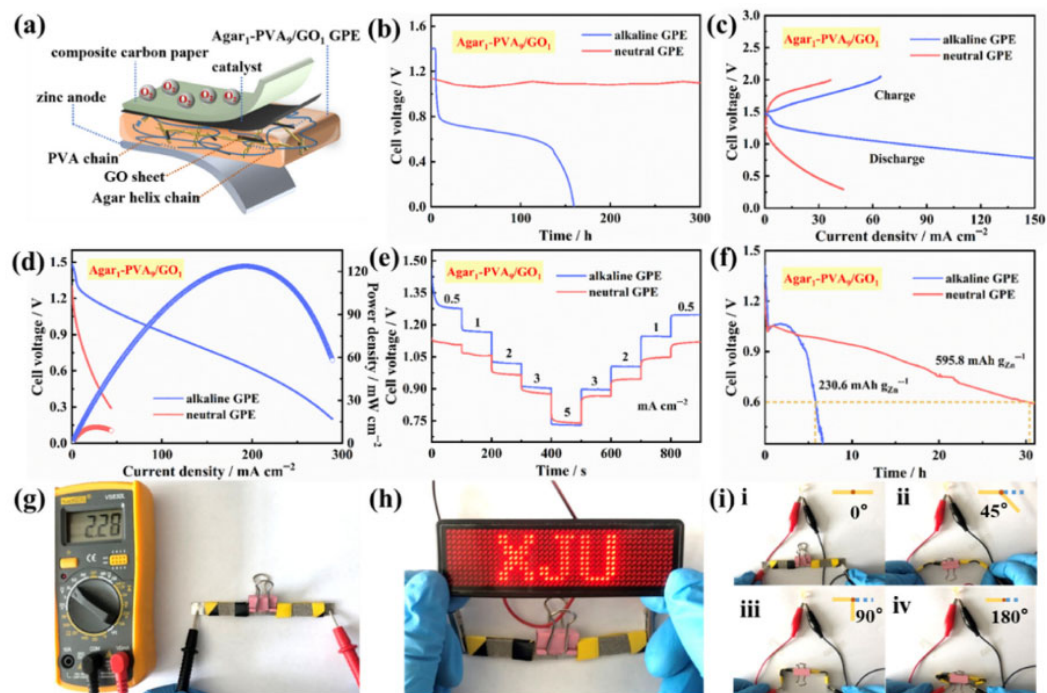


Figure 27. Electrochemical behavior of neutral and alkaline FZABs: (a) sandwich-type FZAB structure using GPE; (b) open-circuit voltages; (c,d) discharge polarization power density; (e) discharge curves between 0.5 and 5 mA/cm²; (f) constant-current discharge curve at a current density of 0.5 mA/cm² (cut-off voltage: 0.6 V). Examples of the neutral and alkaline FZABs: (g) picture of a neutral FZAB and an alkaline FZAB in series with OCV = 2.28 V; (h) series-connected cells powering the LED; (i) image of series-connected cells illuminating the LED at various bending angles of 0°, 45°, 90°, and 180° (reproduced with permission) [163]. Tables 5 and 6 show the various types of agar-based hybrids, and their potential uses in different types of batteries and fuel cells, respectively.

Table 5. Different types of agar-based hybrids and their applications in various types of batteries.

Composite	Role in Battery	Battery Type	Performance Metrics	Ref.
Melamine–agar SSE	Solid-state electrolyte with enhanced mechanical and electrochemical properties	FZAB	Maximum output power: 126 mW/cm ² ; Areal capacity: 24 mAh/cm ² ; improved mechanical strength, water retention, and ionic conductivity; stable performance under extreme conditions	[26]
Agar–polyacrylamide hydrogel polymer electrolyte	Electrolyte for ion transport and mechanical flexibility	Flexible quasi-solid-state aqueous lithium–zinc hybrid ion batteries	Ionic conductivity: high; electrochemical stability: broad window; ion migration number: notable; symmetric cell cycling stability: 350 h at 1 mA/cm ² ; full battery cycle life: retains 80.5% capacity after 500 cycles at 1 C	[264]
CPE3: Ce-LLZO, chitosan/agar–agar, PEG, LiClO ₄	Solid-state polymer electrolyte	Lithium-ion batteries	Lithium-ion conductivity: 5.18×10^{-3} S cm ⁻¹ ; transference number: 0.937; electrochemical stability: up to 4.1 V; coin-cell discharge capacity: 163 mAh/g over 100 cycles at 0.1 C; symmetric cell stability: 550 h at 2.0 mA/cm ²	[265]
Heteroatom-codoped carbon aerogels (ON-CA with O, N, B)	Electrode material	Supercapacitors and ion batteries	Specific capacity and capacitance optimized; contact angle: 9.26° indicating enhanced wetting ability; adsorption capacity: −1.62 eV; diffusion barrier: 0.12 eV for K ⁺ ; energy density: 51.8 Wh kg ⁻¹ ; power density: 443 W kg ⁻¹ ; cycling stability: maintains 83.3% capacity after 10,000 cycles in 1 M KPF6	[206]
Agar-derived carbon/NH ₄ F@nanosilicon composites	Anode material	High-energy-density lithium-ion batteries	First discharge capacity: 2001.0 mAh·g ⁻¹ at 500 mA g ⁻¹ ; residual capacity: 836.7 mAh·g ⁻¹ after 200 cycles; enhanced cyclic stability and electrical conductivity post-NH ₄ F modification	[266]

Table 5. Cont.

Composite	Role in Battery	Battery Type	Performance Metrics	Ref.
Polysulfone/agarose bi-functional protective layer	Protective layer for anode	Zinc-ion batteries	Uniform electric field and Zn^{2+} distribution; low desolvation energy and nucleation overpotential; excellent cycling performance: 4200 h at $1 \text{ mA cm}^{-2}/1 \text{ mAh cm}^{-2}$, 1000 h at $5 \text{ mA cm}^{-2}/5 \text{ mAh cm}^{-2}$; high stability in full cell with ZnVO cathode: maintains 72% capacity after 7000 cycles at 10 A g^{-1}	[267]
Agar interface layer on Zn foil	Interface modification for anode	Aqueous zinc-ion batteries	Enhanced Zn^{2+} desolvation and uniform deposition; reduced hydrogen evolution and corrosion	[268]
Agarose/PVA mesoporous membrane	Separator	SIB	Outperforms conventional separators in thermal stability, electrolyte wettability, and Na^{+} conductivity; limits dendrite growth; stable operation at $200 \mu\text{A cm}^{-2}$; superior performance in $\text{Na}_3\text{V}_2(\text{PO}_4)_3/\text{Na}$ half-cells: 108 mAh g^{-1} after 50 cycles at C/10, with remarkable rate capability	[269]
High-modulus agarose gel electrolyte	Electrolyte	Zinc-ion batteries	Enhances the coordination environment of Zn^{2+} ; reduces H_2O molecule mobility and sulfate ion diffusion; significantly mitigates dendrite formation and inhibits zinc hydroxysulfate by-product	[25]
Ultra-thin polymer electrolyte based on single-helical-structured agarose	Electrolyte	Solid-state lithium batteries	Ionic conductivity: $1.2 \times 10^{-4} \text{ S cm}^{-1}$; tensile strength: 5.5 MPa; thickness: $<32 \mu\text{m}$; Li symmetric-cell cycle life: 600 h at room temperature; $\text{LiFePO}_4/\text{Li}$ battery capacity: 131 mAh g^{-1} over 600 cycles at 1.0 C, retention rate of 92.9%	[270]

7.3. Agar-Based Composites in Fuel Cells

Agar showcases significant advancements in fuel cell technology with patented innovations in membrane structures and electrodes. The robust gelling capability, coupled with its hydrophilic nature, enables agar to function effectively as a foundational material for sophisticated gel polymer electrolytes, enhancing proton conductivity and reducing methanol crossover in fuel cells. Different agar-matrix electrolytes demonstrate their potential as substitutes for synthetic polymers due to their biodegradability and the sustainable environmental benefits they offer [30,271–273]. Through experimentation, it was demonstrated that agar combined with various ionic dopants resulted in enhanced ionic conductivity and thermal stability, making these composite materials ideal candidates for proton-exchange membrane (PEM) construction and fuel cell electrode binders. The use of agar in fuel cell technology integrates environmental sustainability with chemical stability and cost-effectiveness, while also minimizing ecological harm, serving as an alternative material that promotes the progress of green energy initiatives [67,247,271,274].

Lee et al. enhanced the performance of aluminum–air batteries by incorporating agar into the 4 M NaOH electrolyte, effectively reducing self-corrosion and improving fuel efficiency. SEM imaging and computational simulations reveal that the agar film, which adheres to aluminum surfaces through physisorption, offers corrosion protection with an efficiency of 62.8% and enhances fuel efficiency to 35.95%. The validation of agar's effectiveness as an electrolyte additive was achieved through experimental hydrogen evolution tests, as well as DFT and electrochemical assessments [275]. Hernández-Flores et al. found that studies on agar membranes in microbial fuel cells indicated performance improvements at a 4 wt% agar concentration, which reached a peak. However, the addition of KCl during the process did not provide any performance benefits and often led to diminished results. The optimal outcomes for microbial membranes were achieved using pure agar membranes, which notably lowered costs compared to Nafion® 117 [276]. The proton-conducting membrane Park et al. created uses agar, polyethylene oxide (PEO), and silica aerogel. Silica aerogel particles were uniformly dispersed within the agar/PEO matrix during the membrane casting process conducted. The membrane had a room-temperature conductivity of $1 \times 10^{-3} \text{ S cm}^{-1}$ before heat processing, and surface tuning

improved its performance [277]. According to Boopathi et al., solution casting facilitated the fabrication of proton-conducting polymer electrolytes utilizing agar combined with NH_4NO_3 . Upon the incorporation of 60 wt% of NH_4NO_3 , the electrolyte achieved its peak ionic conductivity at room temperature, measuring $6.57 \times 10^{-4} \text{ S cm}^{-1}$, which further increased to $1.09 \times 10^{-3} \text{ S cm}^{-1}$ at 70°C . This specific polymer facilitated a fuel cell's generation of 558 mV output in the absence of a connected load [67].

John conducted a study that developed and evaluated both a clay-based PEM microbial fuel cell and an agar-based equivalent to assess their efficacy in energy generation and pollution reduction in wastewater. The CB-MFC delivered both higher power density at 80.86 mW/m^2 and superior COD treatment efficiency at 64.2% when measured against the performance demonstrated by agar-MFC which achieved 20.93 mW/m^2 and 59.53% removal efficiency. Response surface methodology optimization demonstrated that specific temperature parameters combined with the right pH levels and concentrations resulted in boosted power density and improved COD elimination performance of the clay-based cell. The CB-MFC achieved better results thanks to its superior proton conductivity properties [278]. An et al. developed a unique thermally sensitive agar-based chemical hydrogel binder for clean energy fuel cells, composed of agar, glutaraldehyde, and acetic acid. This novel binder enhances traditional Nafion ionomer-based electrodes by improving fuel cell performance through superior mass and charge transport, all while being cost-effective [65]. Christwardana and Kuntolaksono et al. investigated agar encapsulation as a method for utilizing the yeast *Saccharomyces cerevisiae* in microbial fuel cells. Yeast immobilization in an agar matrix at a concentration of 11.7 mg/mL enables the efficient production of extracellular electrons without the need for external electron mediators. The system functioned for 23 h, generating a current density of 7 mA/m^2 and an MPD output of 0.91 mW/m^2 in this configuration. Agar-immobilized yeast shows significant promise for the advancement of sustainable microbial fuel cells, with a K_m value of $9.15 \pm 1.01 \text{ mg/mL}$, sensitivity measurements of $0.39 \pm 0.03 \text{ (mA/m}^2\text{)/(mg/mL)}$, and maximum current density values of $3.53 \pm 0.16 \text{ mA/m}^2$ [279]. Mai et al. conducted comparative tests on oriented microbial fuel cells (MFCs) by exploring different types of agar–agar and salt additives to assess their impact on efficiency improvement. The MFC configuration, utilizing two chambers with 12% agar, achieved a maximum voltage output of 337.25 mV and a COD removal rate of 64.58%. The study indicated that salt bridges formed with NaCl exhibited greater efficiency compared to those made with KCl. Scientific findings indicate that agar–agar usage is advantageous for microbial fuel cell operations, while also establishing baseline parameters for salt bridge studies in fuel cells [280]. Uddin et al. (2025) [281] investigated the performance of dual-chamber microbial fuel cells (MFCs) using sludges from drains, a textile effluent treatment plant, and the Buriganga River. The MFCs, operating under aerobic conditions with an agar salt bridge for proton exchange, demonstrated the best electrical performance with a maximum voltage of 244.88 mV and current density of 35.16 mA/m^2 . The BOD5 reduction varied, with the highest reduction of 50.15% observed in the drain sludge. The study also documented counts of *Escherichia coli* and *Bacillus subtilis* in the sludges [281].

Zou et al. systematically tested the thermo-electrochemical behavior of an air-breathing direct methanol fuel cell (DMFC) with an agar–wood gel/sponge fuel absorber (Figure 28). Polarization and power curves (Figure 28a,b) show sharp improvement between 22°C and around 70°C : the open-circuit potential (OCP) rises to 0.70 V and the current density at 0.05 V rises to 234 mA cm^{-2} (Figure 28c,d). Based on this, the peak power density increases fourfold to 26.5 mW cm^{-2} (Figure 28e). Both OCP and current density decrease above 70°C , which can be explained by an increased rate of methanol crossover across the Nafion[®] membrane and the consequent mixed potential at the cathode. At high current

densities, the high-temperature data also become noisy, probably due to turbulence in the ambient airflow disrupting oxygen transport in the open-cathode geometry. Thermal survivability is confirmed by Figure 28f–h: following a test run at 80 °C, the membrane-electrode assembly (MEA) as well as the composite exhibit no structural damage, proving that the absorber has a strong immobilizing effect on the fuel and allows it to absorb thermal stress far beyond normal ambient conditions (<50 °C). On scaling up, a four-cell flexible DMFC stack (Figure 29a,b) first provides an OCP of 1.79 V and Pmax of 145 mW (Figure 29c). The damaged stack has an OCP of 1.48 V and Pmax of 52 mW, with no flame, sparks, smoke, or fuel leakage after being fully pierced by the needle with cut edges. Flexibility tests (Figure 29d,e) demonstrate that the stack, with laceration and sharp bending, powered 15 LEDs, and, importantly, remained leak-free under approximately 29.4 kPa compression. This demonstrates that the high methanol retention recorded at the composite level is directly transferred to device safety and omnidirectional functionality. Collectively, Figures 28 and 29 indicate that the addition of an agar-wood gel/sponge matrix significantly increases thermal tolerance, mechanical durability, and practical energy density (13.7 mWh cm^{-2}) in air-breathing DMFCs, suggesting safe, orientation-independent power sources for flexible and wearable electronics [282].

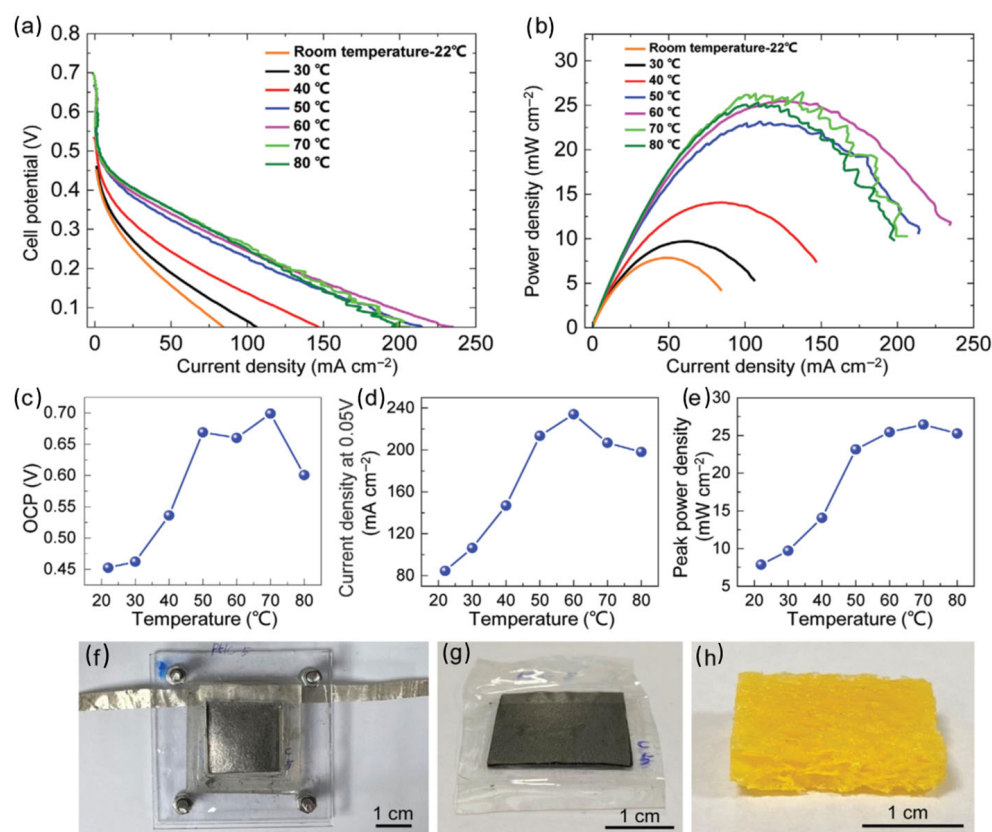


Figure 28. Air-breathing DMFC performance of the composite material at various temperatures: (a) polarization curves at various temperatures; (b) power density at various temperatures; (c) OCP vs. temperature; (d) current density at 0.05 V; (e) peak power density versus temperature; (f) the composite material after measurement of air-breathing DMFC at 80 °C; (g) MEA post-measurement at 80 °C; (h) the composite material measured at 80 °C [282].

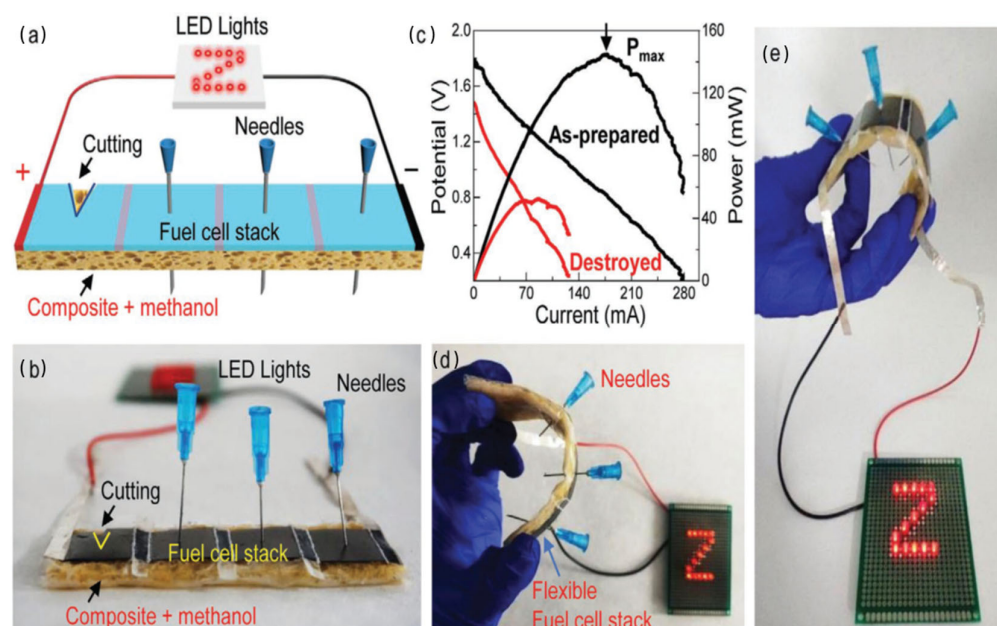


Figure 29. Destructive tests of the DMFC stack composed of composite material and 1.5% agar gel: (a) plan of the destructive experiment. The edge of the first cell is punctured, and the 2nd, 3rd, and 4th cells are pierced by needles, (b) operating condition of a DMFC stack with 4 single cells being manufactured from composite material with 1.5% agar gel; (c) pre- and post-destructive testing performance of the DMFC stack; (d) top view of DMFC stack during destructive experiment; (e) front view of DMFC stack under destructive testing (reproduced with permission) [282].

Table 6. Different types of agar-based hybrids and their applications in various types of fuel cells.

Composite	Role in Fuel Cell	Fuel-Cell Type	Performance Metrics	Ref.
Agar (2, 4, 6, 8 wt%) and agar + KCl (2–8 wt% agar, 10 wt% KCl), agar 2 wt% + KCl (2–10 wt%)	Membrane material and ionic-salt enhancement	Microbial fuel cells	Increase in proton conductivity and O ₂ permeability up to 4 wt% agar; beyond 4 wt% agar, conductivity levels off and O ₂ permeability increases; addition of KCl negatively affects O ₂ permeability; no significant conductivity increase with higher KCl concentrations; worsened O ₂ permeability with higher KCl.	[276]
Agar with immobilized yeast <i>S. cerevisiae</i>	Bio-catalyst for electron transfer	Microbial fuel cells	Current density: 7 mA/m ² in 23 h; maximum power density (MPD): 0.91 mW/m ² ; Km: 9.15 ± 1.01 mg/mL; sensitivity: 0.39 ± 0.03 (mA/m ²)/(mg/mL); Jmax: 3.53 ± 0.16 mA/m ²	[279]
Agarose (4 wt%) in anodic catalyst layer	Enhancer of hydrophilicity and performance under low humidity	PEM fuel cells	Improved low-humidity performance; current density of 960 mA/cm ² at 0.6 V and 500 mA/cm ² at 0.7 V; minimal degradation after 10 h (960 to 840 mA/cm ²) compared to sharp decline in blank MEA without agarose.	[283]
Agar hydrolysate (galactose and glucose)	Renewable carbon source for electricity production	Microbial fuel cells	Enhanced sugar yield with increased HCl concentration, autoclaving temperature, and time; used in a two-compartment MFC reactor to examine the potential of agar as a renewable electricity source.	[284]
Agar chemical hydrogel (ACH) with glutaraldehyde and acetic acid	Electrode binder	Fuel-electrolyte-fed fuel cells	Enhanced mass/charge transport due to hydrophilic nature and water retention of agar; improved cell performance compared to Nafion ionomer-based electrodes, suggesting potential as a cost-effective alternative.	[65]
Agar with 50 M wt% NH ₄ Br	Ion-conducting matrix	PEM fuel cells and batteries	Ionic conductivity: 1.33 × 10 ^{−4} S cm ^{−1} ; temperature dependence follows Arrhenius law; high ionic transference numbers; electrochemical stability confirmed via linear sweep voltammetry; battery output: 1.80 V; PEMFC output: 500 mV	[285]
Agar–Agar with 50 wt% NH ₄	Electrolyte	Electrochemical cells and PEM fuel cells	Conductivity: 1.20 × 10 ^{−4} S/cm; electrochemical cell output: 1.73 V; PEM fuel cell output: 408 mV	[286]

Table 6. Cont.

Composite	Role in Fuel Cell	Fuel-Cell Type	Performance Metrics	Ref.
Agar with 2% ACPC (activated carbon from pine cones)	Salt bridge for ion transfer	Microbial fuel cells	Optimum performance in MFC-1 with open circuit voltage: 421 mV; current: 1.052 A; power density: 61.51 mW/m ² ; COD removal efficiency: 65.84%; stable performance up to day 12, operational up to day 20.	[287]
Agar doped with 40 mol% NH ₄ Cl	Solid polymer electrolyte	Batteries and fuel cells	Ionic conductivity: 4×10^{-3} S cm ⁻¹ ; ionic transference number: 0.99; battery output voltage: 1.89 V; fuel cell output voltage: 541 mV.	[24]
Agar salt bridge with sludges from various sources	Proton-exchange medium	Dual-chamber microbial fuel cells	Best performance with Buriganga sludge: voltage: 244.88 mV, current density: 35.16 mA/m ² , power density: 8.61 mW/m ² ; BOD5 reduction: drain (50.15%), textile plant (43.64%), tannery (47.32%), Buriganga River (35.20%).	[281]

8. Future Perspective

Agar-based composites, as biopolymer alternatives, are gaining significant attention in energy storage devices due to their environmentally friendly nature and promising electrochemical properties. These materials offer unique advantages such as biodegradability, cost-effectiveness, and the potential for enhanced ionic conductivity. However, challenges related to electrochemical stability, mechanical robustness, and scalability must be addressed for their wider adoption. Future research should focus on improving these properties while integrating agar with other materials to boost performance.

- Research should focus on enhancing the electrochemical stability of agar-based composites to prolong their operational life and performance during charge–discharge cycles.
- Enhancing the mechanical properties of agar composites is essential to increase their durability and withstand the stresses encountered in real-world applications.
- Developing scalable fabrication techniques and optimizing the cost of production for agar-based systems will help facilitate their commercialization and widespread adoption.
- Agar's biodegradable nature positions it as a promising material for sustainable energy storage solutions, with less environmental impact compared with traditional synthetic polymers.
- Future advancements should focus on improving the ionic conductivity of agar-based composites, possibly by incorporating advanced dopants or hybrid materials to increase efficiency.
- Agar composites can be combined with other bio-based or conductive materials to enhance performance metrics such as energy density and power output, opening pathways for multifunctional devices.
- AI- and machine learning-guided optimization can revolutionize the development of agar-based energy storage devices by predicting material behaviors, optimizing compositions, and enhancing device performance.

9. Conclusions

In conclusion, agar, as a renewable and biodegradable resource, is proving to be invaluable in pioneering sustainable energy storage solutions. This review highlights how agar-based composites are ingeniously integrated with advanced materials like metallic nanoparticles, graphene, carbon nanotubes, and various natural and synthetic polymers to enhance the functionality and efficiency of energy storage devices, including batteries, supercapacitors, and fuel cells. This burgeoning interest is a testament to the critical role agar composites are poised to play in driving the next generation of energy storage systems, which are crucial for a sustainable future. The ongoing advancements and expanding research landscape indicate that agar and its composites will continue to be at the forefront

of materials science and energy technology, offering promising avenues for environmental sustainability and technological innovation.

Author Contributions: Conceptualization, Z.A.; methodology, Z.A. and S.U.; validation, Z.A. and S.U.; formal analysis, A.P.; investigation, Z.A.; resources, Z.A. and S.U.; data curation, G.J. and A.P.; writing—original draft preparation, Z.A.; writing—review and editing, S.U. and Z.A.; visualization, G.J. and A.P.; supervision, A.P. and G.J. All authors have read and agreed to the published version of the manuscript.

Funding: This research received no external funding.

Data Availability Statement: No new data were created or analyzed in this study.

Acknowledgments: We would like to express our sincere thanks to Arvydas Palevicius and Giedrius Janusas for their review and guidance.

Conflicts of Interest: The authors declare no conflicts of interest.

References

1. Jumaidin, R. Agar based composite as a new alternative biopolymer. In *Composites from the Aquatic Environment*; Springer: Singapore, 2023; pp. 67–82.
2. Kumar, S.; Jahan, K.; Verma, A.; Agarwal, M.; Chandraprakash, C. Agar-based composite films as effective biodegradable sound absorbers. *ACS Sustain. Chem. Eng.* **2022**, *10*, 8242–8253. [\[CrossRef\]](#)
3. Shah, M.; Hameed, A.; Kashif, M.; Majeed, N.; Muhammad, J.; Shah, N.; Rehan, T.; Khan, A.; Uddin, J.; Khan, A. Advances in agar-based composites: A comprehensive review. *Carbohydr. Polym.* **2024**, *346*, 122619. [\[CrossRef\]](#) [\[PubMed\]](#)
4. Xiong, C.; Li, T.; Zhu, Y.; Zhao, T.; Dang, A.; Li, H.; Ji, X.; Shang, Y.; Khan, M. Two-step approach of fabrication of interconnected nanoporous 3D reduced graphene oxide-carbon nanotube-polyaniline hybrid as a binder-free supercapacitor electrode. *J. Alloys Compd.* **2017**, *695*, 1248–1259. [\[CrossRef\]](#)
5. Kakanejadifard, A.; Safarimehr, P.; Karmakar, B.; Pirhayati, M.; Veisi, H. Application of supported palladium nanoparticles over chitosan-agarose encapsulated Fe₃O₄ microspheres as efficient catalyst in the Sonogashira cross-coupling reactions. *J. Organomet. Chem.* **2025**, *1029*, 123553. [\[CrossRef\]](#)
6. Nejad, S.L.; Shekarchizadeh, H. An agar hydrogel-CuNPs/N@ CQDs dual-mode colorimetric/fluorescent indicator for non-destructive monitoring of banana ripening. *Food Chem.* **2025**, *473*, 143098.
7. Belay, M.; Nagarale, R.K.; Verma, V. Preparation and characterization of graphene-agar and graphene oxide-agar composites. *J. Appl. Polym. Sci.* **2017**, *134*, 45085. [\[CrossRef\]](#)
8. Contessa, C.R.; Rosa, G.S.d.; Moraes, C.C.; Burkert, J.F.d.M. Agar-Agar and Chitosan as Precursors in the Synthesis of Functional Film for Foods: A Review. *Macromol* **2023**, *3*, 275–289. [\[CrossRef\]](#)
9. Torres, F.G.; Troncoso, O.P.; Urtecho, A.; Soto, P.; Pachas, B. Recent Progress in Polysaccharide-Based Materials for Energy Applications: A Review. *ACS Appl. Mater. Interfaces* **2024**, *17*, 13179–13196. [\[CrossRef\]](#)
10. Chen, L.; Li, Y.; Du, Q.; Wang, Z.; Xia, Y.; Yedinak, E.; Lou, J.; Ci, L. High performance agar/graphene oxide composite aerogel for methylene blue removal. *Carbohydr. Polym.* **2017**, *155*, 345–353. [\[CrossRef\]](#)
11. Cao, W.; Cheng, X.; Gong, L.; Li, Y.; Zhang, R.; Zhang, H. Thermal conductivity of highly porous ceramic foams with different agar concentrations. *Mater. Lett.* **2015**, *139*, 66–69. [\[CrossRef\]](#)
12. Wu, J.-M.; Ma, Y.-X.; Chen, Y.; Cheng, L.-J.; Chen, A.-N.; Liu, R.-Z.; Li, C.-H.; Shi, Y.-S.; Lin, J.-P. Preparation of Si₃N₄ ceramics by aqueous gelcasting using non-toxic agar powder as gelling agent without cooling crosslink process. *Ceram. Int.* **2019**, *45*, 20961–20966. [\[CrossRef\]](#)
13. Rukmanikrishnan, B.; Lee, J. Montmorillonite clay and quaternary ammonium silane-reinforced pullulan/agar-based nanocomposites and their properties for packaging applications. *Int. J. Biol. Macromol.* **2021**, *191*, 956–963. [\[CrossRef\]](#)
14. Shah, N.; Shah, M.; Khan, F.; Rehan, T.; Shams, S.; Khitab, F.; Khan, A.; Ullah, M.W.; Yousaf, J.; Awwad, F.A.; et al. Fabrication and Characterization of Montmorillonite Clay / Agar-Based Magnetic Composite and Its Biological and Electrical Conductivity Evaluation. *ACS Omega* **2024**, *9*, 15904–15914. [\[CrossRef\]](#) [\[PubMed\]](#)
15. Zhu, Q.; Su, X.; Mai, K.; Huang, R.; Yang, S.; Liu, H.; He, F.; Bao, Y.; Yu, G.; Feng, Y. Amphiphilic colloidal particles/Ca²⁺ reinforced edible agar nanocomposite film by multiple cross-linking/microphase separation strategies. *Food Hydrocoll.* **2025**, *159*, 110602. [\[CrossRef\]](#)
16. Orabi, S.; Ibrahim, A.A.; Gebreil, A.; Kospa, D.A. Sponge-like fluorapatite/expanded graphite@ agar biohydrogel with self-healing and salt resistance ability for solar steam and electricity cogeneration. *Desalination* **2025**, *600*, 118502. [\[CrossRef\]](#)

17. Dongre, M.; Varma, P.; Parthasarathy, A.; Kandasubramanian, B. Algae-Derived Precursors for Sustainable Electrochemical Energy Storage. *Energy Technol.* **2025**, *13*, 2401465. [\[CrossRef\]](#)
18. Ahmed, S.; Arshad, T.; Zada, A.; Afzal, A.; Khan, M.; Hussain, A.; Hassan, M.; Ali, M.; Xu, S. Preparation and Characterization of a Novel Sulfonated Titanium Oxide Incorporated Chitosan Nanocomposite Membranes for Fuel Cell Application. *Membranes* **2021**, *11*, 450. [\[CrossRef\]](#)
19. Liu, Q.; Bi, S.; Xu, X.; Xiao, X.; Lei, Y. N. O-codoped carbon aerogel electrode improves capacitive deionization performance. *J. Colloid Interface Sci.* **2025**, *680*, 54–63. [\[CrossRef\]](#)
20. Ghosh, T. Graphene Oxide–Agar–Agar Hydrogel for Efficient Removal of Methyl Orange from Water. In Proceedings of the International Conference on Transportation Infrastructure Projects: Conception to Execution, Andhra Pradesh, India, 16–18 November 2022; pp. 9–19.
21. Shin, J.; Park, J.-K.; Kim, G.W.; Nam, I.; Park, S. Agarose Gel-Templating Synthesis of a 3D Wrinkled Graphene Architecture for Enhanced Supercapacitor Performance. *Micromachines* **2022**, *13*, 1113. [\[CrossRef\]](#)
22. Belay, M. Preparation of Biodegradable Reduced Graphene Oxide/Agar Composites by In Situ Reduction of Graphene Oxide. *Int. J. Polym. Sci.* **2023**, *2023*, 4583522. [\[CrossRef\]](#)
23. Zhu, P.; Zhuo, S.; Zhang, W.; Ying, X.; Huang, J.; Li, X. Performance and application of microbial fuel cells with sodium alginate/agar/activated carbon composite as efficient biocompatible anode. *J. Appl. Polym. Sci.* **2023**, *140*, e53999. [\[CrossRef\]](#)
24. Selvalakshmi, S.; Vanitha, D.; Saranya, P.; Selvasekarapandian, S.; Mathavan, T.; Premalatha, M. Structural and conductivity studies of ammonium chloride doped agar-agar biopolymer electrolytes for electrochemical devices. *J. Mater. Sci. Mater. Electron.* **2022**, *33*, 24884–24894. [\[CrossRef\]](#)
25. Sun, P.; Liu, W.; Yang, D.; Zhang, Y.; Xiong, W.; Li, S.; Chen, J.; Tian, J.; Zhang, L. Stable Zn anodes enabled by high-modulus agarose gel electrolyte with confined water molecule mobility. *Electrochim. Acta* **2022**, *429*, 140985. [\[CrossRef\]](#)
26. Zuo, Y.; Wang, K.; Wei, M.; Zhang, P.; Zhao, S.; Pei, P.; Wang, H.; Chen, Z.; Shang, N. An Agar gel modulation with melamine foam skeleton for flexible Zn-air batteries. *Chem. Eng. J.* **2023**, *452*, 139301. [\[CrossRef\]](#)
27. Hasan, K.; Bashir, S.; Subramaniam, R.; Kasi, R.; Kamran, K.; Iqbal, J.; Algarni, H.; Al-Sehemi, A.G.; Wageh, S.; Pershaanaa, M. Poly (vinyl alcohol)/agar hydrogel electrolytes based flexible all-in-one supercapacitors with conducting polyaniline/polypyrrole electrodes. *Polymers* **2022**, *14*, 4784. [\[CrossRef\]](#) [\[PubMed\]](#)
28. Dang, A.; Sun, Y.; Fang, C.; Li, T.; Liu, X.; Xia, Y.; Ye, F.; Zada, A.; Khan, M. Rational design of Ti_3C_2 /carbon nanotubes/ MnCo_2S_4 electrodes for symmetric supercapacitors with high energy storage. *Appl. Surf. Sci.* **2022**, *581*, 152432. [\[CrossRef\]](#)
29. Kasprzak, D.; Mayorga-Martinez, C.C.; Pumera, M. Sustainable and flexible energy storage devices: A review. *Energy Fuels* **2022**, *37*, 74–97. [\[CrossRef\]](#)
30. Torres, F.G.; De-la-Torre, G.E. Algal-based polysaccharides as polymer electrolytes in modern electrochemical energy conversion and storage systems: A review. *Carbohydr. Polym. Technol. Appl.* **2021**, *2*, 100023. [\[CrossRef\]](#)
31. Parsimehr, H.; Ehsani, A. Algae-based electrochemical energy storage devices. *Green Chem.* **2020**, *22*, 8062–8096. [\[CrossRef\]](#)
32. Gupta, P.; Gupta, A.K.; Gupta, S.K.; Gupta, S.; Shrivastav, M.; Yadav, R.K. DFT Study on Na-Ion Conducting Solid Biopolymer Electrolyte-Based on Agar-Agar and NaPF_6 for Sodium-Ion Batteries. *Nano Hybrids Compos.* **2023**, *40*, 65–78. [\[CrossRef\]](#)
33. Li, D.; Wang, Y.; Sun, Y.; Lu, Y.; Chen, S.; Wang, B.; Zhang, H.; Xia, Y.; Yang, D. Turning gelidium amansii residue into nitrogen-doped carbon nanofiber aerogel for enhanced multiple energy storage. *Carbon* **2018**, *137*, 31–40. [\[CrossRef\]](#)
34. Padmesh, S.; Singh, A. Agars: Properties and applications. In *Polysaccharides: Properties and Applications*; WILEY: Hoboken, NJ, USA, 2021; pp. 75–93.
35. Yadav, S.K.; Yohannan, A.S.K.; Palanisamy, M. Seaweeds as natural resource for agar-Agar extraction in India-A review. *Agro Econ.—Int. J.* **2023**, *10*, 201–208. [\[CrossRef\]](#)
36. Veerakumar, S.; Manian, R.P. Recombinant β -agarases: Insights into molecular, biochemical, and physiochemical characteristics. *3 Biotech* **2018**, *8*, 445. [\[CrossRef\]](#) [\[PubMed\]](#)
37. Ogrenci, A.S.; Pekcan, O.; Kara, S.; Bilge, A.H. Mathematical characterization of thermo-reversible phase transitions of agarose gels. *J. Macromol. Sci. Part B* **2018**, *57*, 364–376. [\[CrossRef\]](#)
38. Bertasa, M.; Poli, T.; Riedo, C.; Di Tullio, V.; Capitani, D.; Proietti, N.; Canevali, C.; Sansonetti, A.; Scalapone, D. A study of non-bounded/bounded water and water mobility in different agar gels. *Microchem. J.* **2018**, *139*, 306–314. [\[CrossRef\]](#)
39. Armisen, R.; Gaiatas, F. Agar. In *Handbook of Hydrocolloids*; Elsevier: Amsterdam, The Netherlands, 2009; pp. 82–107.
40. Lee, W.-K.; Lim, Y.-Y.; Ho, C.-L. Gracilaria as the major source of agar for food, health and biotechnology applications. In *Sustainable Global Resources of Seaweeds Volume 2: Food, Pharmaceutical and Health Applications*; Springer: Berlin/Heidelberg, Germany, 2022; pp. 145–161.
41. Vijayakumar, M.; Adduru, J.; Rao, T.N.; Karthik, M. Conversion of Solar Energy into Electrical Energy Storage: Supercapacitor as an Ultrafast Energy-Storage Device Made from Biodegradable Agar-Agar as a Novel and Low-Cost Carbon Precursor. *Glob. Chall.* **2018**, *2*, 1800037. [\[CrossRef\]](#) [\[PubMed\]](#)

42. Raphael, E.; Avellaneda, C.; Aegerter, M.; Silva, M.; Pawlicka, A. Agar-based gel electrolyte for electrochromic device application. *Mol. Cryst. Liq. Cryst.* **2012**, *554*, 264–272. [\[CrossRef\]](#)
43. Raphael, E.; Avellaneda, C.O.; Manzolli, B.; Pawlicka, A. Agar-based films for application as polymer electrolytes. *Electrochim. Acta* **2010**, *55*, 1455–1459. [\[CrossRef\]](#)
44. Zhang, X.; Xing, P.; Madanu, T.L.; Li, J.; Shu, J.; Su, B.-L. Aqueous batteries: From laboratory to market. *Natl. Sci. Rev.* **2023**, *10*, nwad235. [\[CrossRef\]](#)
45. García-Gaitán, E.; Morant-Miñana, M.C.; Frattini, D.; Maddalena, L.; Fina, A.; Gerbaldi, C.; Cantero, I.; Ortiz-Vitoriano, N. Agarose-based Gel Electrolytes for Sustainable Primary and Secondary Zinc-Air Batteries. *Chem. Eng. J.* **2023**, *472*, 144870. [\[CrossRef\]](#)
46. Moon, W.G.; Kim, G.-P.; Lee, M.; Song, H.D.; Yi, J. A biodegradable gel electrolyte for use in high-performance flexible supercapacitors. *ACS Appl. Mater. Interfaces* **2015**, *7*, 3503–3511. [\[CrossRef\]](#) [\[PubMed\]](#)
47. Kim, J.S.; Kim, J.-H.; Cho, Y.; Shim, T.S. Agarose/Spherical Activated Carbon Composite Gels for Recyclable and Shape-Configurable Electrodes. *Polymers* **2019**, *11*, 875. [\[CrossRef\]](#) [\[PubMed\]](#)
48. Nath, P.C.; Debnath, S.; Sridhar, K.; Inbaraj, B.S.; Nayak, P.K.; Sharma, M. A Comprehensive Review of Food Hydrogels: Principles, Formation Mechanisms, Microstructure, and Its Applications. *Gels* **2023**, *9*, 1. [\[CrossRef\]](#)
49. Wenger, L.; Radtke, C.P.; Gerisch, E.; Kollmann, M.; Niemeyer, C.M.; Rabe, K.S.; Hubbuch, J. Systematic evaluation of agarose-and agar-based bioinks for extrusion-based bioprinting of enzymatically active hydrogels. *Front. Bioeng. Biotechnol.* **2022**, *10*, 928878. [\[CrossRef\]](#) [\[PubMed\]](#)
50. Zheng, Z.; Shi, W.; Zhou, X.; Zhang, X.; Guo, W.; Shi, X.; Xiong, Y.; Zhu, Y. Agar-based hydrogel polymer electrolyte for high-performance zinc-ion batteries at all climatic temperatures. *iScience* **2023**, *26*, 106437. [\[CrossRef\]](#)
51. Zhang, L.; Liao, W.; Huang, Y.; Wen, Y.; Chu, Y.; Zhao, C. Global seaweed farming and processing in the past 20 years. *Food Prod. Process. Nutr.* **2022**, *4*, 23. [\[CrossRef\]](#)
52. Duceac, I.A.; Stanciu, M.-C.; Nechifor, M.; Tanasă, F.; Teacă, C.-A. Insights on some polysaccharide gel type materials and their structural peculiarities. *Gels* **2022**, *8*, 771. [\[CrossRef\]](#)
53. Lee, W.-K.; Lim, Y.-Y.; Leow, A.T.-C.; Namasivayam, P.; Abdullah, J.O.; Ho, C.-L. Factors affecting yield and gelling properties of agar. *J. Appl. Phycol.* **2017**, *29*, 1527–1540. [\[CrossRef\]](#)
54. Jiang, F.; Xu, X.-W.; Chen, F.-Q.; Weng, H.-F.; Chen, J.; Ru, Y.; Xiao, Q.; Xiao, A.-F. Extraction, modification and biomedical application of agarose hydrogels: A review. *Mar. Drugs* **2023**, *21*, 299. [\[CrossRef\]](#)
55. Zucca, P.; Fernandez-Lafuente, R.; Sanjust, E. Agarose and its derivatives as supports for enzyme immobilization. *Molecules* **2016**, *21*, 1577. [\[CrossRef\]](#)
56. Zarrintaj, P.; Bakhshandeh, B.; Rezaeian, I.; Heshmatian, B.; Ganjali, M.R. A Novel Electroactive Agarose-Aniline Pentamer Platform as a Potential Candidate for Neural Tissue Engineering. *Sci. Rep.* **2017**, *7*, 17187. [\[CrossRef\]](#)
57. Rayung, M.; Aung, M.M.; Azhar, S.C.; Abdullah, L.C.; Su'ait, M.S.; Ahmad, A.; Jamil, S.N.A.M. Bio-Based Polymer Electrolytes for Electrochemical Devices: Insight into the Ionic Conductivity Performance. *Materials* **2020**, *13*, 838. [\[CrossRef\]](#) [\[PubMed\]](#)
58. Kasem, K.K. Electrochemical behavior of some redox systems pendant in agar gel. *J. New Mater. Electrochem. Syst.* **2005**, *8*, 189.
59. Osinska-Broniarz, M.; Martyla, A.; Manczak, R.; Sierczynska, A. Agar as a compound of alkaline solid polymer electrolyte. *Trans. Environ. Dev.* **2018**, *14*, 474–480.
60. Mohd Rafi, N.S.; Abidin, S.Z.Z.; Majid, S.R.; Zakaria, R. Preparation of Agarose-based Biopolymer Electrolytes Containing Calcium Thiocyanate: Electrical and Electrochemical Properties. *Int. J. Electrochem. Sci.* **2022**, *17*, 220713. [\[CrossRef\]](#)
61. Shauli, L.; Salomon, E. A Simple Method for Measuring Agar Gel Strength. *Phycology* **2025**, *5*, 6. [\[CrossRef\]](#)
62. Bertasa, M.; Doderio, A.; Alloisio, M.; Vicini, S.; Riedo, C.; Sansonetti, A.; Scalarone, D.; Castellano, M. Agar gel strength: A correlation study between chemical composition and rheological properties. *Eur. Polym. J.* **2020**, *123*, 109442. [\[CrossRef\]](#)
63. Wüstenberg, T. General overview of food hydrocolloids. In *Cellulose and Cellulose Derivatives in the Food Industry Fundamentals and Applications*; Wüstenberg, T., Ed.; John Wiley & Sons: Hoboken, NJ, USA, 2015; pp. 1–68.
64. Nishinari, K. Gelling properties. In *Food Hydrocolloids: Functionalities and Applications*; Springer: Berlin/Heidelberg, Germany, 2021; pp. 119–170.
65. An, L.; Zhao, T.; Zeng, L. Agar chemical hydrogel electrode binder for fuel-electrolyte-fed fuel cells. *Appl. Energy* **2013**, *109*, 67–71. [\[CrossRef\]](#)
66. Han, X.; Li, M.; Fan, Z.; Zhang, Y.; Zhang, H.; Li, Q. PVA/Agar interpenetrating network hydrogel with fast healing, high strength, antifreeze, and water retention. *Macromol. Chem. Phys.* **2020**, *221*, 2000237. [\[CrossRef\]](#)
67. Boopathi, G.; Pugalendhi, S.; Selvasekarapandian, S.; Premalatha, M.; Monisha, S.; Aristatil, G. Development of proton conducting biopolymer membrane based on agar-agar for fuel cell. *Ionics* **2017**, *23*, 2781–2790. [\[CrossRef\]](#)
68. Zhang, B.; da Silva, M.; Johnston, I.; Aspinall, S.; Cook, M. Poly(vinyl alcohol)-Agar Double Network Hydrogels: Linking Formulation to Mechanical and Rheological Properties. *Macromol. Chem. Phys.* **2005**, *e00257*. [\[CrossRef\]](#)
69. Tang, Z.; Xiong, C. Agar as water soluble binder for lithium-sulfur battery. *Energy Storage Sci. Technol.* **2017**, *6*, 493.

70. Nwanya, A.; Amaechi, C.; Udounwa, A.; Osuji, R.; Maaza, M.; Ezema, F. Complex impedance and conductivity of agar-based ion-conducting polymer electrolytes. *Appl. Phys. A* **2015**, *119*, 387–396. [\[CrossRef\]](#)
71. Zuo, L.; Sun, H.; Yuan, X.; Wen, J.; Chen, X.; Zhou, S.; Wu, Y.; van Ree, T. Agar acts as cathode microskin to extend the cycling life of Zn/ / α -MnO₂ batteries. *Materials* **2021**, *14*, 4895. [\[CrossRef\]](#) [\[PubMed\]](#)
72. Sutharsan, M.; Murugan, K.S.; Narayanan, K.; Natarajan, T.S. Chitosan/agar-agar/TiO₂ biopolymer nanocomposite film for solar photocatalysis, antibacterial activity, and food preservation applications. *Next Mater.* **2025**, *9*, 101225. [\[CrossRef\]](#)
73. Hsieh, S.; Huang, B.; Hsieh, S.; Wu, C.; Wu, C.; Lin, P.; Huang, Y.; Chang, C. Green fabrication of agar-conjugated Fe₃O₄ magnetic nanoparticles. *Nanotechnology* **2010**, *21*, 445601. [\[CrossRef\]](#)
74. Roux, D.C.D.; Caton, F.; Jeacomine, I.; Maîtrejean, G.; Rinaudo, M. Reversibility in the Physical Properties of Agarose Gels following an Exchange in Solvent and Non-Solvent. *Polymers* **2024**, *16*, 811. [\[CrossRef\]](#)
75. Tanaka, F. Thermoreversible gelation strongly coupled to coil-to-helix transition of polymers. *Colloids Surf. B Biointerfaces* **2004**, *38*, 111–114. [\[CrossRef\]](#)
76. Lizundia, E.; Costa, C.M.; Alves, R.; Lanceros-Méndez, S. Cellulose and its derivatives for lithium ion battery separators: A review on the processing methods and properties. *Carbohydr. Polym. Technol. Appl.* **2020**, *1*, 100001. [\[CrossRef\]](#)
77. Turossi, T.C.; Júnior, H.L.O.; Monticeli, F.M.; Dias, O.T.; Zattera, A.J. Cellulose-Derived Battery Separators: A Minireview on Advances Towards Environmental Sustainability. *Polymers* **2025**, *17*, 456. [\[CrossRef\]](#) [\[PubMed\]](#)
78. Rosli, N.A.H.; Loh, K.S.; Wong, W.Y.; Yunus, R.M.; Lee, T.K.; Ahmad, A.; Chong, S.T. Review of Chitosan-Based Polymers as Proton Exchange Membranes and Roles of Chitosan-Supported Ionic Liquids. *Int. J. Mol. Sci.* **2020**, *21*, 632. [\[CrossRef\]](#) [\[PubMed\]](#)
79. Wang, Y.; Lu, Y. Sodium Alginate-Based Functional Materials toward Sustainable Applications: Water Treatment and Energy Storage. *Ind. Eng. Chem. Res.* **2023**, *62*, 11279–11304. [\[CrossRef\]](#)
80. Wang, H.; Yang, L.; Yang, Y. A review of sodium alginate-based hydrogels: Structure, mechanisms, applications, and perspectives. *Int. J. Biol. Macromol.* **2025**, *292*, 139151. [\[CrossRef\]](#) [\[PubMed\]](#)
81. Wang, Y.; Shen, Z.; Wang, H.; Song, Z.; Yu, D.; Li, G.; Liu, X.; Liu, W. Progress in Research on Metal Ion Crosslinking Alginate-Based Gels. *Gels* **2025**, *11*, 16. [\[CrossRef\]](#) [\[PubMed\]](#)
82. Jain, A.; Mahata, K.; Onkarnath; Banerjee, S. Biopolymer Derived Gel Polymer Electrolytes: Current Status and Future Perspectives. *Macromol. Rapid Commun.* **2005**, e00472. [\[CrossRef\]](#)
83. Wang, W.; Guo, X.; Yang, Y. Lithium iodide effect on the electrochemical behavior of agarose based polymer electrolyte for dye-sensitized solar cell. *Electrochim. Acta* **2011**, *56*, 7347–7351. [\[CrossRef\]](#)
84. Fuzlin, A.F.; Aynharan, S.; Hafidz, N.N.A.; Ghazali, N.M.; Diantoro, M.; Nagao, Y.; Samsudin, A.S. Advances in Gel Biopolymer Electrolytes: Sustainable Polymers for Energy Storage Applications. *Polym. Adv. Technol.* **2025**, *36*, e70319. [\[CrossRef\]](#)
85. Dalwadi, S.; Goel, A.; Kapetanakis, C.; Salas-de la Cruz, D.; Hu, X. The Integration of Biopolymer-Based Materials for Energy Storage Applications: A Review. *Int. J. Mol. Sci.* **2023**, *24*, 3975. [\[CrossRef\]](#)
86. Mahajan, P.; Sharma, M. A comprehensive review on developments and future perspectives of biopolymer-based materials for energy storage. *Energy Storage* **2024**, *6*, e634. [\[CrossRef\]](#)
87. Banu, J.R.; Kumar, M.D.; Gunasekaran, M.; Kumar, G. Biopolymer production in bio electrochemical system: Literature survey. *Bioresour. Technol. Rep.* **2019**, *7*, 100283. [\[CrossRef\]](#)
88. Taji, K.; Shekarchizadeh, H. Development of an active agar aerogel with dual antioxidant and UV-blocking activities using chlorine-doped graphene quantum dots. *Heliyon* **2024**, *10*, e34387. [\[CrossRef\]](#)
89. Kandhol, G.; Wadhwa, H.; Verma, A. Glass transition temperature of Agar-Reduced Graphene Oxide (RGO) Composites using 2-D contour mapping of temperature dependent FTIR spectra. *Chem. Phys. Impact* **2024**, *9*, 100690. [\[CrossRef\]](#)
90. Sarwar, O.; Munir, R.; Mushtaq, N.; Ambreen, H.; Bashir, M.Z.; Sana, M.; Muneer, A.; Sayed, M.; Noreen, S. Synthesis, utilization, and recycling of graphene oxide-based nanohybrid biopolymeric hydrogels for purification of dye wastewater. *AQUA—Water Infrastruct. Ecosyst. Soc.* **2024**, *73*, 1228–1256. [\[CrossRef\]](#)
91. Namasivayam, S.K.R.; Pandian, U.K.; Samrat, K.; Bharani, R.A.; John, A.; Kavisri, M.; Kadaikunnan, S.; Thiruvengadam, M.; Moovendhan, M. Fungal derived herbicidal metabolite loaded starch-chitosan-gum acacia-agar based bio composite: Preparation, characterization, herbicidal activity, release profile and biocompatibility. *Int. J. Biol. Macromol.* **2024**, *259*, 129264. [\[CrossRef\]](#) [\[PubMed\]](#)
92. Yin, H.; You, M.; Yu, H.; Si, X.; Zheng, Y.; Cui, W.; Zhu, L.; Chen, Q. Rate-Dependent Fracture Behaviors of Agar-Based Hybrid Double-Network Hydrogels. *Macromolecules* **2024**, *57*, 4024–4033. [\[CrossRef\]](#)
93. Riahi, Z.; Khan, A.; Rhim, J.-W.; Shin, G.H.; Kim, J.T. Synergistic effect of iron-based metal-organic framework hybridized with carbon quantum dots in agar /gelatin films for fruit preservation. *Food Packag. Shelf Life* **2024**, *45*, 101330. [\[CrossRef\]](#)
94. Kumar, S.; Boro, J.C.; Ray, D.; Mukherjee, A.; Dutta, J. Bionanocomposite films of agar incorporated with ZnO nanoparticles as an active packaging material for shelf life extension of green grape. *Heliyon* **2019**, *5*, e01867. [\[CrossRef\]](#) [\[PubMed\]](#)
95. Herath, H.; Jinendra, B. Recent advancement in agarwood induction technology: A comprehensive review for the transformation of artificial agar resin induction methods. *J. Agro-Technol. Rural. Sci.* **2023**, *3*, 6–17. [\[CrossRef\]](#)
96. Fujiwara, E.; Rosa, L.O. Soft optical waveguides made of agar. *MRS Adv.* **2024**, *9*, 574–579. [\[CrossRef\]](#)

97. Elhefian, E.A.; Nasef, M.M.; Yahaya, A.H. Preparation and characterization of chitosan/agar blended films: Part 2. Thermal, mechanical, and surface properties. *J. Chem.* **2012**, *9*, 510–516. [\[CrossRef\]](#)
98. Cuvillier, L.; Passaretti, A.; Guilminot, E.; Joseph, E. Agar and Chitosan Hydrogels' Design for Metal-Uptaking Treatments. *Gels* **2024**, *10*, 55. [\[CrossRef\]](#)
99. Liu, J.; Tang, X.; Chen, X.; Wang, G. Investigation of MXene-modified agar/polyurethane hydrogel elastomeric repair materials with tunable water absorption. *e-Polymers* **2023**, *23*, 20230035. [\[CrossRef\]](#)
100. Oprea, S. Preparation and characterization of the agar/polyurethane composites. *J. Compos. Mater.* **2011**, *45*, 2039–2045. [\[CrossRef\]](#)
101. Sousa, A.M.; Souza, H.K.; Uknalis, J.; Liu, S.-C.; Goncalves, M.P.; Liu, L. Electrospinning of agar/PVA aqueous solutions and its relation with rheological properties. *Carbohydr. Polym.* **2015**, *115*, 348–355. [\[CrossRef\]](#) [\[PubMed\]](#)
102. Madera-Santana, T.; Misra, M.; Drzal, L.; Robledo, D.; Freile-Pelegrin, Y. Preparation and characterization of biodegradable agar/poly (butylene adipate-co-terephthalate) composites. *Polym. Eng. Sci.* **2009**, *49*, 1117–1126. [\[CrossRef\]](#)
103. Giménez, B.; De Lacey, A.L.; Pérez-Santín, E.; López-Caballero, M.; Montero, P. Release of active compounds from agar and agar–gelatin films with green tea extract. *Food Hydrocoll.* **2013**, *30*, 264–271. [\[CrossRef\]](#)
104. Jagadish, R.; Rai, S.K.; Guru, G. Miscibility studies of agar-agar/starch blends using various techniques. *Int. J. Res. Pharm. Chem.* **2012**, *2*, 1049–1056.
105. Entezam, M.; Daneshian, H.; Nasirizadeh, N.; Khonakdar, H.A.; Jafari, S.H. Hybrid hydrogels based on Poly (vinyl alcohol)(PVA)/Agar/Poly (ethylene glycol) (PEG) prepared by high energy electron beam irradiation: Investigation of physico-mechanical and rheological properties. *Macromol. Mater. Eng.* **2017**, *302*, 1600397. [\[CrossRef\]](#)
106. Hamimed, S.; Ammar, N.E.B.; Slimi, H.; Asses, N.; Hamzaoui, A.H.; Chatti, A. Innovative entrapped Yarrowia lipolytica within polyvinylpyrrolidone (PVP)/polyethylene glycol (PEG)/agar for improving olive mill wastewater bioremediation. *J. Clean. Prod.* **2024**, *449*, 141828. [\[CrossRef\]](#)
107. Khan, M.; Tiehu, L.; Hussain, A.; Raza, A.; Zada, A.; Alei, D.; Khan, A.R.; Ali, R.; Hussain, H.; Hussain, J.; et al. Physiochemical evaluations, mechanical attenuations and thermal stability of graphene nanosheets and functionalized nanodiamonds loaded pitch derived carbon foam composites. *Diam. Relat. Mater.* **2022**, *126*, 109077. [\[CrossRef\]](#)
108. Hamid, A.; Khan, M.; Hussain, F.; Zada, A.; Li, T.; Alei, D.; Ali, A. Synthesis and physiochemical performances of PVC-sodium polyacrylate and PVC-sodium polyacrylate-graphite composite polymer membrane. *Z. Phys. Chem.* **2021**, *235*, 1791–1810. [\[CrossRef\]](#)
109. Wang, T.; Li, M.; Zhang, H.; Sun, Y.; Dong, B. A multi-responsive bidirectional bending actuator based on polypyrrole and agar nanocomposites. *J. Mater. Chem. C* **2018**, *6*, 6416–6422. [\[CrossRef\]](#)
110. Sung, J.-H.; Kim, S.-J.; Lee, K.-H. Preparation of compact polyaniline films: Electrochemical synthesis using agar gel template and charge-storage applications. *J. Power Sources* **2004**, *126*, 258–267. [\[CrossRef\]](#)
111. Alves, R.; Fidalgo-Marijuan, A.; Salado, M.; Gonçalves, R.; Silva, M.M.; Bazán, B.a.; del Campo, F.J.; Costa, C.M.; Lanceros-Mendez, S. Agar-Based Solid Polymer Electrolyte-Containing Ionic Liquid for Sustainable Electrochromic Devices. *ACS Sustain. Chem. Eng.* **2023**, *11*, 16575–16584. [\[CrossRef\]](#)
112. Ahmad Ruzaidi, D.A.; Mahat, M.M.; Mohamed Sofian, Z.; Nor Hashim, N.A.; Osman, H.; Nawawi, M.A.; Ramli, R.; Jantan, K.A.; Aizamddin, M.F.; Azman, H.H. Synthesis and characterization of porous, electro-conductive chitosan–gelatin–agar-based PEDOT: PSS scaffolds for potential use in tissue engineering. *Polymers* **2021**, *13*, 2901. [\[CrossRef\]](#)
113. Wang, J.; Khan, M.; Hussain, A.; Khan, I.; Nawaz, A.; Ragab, A.H.; Sayqal, A.; Lei, T.; Zada, A. Carbon foam composites containing carbon nanotubes and graphene oxide as additives for enhanced mechanical, thermal, electrical and catalytic properties. *J. Mater. Res. Technol.* **2023**, *24*, 608–622. [\[CrossRef\]](#)
114. Nie, Z.; Peng, K.; Lin, L.; Yang, J.; Cheng, Z.; Gan, Q.; Chen, Y.; Feng, C. A conductive hydrogel based on nature polymer agar with self-healing ability and stretchability for flexible sensors. *Chem. Eng. J.* **2023**, *454*, 139843. [\[CrossRef\]](#)
115. Kang, M.; Bin Mohammed Khusrin, M.S.; Kim, Y.-J.; Kim, B.; Park, B.J.; Hyun, I.; Imani, I.M.; Choi, B.-O.; Kim, S.-W. Nature-derived highly tribopositive κ -carrageenan-agar composite-based fully biodegradable triboelectric nanogenerators. *Nano Energy* **2022**, *100*, 107480. [\[CrossRef\]](#)
116. Lin, Y.; Zhang, L.; Li, X.; Zhai, C.; Liu, J.; Zhang, R. Effect and characterization of konjac glucomannan on xanthan gum/ κ -carrageenan/agar system. *Int. J. Biol. Macromol.* **2024**, *257*, 128639. [\[CrossRef\]](#) [\[PubMed\]](#)
117. Qiao, D.; Li, H.; Jiang, F.; Zhao, S.; Chen, S.; Zhang, B. Incorporation of κ -carrageenan improves the practical features of agar/konjac glucomannan/ κ -carrageenan ternary system. *Food Sci. Hum. Wellness* **2023**, *12*, 512–519. [\[CrossRef\]](#)
118. Shakya, K.R.; Nigam, K.; Sharma, A.; Jahan, K.; Tyagi, A.K.; Verma, V. Preparation and assessment of agar/TEMPO-oxidized bacterial cellulose cryogels for hemostatic applications. *J. Mater. Chem. B* **2024**, *12*, 3453–3468. [\[CrossRef\]](#)
119. Lee, Y.; Kim, H.J.; Kim, M.W.; Miyawaki, J.; Chae, H.G.; Eom, Y. All-biomass-based strong nanocomposite fibers of agar and cellulose nanocrystals and their dye removal applications. *Korea-Aust. Rheol. J.* **2024**, *36*, 109–118. [\[CrossRef\]](#)
120. Manna, A.; Lahiri, S.; Sen, K.; Banerjee, K. Fe(III) cross-linked cellulose-agar hydrogel beads for efficient phosphate removal from aqueous solutions. *Environ. Monit. Assess.* **2023**, *196*, 54. [\[CrossRef\]](#) [\[PubMed\]](#)

121. How, Y.H.; Wong, L.X.; Kong, I.; Nyam, K.L.; Pui, L.P. Development of Multilayered pH-Sensitive Chitosan–Gelatin–Agar Intelligent Film Incorporated with Roselle Anthocyanin Extract for Monitoring of the Freshness of Snapper Fish. *Food Bioprocess Technol.* **2024**, *17*, 4177–4194. [\[CrossRef\]](#)
122. Safarimehr, P.; Kakanejadifard, A.; Veisi, H. Decorated palladium nanoparticles over chitosan-agarose encapsulated Fe₃O₄ microspheres: Investigation of its catalytic efficiency in the Suzuki-Miaura coupling reactions. *J. Organomet. Chem.* **2024**, *1017*, 123282. [\[CrossRef\]](#)
123. Mohapatra, S.; Behera, L. A stretchable PVA-agar hydrogel patch embedded with metal-doped carbon dots (MCD) for monitoring the Ca²⁺ biomarker. *Mater. Adv.* **2025**, *6*, 1392–1402.
124. Xu, Y.; Hu, Y.; Zhang, H.; Bao, W.; Maimaitiyiming, X. Influence of cellulose on the properties of physically cross-linked poly(vinyl alcohol)/Agar double network hydrogels and investigation of multifunctional flexible sensors. *Colloids Surf. A Physicochem. Eng. Asp.* **2025**, *705*, 135626. [\[CrossRef\]](#)
125. Hamza, R.S.A.; Habeeb, M.A. Reinforcement of morphological, structural, optical, and antibacterial characteristics of PVA/CMC bioblend filled with SiO₂/Cr₂O₃ hybrid nanoparticles for optical nanodevices and food packing industries. *Polym. Bull.* **2024**, *81*, 4427–4448. [\[CrossRef\]](#)
126. Sun, K.; Cui, S.; Gao, X.; Liu, X.; Lu, T.; Wei, H.; Peng, H.; Ma, G. Graphene oxide assisted triple network hydrogel electrolyte with high mechanical and temperature stability for self-healing supercapacitor. *J. Energy Storage* **2023**, *61*, 106658. [\[CrossRef\]](#)
127. Peng, H.; Gao, X.; Sun, K.; Xie, X.; Ma, G.; Zhou, X.; Lei, Z. Physically cross-linked dual-network hydrogel electrolyte with high self-healing behavior and mechanical strength for wide-temperature tolerant flexible supercapacitor. *Chem. Eng. J.* **2021**, *422*, 130353. [\[CrossRef\]](#)
128. Wang, J.; Zhang, J.; Gu, J.; Chen, C.; Xu, Y.; Zhang, X. Plate-type solid-state Ag/AgCl reference electrode modified with KCl agar-PVA and PDMS composites. *IEEE Sens. J.* **2024**, *24*, 29659–29668. [\[CrossRef\]](#)
129. Shukla, M.K.; Singh, R.P.; Reddy, C.; Jha, B. Synthesis and characterization of agar-based silver nanoparticles and nanocomposite film with antibacterial applications. *Bioresour. Technol.* **2012**, *107*, 295–300. [\[CrossRef\]](#)
130. Balalakshmi, C.; Alharbi, N.S.; Kadaikunnan, S.; Khaled, J.M.; Alanzi, K.F.; Gopinath, K.; Arumugam, A.; Govindarajan, M. Development of chitosan/agar-silver nanoparticles-coated paper for antibacterial application. *Green Process. Synth.* **2020**, *9*, 751–759. [\[CrossRef\]](#)
131. Mofidian, R.; Hosseini, S.S.; Miansari, M.; Salmani, H. Separation and Clarification of Mazandaran Wood and Paper Factory Effluent to Remove Heavy Metals Using Zeolite–Agar Nanoadsorbent Immobilized by Cibacron Blue Dye Ligand. *Korean J. Chem. Eng.* **2024**, *41*, 325–336. [\[CrossRef\]](#)
132. Alenad, A.M.; Taha, T.A.; Amin, M.A.; Irfan, A.; Oliva, J.; Al-Hadeethi, Y.; Palamanit, A.; Khan, M.; Hayat, A.; Kumar Baburao Mane, S.; et al. Selectivity, stability and reproducibility effect of Uric acid integrated carbon nitride for photocatalytic application. *J. Photochem. Photobiol. A Chem.* **2022**, *423*, 113591. [\[CrossRef\]](#)
133. Chostak, C.L.; López-Delgado, A.; Padilla, I.; Lapolli, F.R.; Lobo-Recio, M.Á. Agarose-Immobilized LTA Zeolite: A Novel Material to Use in an Improved Treatment Process of Mine-Impacted Water. *Water Air Soil Pollut.* **2023**, *234*, 365. [\[CrossRef\]](#)
134. Xiong, C.; Yang, Q.; Li, B.; Nie, S.; Qin, C.; Dai, L.; Khan, M.; Xu, Y.; Ni, Y. Carbonized porous wood as an effective scaffold for loading flower-like CoS, NiS nanofibers with Co, Ni nanoparticles served as electrode material for high-performance supercapacitors. *Ind. Crops Prod.* **2021**, *167*, 113545. [\[CrossRef\]](#)
135. Magesh, G.; Bhoopathi, G.; Nithya, N.; Arun, A.P.; Ranjith Kumar, E. Structural, morphological, optical and biological properties of pure ZnO and agar/zinc oxide nanocomposites. *Int. J. Biol. Macromol.* **2018**, *117*, 959–966. [\[CrossRef\]](#)
136. Roy, S.; Rhim, J.-W. Preparation of pectin/agar-based functional films integrated with zinc sulfide nano petals for active packaging applications. *Colloids Surf. B Biointerfaces* **2021**, *207*, 111999. [\[CrossRef\]](#)
137. Hu, Y.; Zeng, Q.; Hu, Y.; He, J.; Wang, H.; Deng, C.; Li, D. MXene/zinc ion embedded agar/sodium alginate hydrogel for rapid and efficient sterilization with photothermal and chemical synergetic therapy. *Talanta* **2024**, *266*, 125101. [\[CrossRef\]](#)
138. Rhim, J.W.; Wang, L.F.; Hong, S.I. Preparation and characterization of agar/silver nanoparticles composite films with antimicrobial activity. *Food Hydrocoll.* **2013**, *33*, 327–335. [\[CrossRef\]](#)
139. Ghosh, S.; Kaushik, R.; Nagalakshmi, K.; Hoti, S.L.; Menezes, G.A.; Harish, B.N.; Vasan, H.N. Antimicrobial activity of highly stable silver nanoparticles embedded in agar–agar matrix as a thin film. *Carbohydr. Res.* **2010**, *345*, 2220–2227. [\[CrossRef\]](#) [\[PubMed\]](#)
140. Mostafa, S.I.; Ali, M.A.; El-Wassefy, N.A.; Saad, E.M.; Hussein, M.H. Adsorption and interaction studies of methylene blue dye onto agar-carboxymethylcellulose-silver nanocomposite in aqueous media. *Biomass Convers. Biorefinery* **2024**, *14*, 3363–3383. [\[CrossRef\]](#)
141. Gautam, B.; Nabat Al-Ajrash, S.M.; Hasan, M.J.; Saini, A.; Watzman, S.J.; Ureña-Benavides, E.; Vasquez-Guardado, E.S. Experimental Thermal Conductivity Studies of Agar-Based Aqueous Suspensions with Lignin Magnetic Nanocomposites. *Magnetochemistry* **2024**, *10*, 12. [\[CrossRef\]](#)

142. Gupta, K.K.; Tan, C.-P.; Hsu, C.-M.; Lin, B.-C.; Lu, C.-H. Bio-polymer agar-assisted sol-gel synthesis and electrochemical characterization of bi-pyramidal $\text{LiNi}_0.8\text{Co}_0.1\text{Mn}_0.1\text{O}_2$ cathode materials for lithium-ion batteries. *J. Sol-Gel Sci. Technol.* **2023**, *108*, 685–694. [\[CrossRef\]](#)
143. Lu, C.-H.; Subburaj, T.; Chiou, H.-T.; Som, S.; Ou, C.Y.; Kumar, P.S.; Balaji, S. Facile sol-gel synthesis of $\text{LiMn}_{0.5}\text{Fe}_{0.5}\text{PO}_4$ cathode materials fostered by bio-derived natural agar. *Ionics* **2020**, *26*, 1051–1056. [\[CrossRef\]](#)
144. Azevêdo, H.V.S.B.; Raimundo, R.A.; Ferreira, L.S.; Silva, M.M.S.; Morales, M.A.; Macedo, D.A.; Gomes, U.U.; Cavalcante, D.G.L. Green synthesis of CoWO_4 powders using agar-agar from red seaweed (Rhodophyta): Structure, magnetic properties and battery-like behavior. *Mater. Chem. Phys.* **2020**, *242*, 122544. [\[CrossRef\]](#)
145. Hazaana, S.A.; Joseph, A.; Selvasekarapandian, S.; Naachiyar, R.M.; Vignesh, N.M. Performance of solid-state Li-ion conducting battery using biopolymer electrolyte based on agar-agar/lithium chloride. *J. Solid State Electrochem.* **2023**, *27*, 539–557. [\[CrossRef\]](#)
146. Raphael, E.; Jara, D.H.; Schiavon, M.A. Optimizing photovoltaic performance in CuInS_2 and CdS quantum dot-sensitized solar cells by using an agar-based gel polymer electrolyte. *RSC Adv.* **2017**, *7*, 6492–6500. [\[CrossRef\]](#)
147. Fetyan, A.; Alhammedi, A.; Matouk, Z.; Andisetiawan, A.; Bahaa, A. Influence of eco-friendly agar-derivatives on the electrochemical performance of carbon felts electrodes of vanadium redox flow battery. *J. Energy Storage* **2024**, *84*, 110599. [\[CrossRef\]](#)
148. Xu, C.; Yang, C.; Liu, X.; He, Y.; Xing, X.; Zhao, Y.; Qian, Z.; Zheng, J.; Hao, Z. Agar-stabilized sulfidated microscale zero-valent iron: Its stability and performance in chromate reduction. *J. Hazard. Mater.* **2021**, *417*, 126019. [\[CrossRef\]](#) [\[PubMed\]](#)
149. Sun, P.; Chen, J.; Huang, Y.; Tian, J.-H.; Li, S.; Wang, G.; Zhang, Q.; Tian, Z.; Zhang, L. High-Strength agarose gel electrolyte enables long-endurance wearable Al-air batteries with greatly suppressed self-corrosion. *Energy Storage Mater.* **2021**, *34*, 427–435. [\[CrossRef\]](#)
150. Yan, T.; Zou, Y.; Zhang, X.; Li, D.; Guo, X.; Yang, D. Hydrogen Bond Interpenetrated Agarose/PVA Network: A Highly Ionic Conductive and Flame-Retardant Gel Polymer Electrolyte. *ACS Appl. Mater. Interfaces* **2021**, *13*, 9856–9864. [\[CrossRef\]](#) [\[PubMed\]](#)
151. Liu, J.; Maimaitiyiming, X.; Kuerban, Z. Oxygen reduction performance study of Fe/Ni doped PAAM/Agar double net hydrogel carbon materials. *ChemistrySelect* **2023**, *8*, e202302746. [\[CrossRef\]](#)
152. Liu, G.; Ma, Q.; Zhang, X. Agar-polyacrylamide dual network hydrogel-carbon nanotube composites with long-term stability for high efficient solar water purification. *Compos. Commun.* **2025**, *53*, 102248. [\[CrossRef\]](#)
153. Cirillo, G.; Hampel, S.; Spizzirri, U.G.; Parisi, O.I.; Picci, N.; Iemma, F. Carbon nanotubes hybrid hydrogels in drug delivery: A perspective review. *BioMed Res. Int.* **2014**, *2014*, 825017. [\[CrossRef\]](#)
154. Sivashankari, P.; Prabakaran, M. Three-dimensional porous scaffolds based on agarose/chitosan/graphene oxide composite for tissue engineering. *Int. J. Biol. Macromol.* **2020**, *146*, 222–231. [\[CrossRef\]](#)
155. Xiong, C.; Li, T.; Khan, M.; Li, H.; Zhao, T. A three-dimensional MnO_2 /graphene hybrid as a binder-free supercapacitor electrode. *RSC Adv.* **2015**, *5*, 85613–85619. [\[CrossRef\]](#)
156. Khan, M.; Hussain, A.; Saleh, M.T.; Ibrahim, M.; Attique, F.; Sun, X.; Unalan, H.E.; Shafi, M.; Khan, Y.; Khan, I.; et al. Cutting-edge advancements in MXene-derived materials: Revolutionary electrocatalysts for hydrogen evolution and high-performance energy storage. *Coord. Chem. Rev.* **2024**, *506*, 215722. [\[CrossRef\]](#)
157. Khan, M.; Tiehu, L.; Zaidi, S.B.A.; Javed, E.; Hussain, A.; Hayat, A.; Zada, A.; Alei, D.; Ullah, A. Synergistic effect of nanodiamond and titanium oxide nanoparticles on the mechanical, thermal and electrical properties of pitch-derived carbon foam composites. *Polym. Int.* **2021**, *70*, 1733–1740. [\[CrossRef\]](#)
158. Vaghela, C.; Kulkarni, M.; Karve, M.; Zinjarde, S. Selective electrochemical sensing of bisphenol derivatives using novel bioelectrode of agarose-guar gum-graphene oxide immobilized with tyrosinase. *J. Environ. Chem. Eng.* **2022**, *10*, 107360. [\[CrossRef\]](#)
159. Guo, Z.; Hao, T.; Duan, J.; Wang, S.; Wei, D. Electrochemiluminescence immunosensor based on graphene-CdS quantum dots-agarose composite for the ultrasensitive detection of alpha fetoprotein. *Talanta* **2012**, *89*, 27–32. [\[CrossRef\]](#) [\[PubMed\]](#)
160. Hwang, S.; Zhou, J.; Tang, T.; Goossens, K.; Bielawski, C.W.; Geng, J. Agarose-Based Hierarchical Porous Carbons Prepared with Gas-Generating Activators and Used in High-Power Density Supercapacitors. *Energy Fuels* **2021**, *35*, 19775–19783. [\[CrossRef\]](#)
161. Rehman, A.U.; Khan, M.; Maosheng, Z. Hydration behavior of MgSO_4 - ZnSO_4 composites for long-term thermochemical heat storage application. *J. Energy Storage* **2019**, *26*, 101026. [\[CrossRef\]](#)
162. Xiong, C.; Li, T.; Zhao, T.; Khan, M.; Wang, J.; Ji, X.; Li, H.; Liu, W.; Shang, Y. Preparation of C/C-SiC composite by low temperature compression molding-liquid silicon infiltration and its application in automobile brake. *Ceram. Int.* **2016**, *42*, 1057–1062. [\[CrossRef\]](#)
163. Yang, Y.; Wang, T.; Guo, Y.; Liu, P.; Han, X.; Wu, D. Agar-PVA/GO double network gel electrolyte for high performance flexible zinc-air batteries. *Mater. Today Chem.* **2023**, *29*, 101384. [\[CrossRef\]](#)
164. Ji, Y.; Wang, T.; Yao, X.; Gao, J.; Chu, Y.; Sun, J.; Dong, H.; Sha, J. Regulating microstructure in agar-derived N-doped hard carbon towards enhanced sodium ion storage. *J. Energy Storage* **2025**, *106*, 114640. [\[CrossRef\]](#)
165. Samadi, N.; Sabzi, M.; Babaahmadi, M. Self-healing and tough hydrogels with physically cross-linked triple networks based on Agar/PVA/Graphene. *Int. J. Biol. Macromol.* **2018**, *107*, 2291–2297. [\[CrossRef\]](#) [\[PubMed\]](#)

166. de Araujo, C.M.B.; Rios, A.G.; Ferreira, A.F.P.; da Motta Sobrinho, M.A.; Rodrigues, A.E.; Ghislandi, M.G. Agar/graphene oxide hydrogels as nano-bioadsorbents: A comparative analysis for dye removal. *Environ. Sci. Pollut. Res.* **2024**, *31*, 53629–53641. [[CrossRef](#)] [[PubMed](#)]
167. de Araujo, C.M.B.; Ghislandi, M.G.; Rios, A.G.; da Costa, G.R.B.; do Nascimento, B.F.; Ferreira, A.F.P.; da Motta Sobrinho, M.A.; Rodrigues, A.E. Wastewater treatment using recyclable agar-graphene oxide biocomposite hydrogel in batch and fixed-bed adsorption column: Bench experiments and modeling for the selective removal of organics. *Colloids Surf. A Physicochem. Eng. Asp.* **2022**, *639*, 128357. [[CrossRef](#)]
168. Bezerra de Araujo, C.M.; Wernke, G.; Ghislandi, M.G.; Diório, A.; Vieira, M.F.; Bergamasco, R.; Alves da Motta Sobrinho, M.; Rodrigues, A.E. Continuous removal of pharmaceutical drug chloroquine and Safranin-O dye from water using agar-graphene oxide hydrogel: Selective adsorption in batch and fixed-bed experiments. *Environ. Res.* **2023**, *216*, 114425. [[CrossRef](#)]
169. Felipe Melo Lima Gomes, B.; de Araujo, C.M.B.; do Nascimento, B.F.; da Silva Santos, R.K.; de Luna Freire, E.M.P.; Da Motta Sobrinho, M.A.; Carvalho, M.N. Adsorption of Cd (II) ions and methyl violet dye by using an agar-graphene oxide nano-biocomposite. *Environ. Technol.* **2024**, *45*, 2957–2968. [[CrossRef](#)] [[PubMed](#)]
170. Tang, T.; Goossens, K.; Lu, S.J.; Meng, D.; Bielawski, C.W. Agar-reduced graphene oxide selectively adsorbs organic dyes and strengthens double-network hydrogels. *RSC Adv.* **2020**, *10*, 29287–29295. [[CrossRef](#)] [[PubMed](#)]
171. Bagheri, O.; Esmkhani, M.; Javanshir, S.; Aghabarari, B. Preparation of agar functionalized graphene oxide-immobilized copper ferrite aerogel for dye degradation via dark-Fenton oxidative process. *Int. J. Biol. Macromol.* **2023**, *253*, 127432. [[CrossRef](#)] [[PubMed](#)]
172. Liu, Q.; Wu, D.; Wang, T.; Guo, Y. Polysaccharide of agar based ultra-high specific surface area porous carbon for superior supercapacitor. *Int. J. Biol. Macromol.* **2023**, *228*, 40–47. [[CrossRef](#)]
173. Wang, T.; Sha, J.; Wang, W.; Ji, Y.; Zhang, Z.-M. Agar-derived nitrogen-doped porous carbon as anode for construction of cost-effective lithium-ion batteries. *Chin. Chem. Lett.* **2023**, *34*, 107929. [[CrossRef](#)]
174. Liew, S.Y.; Juan, J.C.; Lai, C.W.; Pan, G.-T.; Yang, T.C.K.; Lee, T.K. An eco-friendly water-soluble graphene-incorporated agar gel electrolyte for magnesium-air batteries. *Ionics* **2019**, *25*, 1291–1301. [[CrossRef](#)]
175. Jiang, J.; Zhao, R.; Wang, T.; Song, B.; Chen, Y.; Zhang, H.; Dong, B. Agar/graphene conductive organogel with self-healable, adhesive, and wearable properties. *J. Mater. Sci.* **2023**, *58*, 5287–5297. [[CrossRef](#)]
176. Lv, L.; Hui, B.; Zhang, X.; Zou, Y.; Yang, D. Lamellar agarose/graphene oxide gel polymer electrolyte network for all-solid-state supercapacitor. *Chem. Eng. J.* **2023**, *452*, 139443. [[CrossRef](#)]
177. Guo, Y.; Wang, T.; Chen, X.; Wu, D. Agar-based porous electrode and electrolyte for flexible symmetric supercapacitors with ultrahigh energy density. *J. Power Sources* **2021**, *507*, 230252. [[CrossRef](#)]
178. Krempirski, A.; Rudnicki, K.; Korzonek, W.; Poltorak, L. 3D-printed gelled electrolytes for electroanalytical applications. *Sci. Rep.* **2025**, *15*, 6917. [[CrossRef](#)]
179. Wei, J.; Wang, J.; Su, S.; Wang, S.; Qiu, J.; Zhang, Z.; Christopher, G.; Ning, F.; Cong, W. 3D printing of an extremely tough hydrogel. *RSC Adv.* **2015**, *5*, 81324–81329. [[CrossRef](#)]
180. Kong, I.; Tshai, K.; Hoque, M.E. Manufacturing of natural fibre-reinforced polymer composites by solvent casting method. In *Manufacturing of Natural Fibre Reinforced Polymer Composites*; Springer: Berlin/Heidelberg, Germany, 2015; pp. 331–349.
181. Siemann, U. Solvent cast technology—a versatile tool for thin film production. In *Scattering Methods and the Properties of Polymer Materials*; Springer: Berlin/Heidelberg, Germany, 2005; pp. 1–14.
182. Munro, C.D.; Plucknett, K.P. Agar-Based Aqueous Gel Casting of Barium Titanate Ceramics. *Int. J. Appl. Ceram. Technol.* **2011**, *8*, 597–609. [[CrossRef](#)]
183. Han, K.; Sathiyaseelan, A.; Lu, Y.; Kim, K.M.; Wang, M.-H. Agar/carboxymethyl cellulose composite film loaded with hydroxyapatite nanoparticles for bone regeneration. *Cellulose* **2024**, *31*, 9319–9334. [[CrossRef](#)]
184. Jayram, J.; Kondaveeti, S.S.; Balu, A.; Madhavan, Y.; Kalachaveedu, M. Polymer blended *Acalypha indica* bioactive for potential wound dressing applications through solvent casting—An experimental interrogation. *Biomass Convers. Biorefinery* **2023**, *15*, 4985–4997. [[CrossRef](#)]
185. Rathore, K.; Upadhyay, D.; Verma, N.; Gupta, A.K.; Matheshwaran, S.; Sharma, S.; Verma, V. Asymmetric Janus Nanofibrous Agar-Based Wound Dressing Infused with Enhanced Antioxidant and Antibacterial Properties. *ACS Appl. Bio Mater.* **2024**, *7*, 7608–7623. [[CrossRef](#)]
186. Diop, C.I.K.; Beltran, S.; Sanz, M.-T.; Garcia-Tojal, J.; Trigo-lopez, M. Designing bilayered composite films by direct agar/chitosan and citric acid-crosslinked PVA/agar layer-by-layer casting for packaging applications. *Food Hydrocoll.* **2023**, *144*, 108987. [[CrossRef](#)]
187. Jiang, S.; Chen, Y.; Duan, G.; Mei, C.; Greiner, A.; Agarwal, S. Electrospun nanofiber reinforced composites: A review. *Polym. Chem.* **2018**, *9*, 2685–2720. [[CrossRef](#)]
188. Lee, J.K.Y.; Chen, N.; Peng, S.; Li, L.; Tian, L.; Thakor, N.; Ramakrishna, S. Polymer-based composites by electrospinning: Preparation & functionalization with nanocarbons. *Prog. Polym. Sci.* **2018**, *86*, 40–84. [[CrossRef](#)]

189. Badshah, F.; Zhou, Y.; Idrees, M.; Ziauddin; Rahmatullah. Vacuum-induced excitation of surface plasmon polaritons. *Phys. Rev. A* **2025**, *112*, 043706. [\[CrossRef\]](#)
190. Duman, O.; Uğurlu, H.; Diker, C.Ö.; Tunç, S. Fabrication of highly hydrophobic or superhydrophobic electrospun PVA and agar/PVA membrane materials for efficient and selective oil/water separation. *J. Environ. Chem. Eng.* **2022**, *10*, 107405. [\[CrossRef\]](#)
191. Rathore, K.; Singh, I.; Balani, K.; Sharma, S.; Verma, V. Fabrication and characterization of multi-layered coaxial agar-based electrospun biocomposite mat, novel replacement for transdermal patches. *Int. J. Biol. Macromol.* **2024**, *275*, 133712. [\[CrossRef\]](#) [\[PubMed\]](#)
192. Wypych, G. *Handbook of Curatives and Crosslinkers*; Elsevier: Amsterdam, The Netherlands, 2024.
193. Trimukhe, K.D. Crosslinking Reactions of Chitosan and Their Applications. Ph.D. Thesis, University of Pune, Pune, India, 2007.
194. Belay, M.; Tyeb, S.; Rathore, K.; Kumar, M.; Verma, V. Synergistic effect of bacterial cellulose reinforcement and succinic acid crosslinking on the properties of agar. *Int. J. Biol. Macromol.* **2020**, *165*, 3115–3122. [\[CrossRef\]](#) [\[PubMed\]](#)
195. Wang, R.; Li, N.; Jiang, B.; Li, J.; Hong, W.; Jiao, T. Facile preparation of agar/polyvinyl alcohol-based triple-network composite hydrogels with excellent mechanical performances. *Colloids Surf. A Physicochem. Eng. Asp.* **2021**, *615*, 126270. [\[CrossRef\]](#)
196. Gürkan Polat, T.; Duman, O.; Tunç, S. Preparation and characterization of environmentally friendly agar/ κ -carrageenan/montmorillonite nanocomposite hydrogels. *Colloids Surf. A Physicochem. Eng. Asp.* **2020**, *602*, 124987. [\[CrossRef\]](#)
197. Hennink, W.E.; van Nostrum, C.F. Novel crosslinking methods to design hydrogels. *Adv. Drug Deliv. Rev.* **2012**, *64*, 223–236. [\[CrossRef\]](#)
198. Li, X.; Zhang, Y.; Yang, Q.; Li, D.; Zhang, G.; Long, S. Agar/PAAc-Fe³⁺ hydrogels with pH-sensitivity and high toughness using dual physical cross-linking. *Iran. Polym. J.* **2018**, *27*, 829–840. [\[CrossRef\]](#)
199. Mahamoud, M.M.; Ketema, T.M.; Kuwahara, Y.; Takafuji, M. Enhancement of Mechanical Properties of Benign Polyvinyl Alcohol/Agar Hydrogel by Crosslinking Tannic Acid and Applying Multiple Freeze/Thaw Cycles. *Gels* **2024**, *10*, 527. [\[CrossRef\]](#)
200. Li, W.; Wu, Z.; Zhao, J.; Jiang, M.; Yuan, L.; Guo, Y.; Li, S.; Hu, L.; Xie, X.; Zhang, Y.; et al. Fabrication of dual physically cross-linked polyvinyl alcohol/agar hydrogels with mechanical stability and antibacterial activity for wound healing. *Int. J. Biol. Macromol.* **2023**, *247*, 125652. [\[CrossRef\]](#)
201. Huang, D.; Quan, Q.; Zheng, Y.; Tang, W.; Zhang, Z.; Qiang, X. Dual-network design to enhance the properties of agar aerogel adsorbent by incorporating in situ ion cross-linked alginate. *Environ. Chem. Lett.* **2020**, *18*, 251–255. [\[CrossRef\]](#)
202. Hu, W.; Yu, L.; Ma, Z.; Liu, Y. W-Y₂O₃ composite nanopowders prepared by freeze-drying method and its sintering characteristics. *J. Alloys Compd.* **2019**, *806*, 127–135. [\[CrossRef\]](#)
203. Du, Y.; Zhang, M.; Mujumdar, A.S.; Liu, W.; Yang, C. Innovative applications of freeze-drying to produce compound formula instant foods: A review. *Dry. Technol.* **2022**, *40*, 2583–2597. [\[CrossRef\]](#)
204. Badshah, F.; Lü, D.-Y.; Xie, J.; Shi, Z.; He, Q.; Idrees, M. Manipulation of photonic spin Hall effect via controllable double-tunneling induced transparency in quantum dot molecules. *Opt. Laser Technol.* **2025**, *192*, 113816. [\[CrossRef\]](#)
205. Ajisafe, V.A.; Raichur, A.M. Snail Mucus-Enhanced Adhesion of Human Chondrocytes on 3D Porous Agarose Scaffolds. *ACS Appl. Mater. Interfaces* **2024**, *16*, 11324–11335. [\[CrossRef\]](#) [\[PubMed\]](#)
206. Xie, K.; Liu, X.; Li, H.; Fang, L.; Xia, K.; Yang, D.; Zou, Y.; Zhang, X. Heteroatom tuning in agarose derived carbon aerogel for enhanced potassium ion multiple energy storage. *Carbon Energy* **2024**, *6*, e427. [\[CrossRef\]](#)
207. Duman, O.; Diker, C.Ö.; Uğurlu, H.; Tunç, S. Highly hydrophobic and superoleophilic agar/PVA aerogels for selective removal of oily substances from water. *Carbohydr. Polym.* **2022**, *286*, 119275. [\[CrossRef\]](#) [\[PubMed\]](#)
208. Sang, S.; Zhao, Y.; Shen, Z.; Cao, Y.; Cheng, R.; Yan, Y.; Jian, A.; Wang, J. Collagen-coated agarose–chitosan scaffold used as a skin substitute. *Biotechnol. Appl. Biochem.* **2023**, *70*, 1206–1216. [\[CrossRef\]](#)
209. Kumar, N.; Desagani, D.; Chandran, G.; Ghosh, N.N.; Karthikeyan, G.; Waigaonkar, S.; Ganguly, A. Biocompatible agarose–chitosan coated silver nanoparticle composite for soft tissue engineering applications. *Artif. Cells Nanomed. Biotechnol.* **2018**, *46*, 637–649. [\[CrossRef\]](#)
210. Prabhakar, M.M.; Saravanan, A.; Lenin, A.H.; Mayandi, K.; Ramalingam, P.S. A short review on 3D printing methods, process parameters and materials. *Mater. Today Proc.* **2021**, *45*, 6108–6114. [\[CrossRef\]](#)
211. Zhang, D.; Liu, X.; Qiu, J. 3D printing of glass by additive manufacturing techniques: A review. *Front. Optoelectron.* **2021**, *14*, 263–277. [\[CrossRef\]](#)
212. Ngo, T.D.; Kashani, A.; Imbalzano, G.; Nguyen, K.T.; Hui, D. Additive manufacturing (3D printing): A review of materials, methods, applications and challenges. *Compos. Part B Eng.* **2018**, *143*, 172–196. [\[CrossRef\]](#)
213. El-Sayegh, S.; Romdhane, L.; Manjikian, S. A critical review of 3D printing in construction: Benefits, challenges, and risks. *Arch. Civ. Mech. Eng.* **2020**, *20*, 34. [\[CrossRef\]](#)
214. Prashar, G.; Vasudev, H.; Bhuddhi, D. Additive manufacturing: Expanding 3D printing horizon in industry 4.0. *Int. J. Interact. Des. Manuf.* **2023**, *17*, 2221–2235. [\[CrossRef\]](#)

215. Ghaedamini, S.I.; Karbasi, S.; Hashemibeni, B.; Honarvar, A.; Rabiei, A. PCL/Agarose 3D-printed scaffold for tissue engineering applications: Fabrication, characterization, and cellular activities. *Res. Pharm. Sci.* **2023**, *18*, 566–579. [\[CrossRef\]](#) [\[PubMed\]](#)
216. Yang, B.; Liu, T.; Gao, G.; Zhang, X.; Wu, B. Fabrication of 3D GelMA Scaffolds Using Agarose Microgel Embedded Printing. *Micromachines* **2022**, *13*, 469. [\[CrossRef\]](#)
217. Wang, J.; Liu, Y.; Zhang, X.; Rahman, S.E.; Su, S.; Wei, J.; Ning, F.; Hu, Z.; Martínez-Zaguilán, R.; Sennoune, S.R.; et al. 3D printed agar/calcium alginate hydrogels with high shape fidelity and tailorable mechanical properties. *Polymer* **2021**, *214*, 123238. [\[CrossRef\]](#)
218. Vijayaraghavan, R.; Loganathan, S.; Valapa, R.B. Fabrication of GelMA–Agarose Based 3D Bioprinted Photocurable Hydrogel with In Vitro Cytocompatibility and Cells Mirroring Natural Keratocytes for Corneal Stromal Regeneration. *Macromol. Biosci.* **2024**, *24*, 2400136. [\[CrossRef\]](#) [\[PubMed\]](#)
219. Mukundan, L.M.; Rajasekaran, R.; Das, S.; Seesala, V.S.; Ganguly, D.; Kumar, N.; Dhara, S.; Chattopadhyay, S. Tailoring of agarose hydrogel to modulate its 3D bioprintability and mechanical properties for stem cell mediated bone tissue engineering. *Int. J. Biol. Macromol.* **2025**, *309*, 142795. [\[CrossRef\]](#) [\[PubMed\]](#)
220. Sartip, E.; Behzad, T.; Kharaziha, M. Fabrication and characterization of 3D printed agarose/poly(ethylene glycol) diacrylate/hydroxyapatite nanocomposite hydrogel for cartilage tissue engineering. *Int. J. Biol. Macromol.* **2025**, *320*, 145573. [\[CrossRef\]](#) [\[PubMed\]](#)
221. Zhang, W.; Hao, M.-F.; Peng, H.; Wei, D.-Y.; Yao, J.-J.; Guo, T.; Yang, L.-M.; Wang, H.-J. Fabrication of PBS/PLA/Fibroin-Agarose nerve guidance conduit with sandwich compression resistant wall structure for repairment of 10 mm-sciatic nerve defect. *Chem. Eng. J.* **2025**, *505*, 159312. [\[CrossRef\]](#)
222. Cao, F.; Zadeh, H.N.; Świacka, K.; Maculewicz, J.; Bowles, D.; Huber, T.; Clucas, D. An additive manufacturing approach for fabrication of agarose hydrogel structures for protein sorption application. *Mater. Des.* **2025**, *250*, 113581. [\[CrossRef\]](#)
223. Chaudhary, J.; Thakur, S.; Sharma, M.; Gupta, V.K.; Thakur, V.K. Development of biodegradable agar-agar/gelatin-based superabsorbent hydrogel as an efficient moisture-retaining agent. *Biomolecules* **2020**, *10*, 939. [\[CrossRef\]](#)
224. Oe, T.; Dechojarassri, D.; Kakinoki, S.; Kawasaki, H.; Furuie, T.; Tamura, H. Microwave-assisted incorporation of AgNP into chitosan–alginate hydrogels for antimicrobial applications. *J. Funct. Biomater.* **2023**, *14*, 199. [\[CrossRef\]](#) [\[PubMed\]](#)
225. Qi, B.; Yang, S.; Zhao, Y.; Wang, Y.; Yang, X.; Chen, S.; Wu, Y.; Pan, C.; Hu, X.; Li, C. Comparison of the Physicochemical Properties of Carboxymethyl Agar Synthesized by Microwave-Assisted and Conventional Methods. *Gels* **2022**, *8*, 162. [\[CrossRef\]](#) [\[PubMed\]](#)
226. Kabir, E. Application of microwave heating in polymer synthesis: A review. *Results Chem.* **2023**, *6*, 101178. [\[CrossRef\]](#)
227. Chen, X.; Yang, J.; Shen, M.; Chen, Y.; Yu, Q.; Xie, J. Structure, function and advance application of microwave-treated polysaccharide: A review. *Trends Food Sci. Technol.* **2022**, *123*, 198–209. [\[CrossRef\]](#)
228. More, A.P.; Chapekar, S. Irradiation assisted synthesis of hydrogel: A Review. *Polym. Bull.* **2024**, *81*, 5839–5908. [\[CrossRef\]](#)
229. Wali, A.S.; Kumar, S.; Khan, D. A review on recent development and application of radiation curing. *Mater. Today Proc.* **2023**, *82*, 68–74. [\[CrossRef\]](#)
230. Abliz, D.; Duan, Y.; Steuernagel, L.; Xie, L.; Li, D.; Ziegmann, G. Curing methods for advanced polymer composites-a review. *Polym. Polym. Compos.* **2013**, *21*, 341–348. [\[CrossRef\]](#)
231. Tudoran, C.; Roşu, M.C.; Coroş, M. A concise overview on plasma treatment for application on textile and leather materials. *Plasma Process. Polym.* **2020**, *17*, 2000046. [\[CrossRef\]](#)
232. Chang, G.; Yang, M.; Xu, Z.; Wang, X.; Li, W.; He, M.; Zhang, J.; Xu, Y.; Wang, L.; Zhang, L. Preparation of agarose microspheres with large pore size and high load and purification of antibody in serum based on microfluidic technology. *Colloid. Polym. Sci.* **2025**, *303*, 693–711. [\[CrossRef\]](#)
233. Wang, J.; Hu, H.; Yang, Z.; Wei, J.; Li, J. IPN hydrogel nanocomposites based on agarose and ZnO with antifouling and bactericidal properties. *Mater. Sci. Eng. C* **2016**, *61*, 376–386. [\[CrossRef\]](#)
234. Xie, K.; Xia, K.; Ding, X.; Fang, L.; Liu, X.; Zhang, X. Facile preparation of 3D porous agar-based heteroatom-doped carbon aerogels for high-energy density supercapacitors. *RSC Adv.* **2022**, *12*, 20975–20982. [\[CrossRef\]](#)
235. Hu, X.; Zhuo, K.; Sun, D.; Du, Q.; Sun, L.; Chen, Y.; Bai, G.; Wang, J. Nitrogen-doped agar-derived porous carbon with long cycle life for high-performance ionic liquid-based supercapacitors. *Diam. Relat. Mater.* **2023**, *139*, 110332. [\[CrossRef\]](#)
236. Wang, T.; Liu, L.; Wei, Y.; Gao, Y.; Wang, S.; Jia, D.; Zhang, W.; Sha, J. Agar-Derived Slope-Dominated Carbon Anode with Puparium Like Nano-Morphology for Cost-Effective SIBs. *Small* **2024**, *20*, 2309809. [\[CrossRef\]](#) [\[PubMed\]](#)
237. Cao, C.; Liu, S.; Fan, J.; Li, G.; Arenal, R.; Wang, C.; Li, W.; Xie, F. MoS₂ Anchored on Agar-Derived 3D Nitrogen-Doped Porous Carbon for Electrocatalytic Hydrogen Evolution Reaction and Lithium-Ion Batteries. *Adv. Sustain. Syst.* **2022**, *6*, 2100393. [\[CrossRef\]](#)
238. Wustoni, S.; Nikiforidis, G.; Ohayon, D.; Inal, S.; Indartono, Y.S.; Suendo, V.; Yuliarto, B. Performance of PEDOT/PEO-based Supercapacitors in Agarose Gel Electrolyte. *Chem. Asian J.* **2022**, *17*, e202200427. [\[CrossRef\]](#) [\[PubMed\]](#)
239. Appiah, E.S.; Dzikunu, P.; Mahadeen, N.; Ampong, D.N.; Mensah-Darkwa, K.; Kumar, A.; Gupta, R.K.; Adom-Asamoah, M. Biopolymers-derived materials for supercapacitors: Recent trends, challenges, and future prospects. *Molecules* **2022**, *27*, 6556. [\[CrossRef\]](#)

240. Tanwar, S.; Sharma, A. Insight into use of biopolymer in hybrid electrode materials for supercapacitor applications—A critical review. *J. Appl. Phys.* **2023**, *133*, 180701. [\[CrossRef\]](#)
241. Ding, J.; Yang, Y.; Poisson, J.; He, Y.; Zhang, H.; Zhang, Y.; Bao, Y.; Chen, S.; Chen, Y.M.; Zhang, K. Recent advances in biopolymer-based hydrogel electrolytes for flexible supercapacitors. *ACS Energy Lett.* **2024**, *9*, 1803–1825. [\[CrossRef\]](#) [\[PubMed\]](#)
242. Liang, W.; Ge, X.; Ge, J.; Li, T.; Zhao, T.; Chen, X.; Song, Y.; Cui, Y.; Khan, M.; Ji, J.; et al. Reduced Graphene Oxide Embedded with MQ Silicone Resin Nano-Aggregates for Silicone Rubber Composites with Enhanced Thermal Conductivity and Mechanical Performance. *Polymers* **2018**, *10*, 1254. [\[CrossRef\]](#) [\[PubMed\]](#)
243. Yasmeen, H.; Zada, A.; Ali, S.; Khan, I.; Ali, W.; Khan, W.; Khan, M.; Anwar, N.; Ali, A.; Huerta-Flores, A.M.; et al. Visible light-excited surface plasmon resonance charge transfer significantly improves the photocatalytic activities of ZnO semiconductor for pollutants degradation. *J. Chin. Chem. Soc.* **2020**, *67*, 1611–1617. [\[CrossRef\]](#)
244. Zhou, Y.; Wang, J.-W.; Cao, L.-Z.; Wang, G.-H.; Shi, Z.-Y.; Lü, D.-Y.; Huang, H.-B.; Hu, C.-S. Realization of chiral two-mode Lipkin–Meshkov–Glick models via acoustics. *Rep. Prog. Phys.* **2024**, *87*, 100502. [\[CrossRef\]](#) [\[PubMed\]](#)
245. Wang, Z.; Li, H.; Tang, Z.; Liu, Z.; Ruan, Z.; Ma, L.; Yang, Q.; Wang, D.; Zhi, C. Hydrogel electrolytes for flexible aqueous energy storage devices. *Adv. Funct. Mater.* **2018**, *28*, 1804560. [\[CrossRef\]](#)
246. Chan, C.Y.; Wang, Z.; Jia, H.; Ng, P.F.; Chow, L.; Fei, B. Recent advances of hydrogel electrolytes in flexible energy storage devices. *J. Mater. Chem. A* **2021**, *9*, 2043–2069. [\[CrossRef\]](#)
247. Xu, T.; Liu, K.; Sheng, N.; Zhang, M.; Liu, W.; Liu, H.; Dai, L.; Zhang, X.; Si, C.; Du, H. Biopolymer-based hydrogel electrolytes for advanced energy storage/conversion devices: Properties, applications, and perspectives. *Energy Storage Mater.* **2022**, *48*, 244–262. [\[CrossRef\]](#)
248. Badshah, F.; Sohrab, A.; Chuang, Y.-L.; Ziauddin; Shi, Z.; Dong, S.-H. Advanced manipulation of surface plasmon resonance and the Goos–Hänchen shift in a coupler-free system. *Phys. Rev. A* **2025**, *111*, 033702. [\[CrossRef\]](#)
249. Ji, X.; Geng, H.; Akhtar, N.; Yang, X. Floquet engineering of point-gapped topological superconductors. *Phys. Rev. B* **2025**, *111*, 195419. [\[CrossRef\]](#)
250. Zhang, M.; Cheng, J.; Zhang, L.; Li, Y.; Chen, M.; Chen, Y.; Shen, Z. Activated Carbon by One-Step Calcination of Deoxygenated Agar for High Voltage Lithium Ion Supercapacitor. *ACS Sustain. Chem. Eng.* **2020**, *8*, 3637–3643. [\[CrossRef\]](#)
251. Kim, S.-K.; Koo, H.-J.; Liu, J.; Braun, P.V. Flexible and Wearable Fiber Microsupercapacitors Based on Carbon Nanotube–Agarose Gel Composite Electrodes. *ACS Appl. Mater. Interfaces* **2017**, *9*, 19925–19933. [\[CrossRef\]](#) [\[PubMed\]](#)
252. Lizundia, E.; Kundu, D. Advances in natural biopolymer-based electrolytes and separators for battery applications. *Adv. Funct. Mater.* **2021**, *31*, 2005646. [\[CrossRef\]](#)
253. Singh, R.; Polu, A.R.; Bhattacharya, B.; Rhee, H.-W.; Varlikli, C.; Singh, P.K. Perspectives for solid biopolymer electrolytes in dye sensitized solar cell and battery application. *Renew. Sustain. Energy Rev.* **2016**, *65*, 1098–1117. [\[CrossRef\]](#)
254. Ghazali, N.M.; Samsudin, A.S. Progress on biopolymer as an application in electrolytes system: A review study. *Mater. Today Proc.* **2022**, *49*, 3668–3678. [\[CrossRef\]](#)
255. Lin, A.; Yang, X. Seaweed extractions as promising polymer electrolytes for lithium batteries. *E3S Web Conf.* **2021**, *308*, 01022. [\[CrossRef\]](#)
256. Lu, C.-H.; Li, K.-C.; Balaji, S.; Kumar, P.S. Agar-assisted sol-gel synthesis and electrochemical characterization of TiNb₂O₇ anode materials for lithium-ion batteries. *Ceram. Int.* **2021**, *47*, 18619–18624. [\[CrossRef\]](#)
257. Sowmiya, S.; Shanthi, C. Preparation and characterization of sodium-ion conducting biopolymer electrolyte membrane based on agar-agar with sodium nitrite for primary Na-ion battery. *Mater. Sci. Chem. Eng.* **2024**.
258. Zhang, K.; Zhou, J.; Liu, H.; Wang, X.; Gao, J.; Chen, J.-L.; Qin, H.; Liu, W.; Lei, X.; Miao, L. Facile formation of Mg-containing interphase on nanosilicon from Agar/MgCO₃ precursor for lithium-ion battery anodes. *Prog. Nat. Sci. Mater. Int.* **2024**, *35*, 177–186. [\[CrossRef\]](#)
259. Lu, C.-H.; Li, W.Y.; Subburaj, T.; Ou, C.Y.; Kumar, P.S. Influence of bio-derived agar addition on the electrochemical performance of LiFePO₄ cathode powders for Li-ion batteries. *Ceram. Int.* **2019**, *45*, 12218–12224. [\[CrossRef\]](#)
260. Ali, N.I.; Abidin, S.Z.Z.; Majid, S.R. The High-Performance Polymer Electrolytes Based on Agarose–Mg (ClO₄)₂ for Application in Electrochemical Energy Storage Devices. *J. Adv. Res. Fluid Mech. Therm. Sci.* **2024**, *118*, 65–85.
261. Hu, C.; Zhang, W.; Zhang, J.; Zhao, X.; Xu, C.; Yang, L.; Jiang, N.; Yin, S. Three-Dimensional Porous Spongy Ti₃C₂T_x MXene/Polyvinyl Alcohol/Agar Gel Electrolyte with High Ionic Conductivity Enables Highly Reversible Zinc-Ion Batteries. *Energy Technol.* **2024**, *12*, 2400772. [\[CrossRef\]](#)
262. Mittal, N.; Ojanguren, A.; Kundu, D.; Lizundia, E.; Niederberger, M. Bottom-Up Design of a Green and Transient Zinc-Ion Battery with Ultralong Lifespan. *Small* **2023**, *19*, 2206249. [\[CrossRef\]](#)
263. Li, B.; Ullah Khan, M.; Qv, C.; Chen, L.; Xiong, Y.; Zhang, L.; Wu, M. A wearable zinc-air battery based on an Agar hydrogel electrolyte for stable operation at −30 °C. *Chem. Phys. Lett.* **2023**, *832*, 140883. [\[CrossRef\]](#)
264. Zheng, Z.; Liu, Y.; Li, Y.; Zhou, J.; Fu, G.; Yang, B.; Zhu, Y. Agar/polyacrylamide-based hydrogel polymer electrolyte for ultra-stable flexible aqueous lithium-zinc hybrid ion batteries. *Appl. Mater. Today* **2025**, *42*, 102585. [\[CrossRef\]](#)

265. Leo Edward, M.; Roselin Ranjitha, M.; Thennarasu, G.; Ranjith Kumar, E.; Abd El-Rehim, A.F.; Jaisankar, V. A high-performance flexible biopolymer-based Ce oxide composite electrolyte for lithium-ion battery dendrite reduction. *Mater. Sci. Semicond. Process.* **2025**, *187*, 109101. [\[CrossRef\]](#)
266. Li, Z.; Wu, Q.; Zhou, J.; Qin, H.; Miao, L.; Liu, W.; Lei, X.; Zhang, Z.; Lu, A.; Mo, Z. Agar-coated and NH₄F Modified Nanosilicon as Anode Material for Lithium-ion Battery. *J. Ceram.* **2024**, *45*, 501–507. [\[CrossRef\]](#)
267. Zhang, X.; Huang, Y.; Liu, Z.; Yang, Q.; Li, M.; Jiang, Y.; Wang, Z.; Chen, X.; Liu, Z.; Zhang, K. Bi-Functional Agarose-Filled Porous Polysulfone Protective Layer for Dendrite-Free Zn Anode. *Small* **2024**, *21*, 2407411. [\[CrossRef\]](#)
268. Qu, Y.F.; Liu, X.; Qian, J.W.; Chen, J.; Chen, L.F. Agar-Based Interface for Suppressing Parasitic Reactions toward High-Performance Aqueous Zn-Ion Batteries. *Batter. Supercaps* **2024**, *7*, e202400159. [\[CrossRef\]](#)
269. Ojanguren, A.; Mittal, N.; Lizundia, E.; Niederberger, M. Stable Na Electrodeposition Enabled by Agarose-Based Water-Soluble Sodium Ion Battery Separators. *ACS Appl. Mater. Interfaces* **2021**, *13*, 21250–21260. [\[CrossRef\]](#) [\[PubMed\]](#)
270. Zhang, X.; Chu, Y.; Cui, X.; Li, Y.; Pan, Q. An ultra-thin polymer electrolyte based on single-helical-structured agarose for high performance solid-state lithium batteries. *J. Mater. Chem. A* **2021**, *9*, 26939–26948. [\[CrossRef\]](#)
271. Joshi, J.S.; Langwald, S.V.; Ehrmann, A.; Sabantina, L. Algae-Based Biopolymers for Batteries and Biofuel Applications in Comparison with Bacterial Biopolymers—A Review. *Polymers* **2024**, *16*, 610. [\[CrossRef\]](#) [\[PubMed\]](#)
272. Musa, M.T.; Shaari, N.; Kamarudin, S.K.; Wong, W.Y. Recent biopolymers used for membrane fuel cells: Characterization analysis perspectives. *Int. J. Energy Res.* **2022**, *46*, 16178–16207. [\[CrossRef\]](#)
273. Palanisamy, G.; Thangarasu, S.; Dharman, R.K.; Patil, C.S.; Negi, T.P.P.S.; Kurkuri, M.D.; Pai, R.K.; Oh, T.H. The growth of biopolymers and natural earthen sources as membrane/separator materials for microbial fuel cells: A comprehensive review. *J. Energy Chem.* **2023**, *80*, 402–431. [\[CrossRef\]](#)
274. Shi, J.; Shi, B. Environment-friendly design of lithium batteries starting from biopolymer-based electrolyte. *Nano* **2021**, *16*, 2130006. [\[CrossRef\]](#)
275. Lee, W.-H.; Choi, S.-R.; Kim, J.-G. Effect of agar as electrolyte additive on the aluminum-air batteries. *J. Electrochem. Soc.* **2020**, *167*, 110503. [\[CrossRef\]](#)
276. Hernández-Flores, G.; Andrio, A.; Compañ, V.; Solorza-Feria, O.; Poggi-Varaldo, H.M. Synthesis and characterization of organic agar-based membranes for microbial fuel cells. *J. Power Sources* **2019**, *435*, 226772. [\[CrossRef\]](#)
277. Park, Y.-S.; Choe, Y.-J.; Lee, K.-J.; Yoon, K.-Y.; Hwang, H.-J. Fabrication and performance of an agar-aerogel composite membrane for polymer electrolyte membrane fuel cells. *Int. J. Nanotechnol.* **2018**, *15*, 568–577. [\[CrossRef\]](#)
278. John, N. Comparative Study of the Effect of Clay-Based Proton Exchange Membrane and Agar-Agar in a Microbial Fuel Cell. *UNIZIK J. Eng. Appl. Sci.* **2020**, *17*, 228–241.
279. Christwardana, M.; Kuntolaksono, S. Immobilization of *Saccharomyces cerevisiae* in agar polymer matrix to improves the performance of a yeast microbial fuel cell. *AIP Conf. Proc.* **2023**, *2626*, 100001.
280. Singh, K. Optimization and performance evaluation of microbial fuel cell by varying agar concentration using different salts in salt bridge medium. *Arch. Mater. Sci. Eng.* **2020**, *101*, 79–84. [\[CrossRef\]](#)
281. Uddin, S.S.; Prodhana, M.M.H.; Nurnabi, M. Studies on agar salt bridge based dual chamber microbial fuel cells using sludge and dustbin waste. *Biomass Convers. Biorefinery* **2025**, *15*, 9435–9443. [\[CrossRef\]](#)
282. Zou, S.; Li, Y.; Jin, H.; Ning, F.; Xu, P.; Wen, Q.; Pan, S.; Dan, X.; Li, W.; Zhou, X. Highly Safe, Durable, Adaptable, and Flexible Fuel Cell Using Gel/Sponge Composite Material. *Adv. Energy Mater.* **2022**, *12*, 2103178. [\[CrossRef\]](#)
283. Hou, S.; Liao, S.; Xiong, Z.; Zou, H.; Dang, D.; Zheng, R.; Shu, T.; Liang, Z.; Li, X.; Li, Y. Improvement of proton exchange membrane fuel cell performance in low-humidity conditions by adding hygroscopic agarose powder to the catalyst layer. *J. Power Sources* **2015**, *273*, 168–173. [\[CrossRef\]](#)
284. Park, D.; Ok, J.; Lim, S.-R.; Lee, D.S. Saccharification of Agar for Electricity Production in Microbial Fuel Cells. *J. Nanoelectron. Optoelectron.* **2012**, *7*, 508–512. [\[CrossRef\]](#)
285. Selvalakshmi, S.; Mathavan, T.; Selvasekarapandian, S.; Premalatha, M. Characterization of biodegradable solid polymer electrolyte system based on agar-NH₄Br and its comparison with NH₄I. *J. Solid State Electrochem.* **2019**, *23*, 1727–1737. [\[CrossRef\]](#)
286. Selvalakshmi, S.; Mathavan, T.; Selvasekarapandian, S.; Premalatha, M. A study of electrochemical devices based on Agar-Agar-NH₄I biopolymer electrolytes. *AIP Conf. Proc.* **2018**, *1942*, 140019.
287. Saini, A.; Shankar, V. Investigating microbial fuel cell performance by developing salt bridge from agar and activated carbon derived from pine cones. *Adv. Environ. Technol.* **2025**, *11*, 116–129.

Disclaimer/Publisher's Note: The statements, opinions and data contained in all publications are solely those of the individual author(s) and contributor(s) and not of MDPI and/or the editor(s). MDPI and/or the editor(s) disclaim responsibility for any injury to people or property resulting from any ideas, methods, instructions or products referred to in the content.